DESIGN OF PHOTOACTIVATED DNA CLEAVING AGENTS: SYNTHESIS AND STUDY OF PHOTOPHYSICAL AND PHOTOBIOLOGICAL PROPERTIES OF BIFUNCTIONAL ORGANIC LIGANDS

THESIS SUBMITTED TO
THE UNIVERSITY OF KERALA
FOR THE DEGREE OF
DOCTOR OF PHILOSOPHY
IN CHEMISTRY
UNDER THE FACULTY OF SCIENCE

By

MAHESH HARIHARAN

PHOTOSCIENCES AND PHOTONICS
CHEMICAL SCIENCES AND TECHNOLOGY DIVISION
REGIONAL RESEARCH LABORATORY (CSIR)
TRIVANDRUM 695 019, KERALA, INDIA

OCTOBER 2006

STATEMENT

I hereby declare that the matter embodied in the thesis entitled: "**Design of Photoactivated DNA Cleaving Agents: Synthesis and Study of Photophysical and Photobiological Properties of Bifunctional Organic Ligands**" is the result of investigations carried out by me at the Photosciences and Photonics, Chemical Sciences and Technology Division of the Regional Research Laboratory (CSIR), Trivandrum, under the supervision of Dr. D. Ramaiah and the same has not been submitted elsewhere for a degree.

In keeping with the general practice of reporting scientific observations, due acknowledgement has been made wherever the work described is based on the findings of other investigators.

Mahesh Hariharan

PHOTOSCIENCES AND PHOTONICS
CHEMICAL SCIENCES AND TECHNOLOGY DIVISION
REGIONAL RESEARCH LABORATORY (CSIR)
TRIVANDRUM 695 019, INDIA

Dr. D. Ramaiah
Scientist

Telephone: (91)-471-2515362; Fax: (91)-471-2490186 or 2491712
E. Mail: d_ramaiah@rediffmail.com or rama@csrrltrd.ren.nic.in

October 16, 2006

CERTIFICATE

This is to certify that the work embodied in the thesis entitled: "**Design of Photoactivated DNA Cleaving Agents: Synthesis and Study of Photophysical and Photobiological Properties of Bifunctional Organic Ligands**" has been carried out by Mr. Mahesh Hariharan under my supervision and the same has not been submitted elsewhere for a degree.

D. Ramaiah
Thesis Supervisor

ACKNOWLEDGEMENTS

I have great pleasure in placing on record my deep sense of gratitude to Dr. D. Ramaiah, my thesis supervisor, for suggesting the research problem and for his guidance, support and encouragement, leading to the successful completion of this work.

I would like to express my sincere thanks to Professor M. V. George for his constant help and encouragement during the tenure of this work.

I wish to thank Professor T. K. Chandrashekar, Director and Dr. G. Vijay Nair and Professor Javed Iqbal, former Directors of the Regional Research Laboratory, Trivandrum for providing me the necessary facilities for carrying out the work.

I sincerely thank Dr. Suresh Das, Dr. K. R. Gopidas, Dr. A. Ajayaghosh and Dr. K. George Thomas, Scientists of the Photosciences and Photonics, Chemical Sciences and Technology Division, for all the help and support extended to me.

I sincerely thank Professor Dr. Bernd Epe, Institute for Pharmacy, University of Mainz, Germany for the guidance and Mrs. Ina Schulz and Mrs. Karin Paulie for the help in carrying out the photobiological studies reported in this thesis during my visit to University of Mainz, Germany under the DST-DAAD exchange programme.

I thank all the members of the Photosciences and Photonics and in particular, Dr. N. V. Eldho, Dr. Joshy Joseph, Dr. K. T. Arun, Ms. Elizabeth Kuruvilla, Mr. K. Jyothish, Mr. P. N. Prakash, Ms. V. S. Jisha, Ms. Rekha Rachel, Mr. Robert Philip and Mrs. Sarada Nair for their help and cooperation. I also thank members of other Divisions of the Regional Research Laboratory, Trivandrum for their help and cooperation. I would like to thank Mrs. Saumini Shoji and Mrs. S. Viji for recording NMR spectra and for elemental analyses.

Financial assistance from the Council of Scientific and Industrial Research (CSIR) and the Department of Science and Technology (DST), Government of India and DAAD, Germany is gratefully acknowledged.

Mahesh Hariharan

CONTENTS

PREFACE

There is a widespread interest in the study of interactions of small molecules including drugs, dyes and toxic compounds with DNA and also in the design of compounds that can cleave DNA in unique and controllable ways. These studies, not only lead to the development of molecular probes for biochemical and medicinal applications, but also provide the chemical basis for carcinogenesis and serve as model systems for DNA-protein interactions. Recently, there have been significant efforts made towards understanding of factors that govern DNA cleaving efficiency and specificity of various ligands. In this context, the present thesis entitled: "Design of Photoactivated DNA Cleaving Agents: Synthesis and Study of Photophysical and Photobiological Properties of Bifunctional Organic Ligands" reports our efforts towards the design of bifunctional molecules that can bind efficiently with DNA and cleave DNA purely through co-sensitization mechanism.

The first Chapter of the thesis presents a brief description of DNA, DNA non-covalent interactions and DNA cleaving agents with particular emphasis on photoactivated DNA cleaving agents. The objectives of the present thesis are also briefly indicated in this Chapter.

In the second Chapter, synthesis and photophysical properties of a few bifunctional viologen linked pyrene conjugates **1-3** and the model compounds **4** and **5** as well as their interactions with nucleosides are presented. These compounds were synthesized by the S_N2 reaction of the corresponding bromoalkylpyrene derivatives

with 1-butyl-4,4'-bipyridinium bromide and were characterized on the basis of analytical and spectral evidence. The conjugates **1-3** exhibited characteristic fluorescence emission of the pyrene chromophore centered around 380 nm, but with significantly reduced quantum yields, when compared to the model compound **4**. The fluorescence quenching observed in the viologen linked pyrene derivatives **1-3** could be explained due to an electron transfer mechanism based on calculated favorable change in free energy of ΔG_{ET} = -1.59 eV and the transient species characterized through laser flash photolysis studies. The photoactivation of these systems in the presence of guanosine / DNA initiate electron transfer from the singlet excited state of the pyrene chromophore to the viologen moiety followed by an electron transfer from guanosine / DNA to the oxidized pyrene. This reaction results in the formation of stable charge separated species such as radical cations of both guanosine / DNA and reduced viologen as characterized by laser flash photolysis studies. The results presented in this Chapter demonstrate that these bifunctional conjugates are soluble in buffer media, stable under irradiation conditions and oxidize guanosine efficiently and selectively through co-sensitization mechanism and hence can be useful as photoactivated DNA oxidizing agents.

The third Chapter of the thesis deals with the evaluation of DNA binding and *in vitro* photobiological properties of a few selected bifunctional viologen linked pyrene conjugates **1-3**. The DNA binding studies have been carried out through photophysical, chiroptical, viscometric, electrochemical and thermal denaturation

techniques employing calf thymus DNA (CT DNA) and polyoligonucleotides. These studies demonstrate that these conjugates undergo effective DNA intercalation with association constants (K_{DNA}) in the range 1.1-2.6 x 10^4 M^{-1}. The efficiency and mechanism of DNA cleavage analysis in the presence of various additives and scavengers indicate that these systems show spacer length dependent DNA damage that is sensitive to formamidopyrimidine-DNA glycosylase (Fpg). This damage was found to increase with increasing in irradiation time as well as the concentration of the probe. The presence of the additives such as superoxide dismutase, catalase and D_2O showed negligible influence on the extent of DNA damage. The viologen linked pyrene derivatives **1-3**, under investigation, were found to be non-toxic in the dark but interestingly exhibited significant photocytotoxicity in L1210 Murine leukemia cells. The comparison of the cytotoxicity induced by various derivatives indicates that substituents such as polymethylene spacer groups play a major role in their cellular uptake as well as their efficiency of generation of cytotoxic agents. The results of these investigations clearly demonstrate that these bifunctional systems, which are soluble in aqueous medium and exhibit efficient DNA binding and photoactivated DNA cleaving properties, can have potential applications in phototherapy.

Investigation of interactions of β-cyclodextrin (β–CD) with a few novel viologen linked acridine conjugates **1a-c** and **2a-c** containing rigid aromatic and flexible methylene spacer groups, respectively, is the subject matter of the fourth

Chapter. The dyads with *para*-tolyl **1a** and biphenyl **1c** spacer groups exhibited significantly decreased fluorescence quantum yields and lifetimes when complexed with β–CD, while negligible changes were observed for the *ortho*-isomer **1b**. In contrast, the dyads **2a-c** with flexible spacer units in the presence of β–CD showed spacer length dependent significantly increased fluorescence quantum yields and lifetimes. Association constants for the complexes formed between β–CD and various dyads have been calculated and the complexation was confirmed using competitive ligand displacement, circular dichroism (CD), cyclic voltammetry (CV), ^{1}H NMR and AFM techniques and further by AM1 calculations. The intramolecular electron transfer rates (k_{ET}) have been estimated and are found to increase by nearly 2-fold for the dyads with *para*-tolyl **1a** and biphenyl **1c** spacer groups when complexed with β–CD, whereas significantly decreased k_{ET} (ca. 15-fold for **2c**) were observed for the dyads with flexible spacer group. These results demonstrate that the complexation of donor-acceptor conjugates **1a** and **1c** with aromatic spacer group with β–CD leads to the unusual planarization of the conjugate resulting in enhanced electron transfer processes between the donor and acceptor moieties, while conformational unfolding of sandwich type of structure occurs in the dyads **2a-c** having flexible spacer groups.

Note: *The numbers of various compounds given here correspond to those given under the respective Chapters.*

Chapter 1

AN OVERVIEW ON PHOTOACTIVATED DNA CLEAVING AGENTS

1.1. Introduction

Design of small molecules that selectively recognize nucleic acids and induce strand scission in presence of light is an active area of research that has important biochemical and therapeutic applications.[1-3] While natural enzymes have been extremely useful in many applications, their large size and/or limited range of sequence-recognition capabilities prevent their general use. For example, type II restriction enzymes which cleave within or near specific recognition sites, usually require Mg^{2+} ions as cofactor. Moreover, efficient cleavage is only observed with DNA containing two or more recognition sites, suggesting that the active complex binds at two sites.[4,5] An application, which demands cleavage with a higher level of sequence selectivity or at single recognition site requires a new cleavage agent with expanded recognition features. Such shortcomings of natural nucleic acid cleaving agents provide opportunities for chemists to design novel chemotherapeutics targeted to DNA and in the development of probes useful in biology and medicine. In order for a single molecule to recognize and cleave both

strands of duplex DNA at a given site and to act as an artificial restriction enzyme, the cleaving agent must be either bifunctional or recyclable.

In this context, a large number of compounds have been reported in the literature, which have the ability to recognize and bind to specific sequences in DNA and are found to exhibit nucleolytic activity under physiological conditions (chemical nucleases) or upon photoactivation (photonucleases). Of these, photonucleases have been found to possess significant practical advantages over the reagents that cleave DNA under thermal conditions. This is because of the fact that the photonuclease activity can be triggered only when the light of the correct wavelength is employed. The ability to control light, in both spatial and temporal sense, would be advantageous for applications ranging from the time-resolved probing of various biochemical processes such as transcription and translation to therapeutic agents. In the light of these facts, we have undertaken the design, photophysical and photobiological aspects of a series of novel viologen linked pyrene conjugates, which can in principle bind to DNA efficiently and cleave DNA through photoinduced electron transfer mechanism. This Chapter deals with a brief description of DNA and DNA cleaving agents with particular emphasis on photoactivated DNA cleaving agents. Moreover, the detailed information on DNA cleaving agents and their applications in biology can be obtained from the recently published reviews.[1-3] The objectives of the present thesis are also briefly indicated in this Chapter.

1.2. Structure of DNA

The primary structure of DNA has a string of nucleosides each joined to its two neighbours through phosphodiester linkages as shown in Figure 1.1A.[6,7] Each

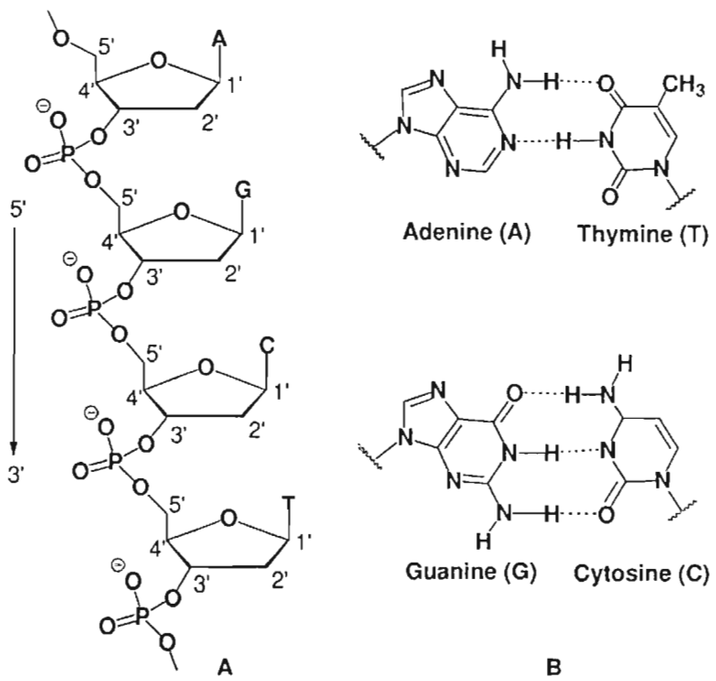

Figure 1.1. (**A**) Schematic representation of the primary structure of DNA and (**B**) Watson-Crick base pairing of adenine-thymine (A-T) and guanine-cytosine (G-C).

regular 5'-hydroxyl group is linked through a phosphate to a 3'-hydroxyl group and the uniqueness of any primary structure depends only on the sequence of bases present in its chain. DNA secondary structure consists of two chains, which run in opposite directions (anti-parallel) and are coiled around each other to form a double helix. These two chains are linked together by a large number of weak

hydrogen bonds formed between the complementary bases (Figure 1.1B). The complementary base pairs in the case of DNA are adenine-thymine and guanine-cytosine. The bases, which are hydrophobic and paired by hydrogen bonding lie inside and perpendicular to the helix axis, whereas the hydrophilic and negatively charged sugar-phosphate backbone face out into the aqueous medium. The double helical structure of DNA is stabilized by hydrogen bonding between the complementary base pairs and also by hydrophobic interactions between the stacked bases.

DNA adopts different secondary helical structures based on the environmental conditions such as humidity and salt concentration. A-DNA and B-DNA are the predominant DNA secondary structures (Figure 1.2) with right

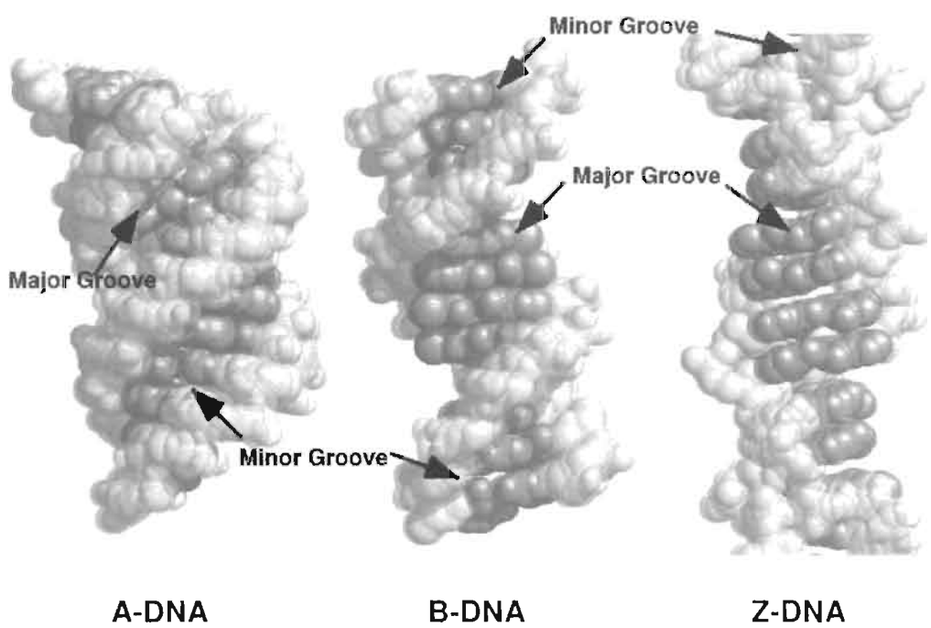

Figure 1.2. The structures of various forms of duplex DNA.

handed double helices and Watson-Crick base pairing, whereas Z-DNA is a left handed double helical structure that is stabilized by high concentrations of $MgCl_2$ and NaCl.[8] Only B-DNA is the one that exists under physiological pH conditions, while A-DNA exists under dehydrated conditions. Table 1.1 summarizes the properties of these three morphological forms of DNA.

Table 1.1. Characteristics of A, B and Z forms of DNA.

Property	A	B	Z
Relative humidity (%)	75	92	66
Pitch (Å)	28	34	31
Residues per turn	11	10	9.3
Inclination of base pair from horizontal	20°	0°	6°
Sugar ring conformation	C3'endo	C2'endo	
Base conformation (rotated relative to sugar)	anti	anti	syn
Major groove	Fully hidden	Accessible (10 Å in width)	Accessible
Minor groove	Accessible	Accessible	Fully hidden

Figures 1.3A and 1.3B represent the secondary structure of B-DNA extrapolated from the crystal structure of stacked decamer of a sequence of d(CCAACGTTGG).[8a] The B-DNA structure shown in Figure 1.3B has 10 base pairs per turn with little tilting of bases. The wide major groove and narrow minor groove are of moderate depth and hence both these grooves are well solvated by

water molecules. Another promising feature of B-DNA is that its structure is sufficiently flexible to permit a conformational response in the backbone to particular base sequences.

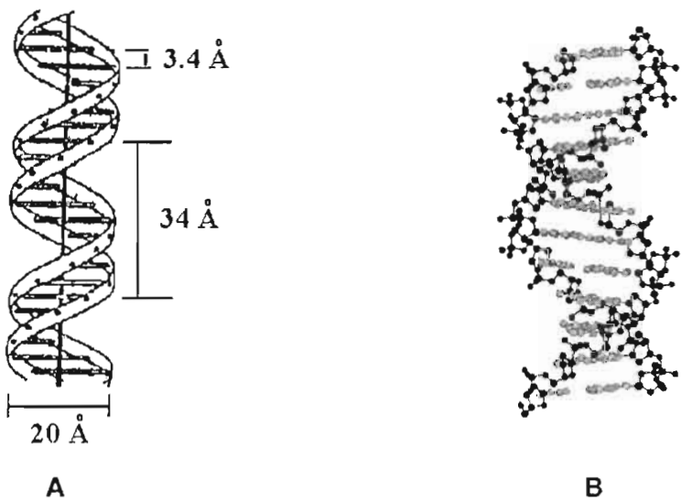

Figure 1.3. (**A**) Double helix model for the B-form of DNA and (**B**) twelve base pairs of B-DNA extrapolated from the crystal structure of stacked decamer of sequence d(CCAACGTTGG).

1.3. Ligand-DNA Interactions

DNA secondary structure possesses a variety of sites for the ligands to interact including the sugar-phosphate backbone, the central base core and the major and minor grooves. Figure 1.4 schematically represents the possible sites of ligand binding to B-DNA structure. The DNA structure by itself is stabilized by a 'spine of hydration' on the grooves and stacked cations around the anionic sugar-phosphate backbone. Therefore, there exist a number of possible pathways for the

ligands to interact with DNA through either covalent or non-covalent interactions. Although, DNA can be modified without any specific interactions with ligand, the selectivity and efficiency of modification is marginal for such ligands. This Chapter presents mainly photocleaving agents, which bind to DNA through non-covalent interactions (reversible interactions). Moreover, the important examples of

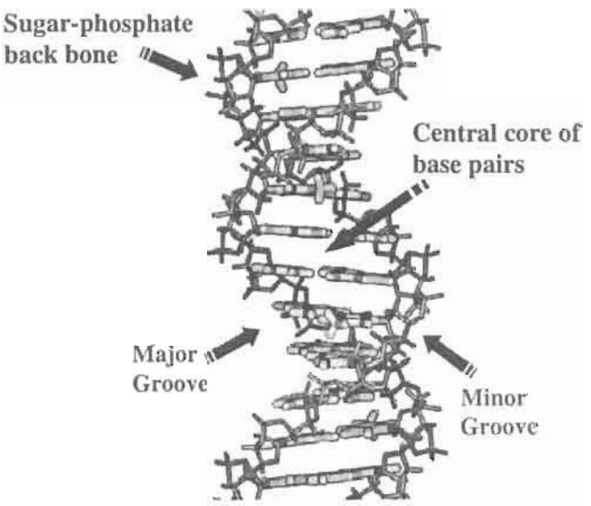

Figure 1.4. Schematic representation of B-DNA and probable ligand-binding sites.

molecules that cleave DNA without any specific interactions as well as covalent interactions can be obtained from the published reviews.[9,10]

1.4. DNA Cleaving Agents

Cellular DNA is by no means inert, stable structure holding genetic information in dead storage. It continually suffers assault from exogenous and endogenous agents, which result in a wide variety of modifications. These include

base modifications, abasic sites, strand breaks and DNA protein cross links.[11] When these lesions escape repair by cellular mechanisms, they lead to mutagenesis, carcinogenesis, aging and cell death.[12] While cleavage of DNA is generally considered to be deleterious, synthetic DNA cleaving agents have been developed in recent years that have been extremely useful in the treatment of diseases and also as probes for understanding DNA-protein interactions and macromolecular structure.[1-4] Hydrolysis of phosphodiester bonds and oxidation of sugar and nucleobases can cause DNA cleavage. Most enzymatic nucleases (e.g. repair enzymes) cleave DNA by the hydrolysis of phosphodiester bonds, whereas the synthetic reagents typically involve an initial oxidation reaction of either sugar or nucleobase, which indirectly results in phosphodiester cleavage. This chapter deals with a brief description on small and hybrid molecules that can cleave DNA upon photoexcitation.

1.5. Photoactivated DNA Cleaving Agents

Photonucleases are those compounds that react directly with the nucleic acids while in an electronically excited state and cause an immediate scission of the nucleic acid chain. In the strictest sense, the cleaving agent should not be consumed in the process, permitting it to react catalytically with the nucleic acid, similar to the reaction of enzymes. But in reality, only very few compounds meet this criteria. Thus photonucleases can be referred to as those compounds, whose excited states can initiate a series of chemical reactions, which ultimately lead to

nucleic acid cleavage. One appealing aspect of the photoactivated cleaving agent is that it allows the reaction to be controlled spatially and temporally by combining all the components of the reaction mixture before the irradiation. Excitation of the reaction mixture with an appropriate light source initiates the reaction, which continues until the light is shut off. Several types of photoactive compounds are reported in the literature,[1a,5] but very few compounds cleave DNA catalytically. Hence majority of these compounds can be referred to as "photoactivated DNA cleaving agents," and are defined as those compounds whose excited states can initiate a series of chemical reactions, which ultimately lead to the nucleic acid cleavage. The ability to control light, in both spatial and temporal sense, would be advantageous for applications such as the time-resolved probing of various biochemical processes. These include transcription or translation, to therapeutic agents, which are activated under in vivo conditions by laser sources coupled into the body through fiber optics. Perhaps the most important feature of these reagents is the fact that light can be a very selective cofactor in a chemical reaction. Moreover, if the photocleaver is sensitive to light at wavelengths longer than 360 nm, selective excitation of the photocleavage agent is possible. This is critical in limiting the number of side reactions in the system as well as in analyzing the reaction mechanisms.

The mechanisms of DNA cleavage through photosensitization can be broadly classified into (i) by generation of diffusible (singlet oxygen) and non-diffusible (hydroxyl radicals) reactive intermediates, (ii) hydrogen atom

abstraction and (iii) electron transfer mechanism. The energy transfer from the excited state of photosensitizer to the ground state of triplet molecular oxygen can yield singlet oxygen. Hydroxyl radical intermediates, on the other hand, can be generated by direct homolysis of the peroxide bond in the excited state of the substrate or by an energy/electron transfer mediated heterolytic cleavage. Alternatively, photosensitizers can also initiate formation of hydroxyl radicals by electron transfer to superoxide radical anion to yield hydrogen peroxide, which can in turn generate hydroxyl radicals through Fenton reaction.[13]

Photosensitizers can also initiate hydrogen atom abstraction by mechanisms not involving hydroxyl radicals. Many n,π^* excited states of photosensitizers readily abstract hydrogen atoms, and radicals derived from them are capable of hydrogen atom abstraction from the deoxyribose sugar.[2b] In the case of electron transfer mechanism, the first step in DNA cleavage involves the oxidation of nucleobases by the excited state of the photosensitizer. The free energy for electron transfer from a nucleic acid base to an excited state sensitizer will depend on the oxidation potential of the ground state base and the reduction potential and excited state energy of the sensitizer. Of all the nucleobases, guanine has the lowest oxidation potential,[14] and hence guanine is implicated as the base in an electron transfer mechanism in DNA.

A variety of compounds, from ketones to organometallic complexes to polycyclic heteroaromatic drugs have been reported in the literature, which photosensitize the cleavage of DNA. Some of these involve direct reaction of an

excited state of the photosensitizer or its radical with the nucleic acids, while others generate intermediates such as singlet oxygen or hydroxyl radical. Some photosensitizers initiate photocleavage by more than one mechanism. Here we present salient features of some selected photoactivated cleaving agents, which cleave DNA through different mechanisms. For convenience, these compounds have been divided into two groups on the basis of their likely sites of reactivity in DNA, namely, sugar or nucleobase.

1.5.1. Photoactivated Cleaving Agents Selective for Oxidation of Sugar Moiety in DNA

Oxidation of deoxyribose due to hydrogen atom abstraction from the sugar furanose is quite often the key step in DNA cleavage. The resulting sugar radicals can decompose by a variety of pathways to yield small molecules and DNA fragments.[2b] Since identical deoxyribose residues are found at every step along the DNA duplex, the cleavage by hydrogen abstraction is inherently non-selective with respect to the sequence. The sequence selectivity depends on the local structure of the DNA and the physicochemical properties of the hydrogen abstracting sensitizer. The ability to alter the sequence selectivity of cleavage by varying the structure of the photocleavage agent is a key component in the design of new DNA cleavage agents. Therefore, this section deals with the reagents, which cleave DNA by the oxidation of sugar moiety.

1.5.1.1. DNA Photocleavage Induced by Metal Complexes

The first DNA photocleaving agent based on uranyl ion (UO_2^{2+}) was introduced by Nielsen and co-workers in 1988.[15] The photoactivated uranyl salts were found to spontaneously cleave both supercoiled and linear DNA targets resulting in nicks in the DNA. Mechanistic studies indicated that the cleavage occurs through abstraction of a hydrogen atom. The intact nucleobases are observed as byproducts of the photocleavage and the quantum yield for their production ($\sim 10^{-4}$) matches the quantum yield for plasmid nicking, consistent with a mechanism in which the damage is targeted to the sugar and not the nucleobase. UO_2^{2+} binds to the DNA by coordinating with phosphate backbone across the minor groove with an affinity of the order of $10^{10}\ M^{-1}$, making it a valuable probe of local structure. Subsequently, the uranyl salts have been successfully employed as photofootprinting agents to probe a wide variety of nucleic acid structures and protein-nucleic acid complexes including imaging of DNA triplexes and gene expression regulator/DNA complexes.[16] The uranyl salts are the most useful photocleavage agents developed so far, however, there are a few disadvantages associated with these salts. One of the drawbacks of these salts is that they need either neutral or acidic pH, otherwise uranyl ion forms insoluble uranyl hydroxide aggregates, which makes it inefficient in cleaving DNA.

Biological applications of rhodium complexes, such as DNA and RNA photocleavage, have been extensively reviewed.[1a] Photocleavage of DNA by

rhodium (II) complexes (Chart 1.1) containing the phi ligand (phi = 9,10-phenanthrenequinone diimine) (**1**) has been studied by Barton and co-workers.[17,18] Irradiation of solutions containing Rh(phi) complexes in the presence

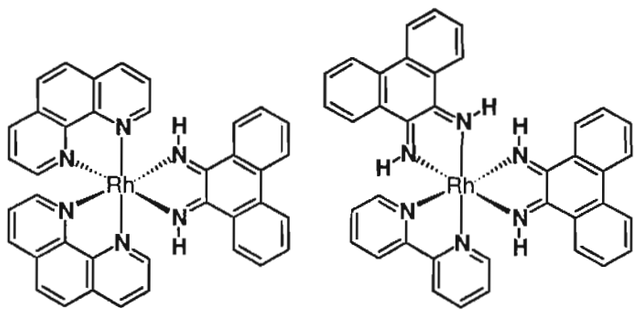

1 **2**

Chart 1.1

of DNA results in spontaneous cleavage. Analysis of the product mixture revealed the presence of free bases and base propenoic acids, while DNA fragments are terminated by 3'-phosphates. These products correspond to those expected from hydrogen abstraction from the 3'-carbon of the deoxyribose. The Rh(phi) complexes bind to B-form DNA through intercalation of the phi ligand from the major groove and the excited state of the complex abstracts a hydrogen atom from C-3' of sugar at the intercalation site.

It has also been reported that rhodium complexes with different ligands can generate complexes with varying selectivities for DNA. For example, the complex bis(phenanthrenequinone diimine)bipyridylrhodium(III) ($Rh(phi)_2(bpy)^{3+}$) (**2**, Chart 1.1) is a sequence neutral complex in its reactions with DNA. The role of ancillary (non-intercalating) ligands on the DNA cleavage by Rh(phi) complexes

is quite interesting.[18] For example, the Δ-isomer of $[Rh(en)_2phi]^{3+}$ (**3**, Chart 1.2) (en = ethylenediamine) cleaves DNA with high selectivity for 5'-GG-3' dinucleotide steps, whereas the Λ-isomer (**4**, Chart 1.2) exhibits cleavage at all sites, with some preference for A/T sites. Thus, the Rh(phi) complexes represent excellent examples of how the cleavage selectivity can be determined through the binding selectivity of the photocleaver. The ability to alter the cleavage selectivity by varying the ancillary ligands of the complexes provides control, unavailable in most other systems.

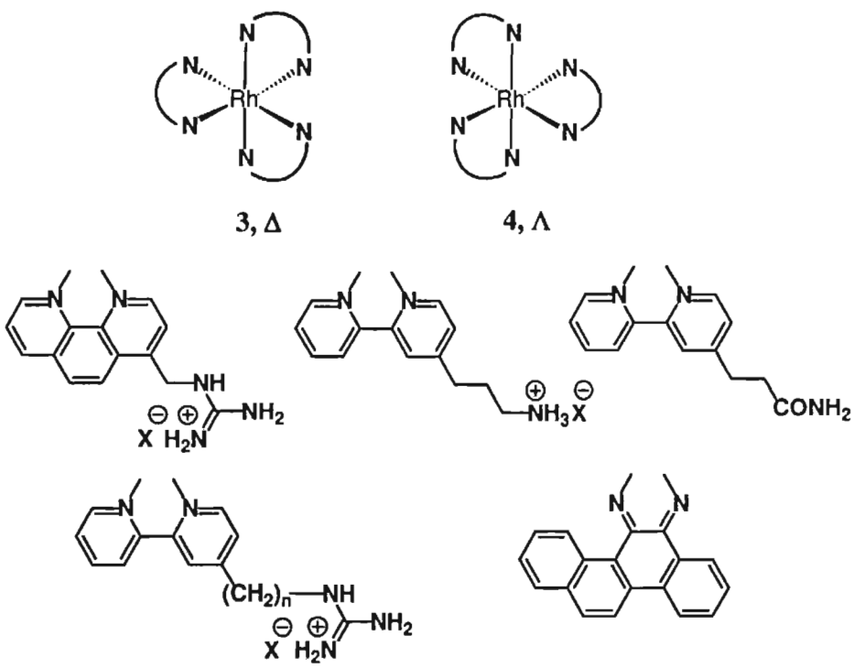

Chart 1.2

Bleomycin, a product of streptomyces fermentation, cleaves DNA via an iron-oxo intermediate and has played a heuristic role in our understanding of the

reactions of abiological coordination complexes. In 1982, Chang and Meares[19] have first reported the DNA cleavage by photoactivated cobalt(III)-bleomycin complex (**5**, Chart 1.3) and later Saito, Hecht and co-workers[20] have studied in detail through characterization of the Co(III)-BLM(Green) complex (**5**) and employing model systems. When the self-complementary dodecamer 5'-CGCTTTAAAGCG-3' was used as the target, selective cleavage was observed after alkali treatment at positions C-3 and C-11 and initiation of hydrogen abstraction from the C-4' of the deoxyribose moiety leading to the cleavage at

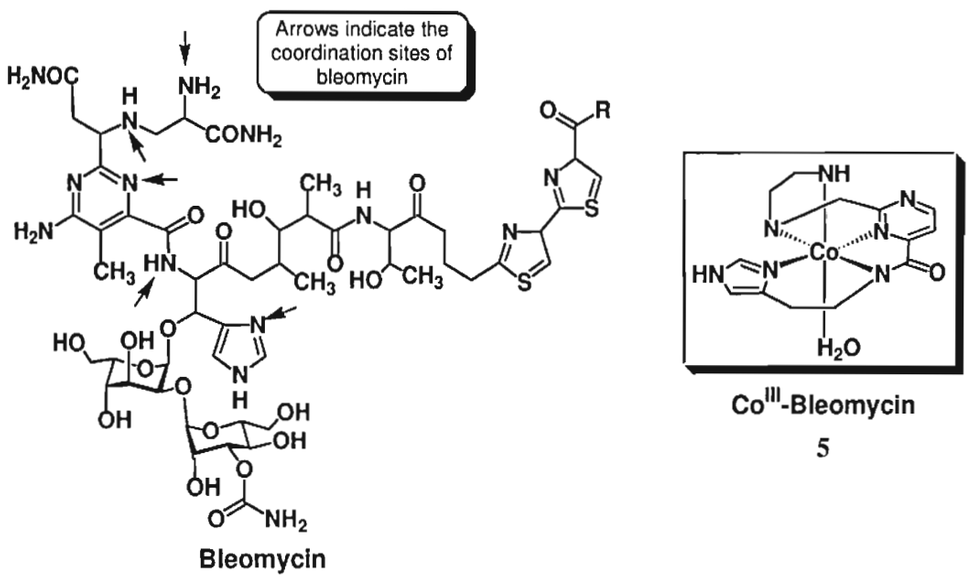

Chart 1.3

C-3 center. However, experimental details do not offer insights into the nature of oxidizing species nor for the mechanism of their function. Catalytic photocleavage of DNA by tetraanionic diplatinum complex, $Pt_2(pop)_4^{4-}$(pop = pyrophosphito) (**6**, Chart 1.4) has been studied by Thorp and co-workers.[21] The DNA fragments that

arise from the cleavage possess 3'-phosphate and 3'-phosphoglycolate as well as 5'-phosphate and 5'-aldehyde termini. This indicates that the cleavage by platinum complex is the result of hydrogen abstraction from both C-4' and C-5' of deoxyribose, respectively. Zaleski and co-workers[22] reported that bis(9-diazo-4,5-diazafluorene)copper (II) nitrate complex (**7**, Chart 1.4) cleaves DNA in the presence of visible light under anaerobic conditions and act as a transition metal kinamycin model. On the other hand, irradiation of the Fe(III) complex (**8**) in the

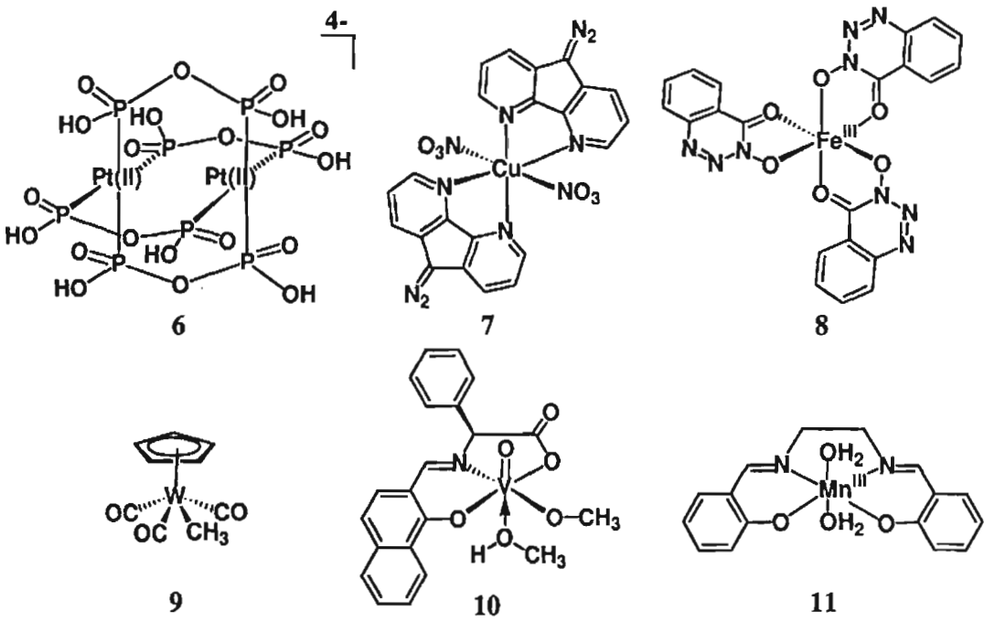

Chart 1.4

presence of plasmid DNA affords both single- and double-strand cleavage,[23] with significantly greater efficiency than photolysis of free ligand in threefold higher concentration. From a mechanistic perspective, detection of Fe(II) as a reaction product raises important questions concerning the mode of activation of the

kinamycins and 6-diazo-5-oxo-L-norleucine. However, ligand to metal charge transfer (LMCT) activated N_2 release from Fe(III) complex produces localized ligand radical intermediates capable of cleaving DNA and represents a new chemical approach for the design of photoactivated cleaving agents.

The photolysis of $CpW(CO)_3Me$ (**9**, Chart 1.4) has been shown to produce methyl radicals and to cleave DNA in a single-stranded manner. The experimental evidence suggests the involvement of carbon-centered radical in this process.[24] In this work, the mechanism of strand scission was determined to occur by hydrogen atom abstraction from the 4′- and 5′-positions of the deoxyribose moiety of the backbone of DNA. Additionally, in a side reaction that does not lead to frank strand scission, all four bases of DNA are methylated under these conditions; however, none of these bases or backbone modifications lead to the formation of abasic sites.

Chen and co-workers[25] have reported that vanadyl (V) complexes serve as efficient reagents for cleaving supercoiled plasmid DNA by photoinitiation. Complex (**10**, Chart 1.4), derived from 2-hydroxy-1-naphthaldehyde and L-phenylalanine, exhibits a unique wedge feature, inducing a site-selective photocleavage at the C22-T23 of the bulge backbone for a HIV-27 DNA system at 0.1-5 μM. Transient absorption experiments indicate the involvement of ligand to metal charge transfer (LMCT) with concomitant tautomerization. This results in the formation of an *ortho*-quinone-methide V-bound hydroxyl species, which is found to be responsible for the cleavage profiles. Fujii and co-workers[26] reported

photoinduced cleavage of DNA by a cationic Schiff base complex of manganese (**11**, Chart 1.4). The cationic complex effectively cleaved T-site of DNA in ca. 88% selectivity upon visible light irradiation. The high selectivity observed for the cationic complex suggests that the cationic organic radical formed by photolysis of **11** selectively attacks thymine or thymidine, thereby cleaving DNA at the T site.

1.5.1.2. DNA Photocleavage Induced by Organic Compounds

Several photoactivated organic compounds have been found to cause the sugar oxidation followed by DNA cleavage either by hydrogen abstraction in the excited state or they generate free radicals and hydroxyl radicals *in situ*, which in turn abstract hydrogen atom from the deoxyribose. These include enediyenes (**12** and **13**),[27] nitroaromatics, triazoles (**14**), anthraquinones (**15** and **16**), flavin-oligopyrroles, halogenated bithiazoles, N-hydroxypyridones (**20**), hydroperoxides, (**18** and **21**) etc (Charts 1.5 and 1.6). This section deals with salient features of some of these compounds.

Enediyne antitumor antibiotics are natural products and are believed to destroy cancer cells by damaging DNA. These compounds bind to DNA in the minor groove and, upon activation, undergo rearrangements to produce diradicals.[2b,27] These are potent DNA cleavage agents, capable of producing single and double strand breaks, suggesting their use in a variety of diagnostic and therapeutic applications. Compounds that are active and involve diradical intermediates *in situ* include neocarzinostatin, esperamicin A1, dynemicin A,

C1027 (**12**), calicheamicin etc.[2b] These compounds are normally activated by reduction, but irradiation also leads to the cleavage of supercoiled DNA.

Due to the structural complexity of the natural enediynes, a large number of simplified model compounds designed to generate diradicals have been studied as photocleavers. Goldberg and co-workers[28] have demonstrated that the enediyne antibiotic C1027 (**12**, Chart 1.5) produces sequence specific covalent DNA drug

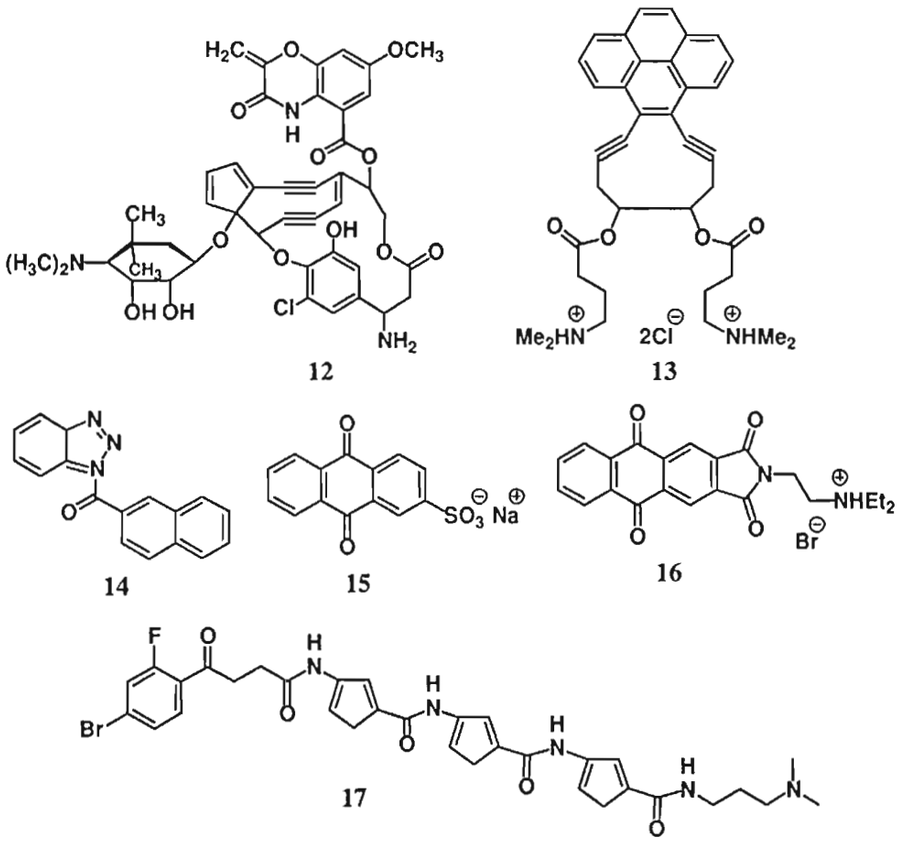

Chart 1.5

adducts and DNA interstrand cross-links under anaerobic conditions. After binding to DNA by intercalation, the enediyne core of C1027 (**12**) chromophore

rearranges to the 3,6-diradical form. The diradical is positioned in such a way that one of the radicals abstracts a hydrogen atom from C-4' position of the A1 nucleotide (A = adenine) and the other radical, from either C-1' of A2 or C-5' of A3, ultimately leading to DNA cleavage.

Wender and co-workers[29] used a similar strategy in developing a series of triazole compounds as new photocleavers. Irradiation of triazole (**14**, Chart 1.5) in presence of ethanol led to formation of hydrogen abstraction products, consistent with diradical intermediates. The triazoles photonick plasmid DNA and radiolabelled restriction fragments spontaneously. It was found that there is some preference for cleavage at GG sites as observed for many photocleavers that react with DNA nucleobases by electron transfer. However, the spontaneous nature of the cleavage and a distinct preference for cleavage at 3'-G of the GG steps by the triazoles argues against cleavage by an electron transfer pathway.

Schuster and co-workers[30] showed that anthraquinones (AQ) photocleave DNA by three distinct pathways, which are differentiated by the binding mode of the AQ as well as the composition of the buffer (Chart 1.5). One mechanism involves an electron transfer from the DNA nucleobases to an intercalated AQ and the other two pathways involve hydrogen atom abstraction from deoxyribose.[31] Anthraquinones possessing electron withdrawing substituents are capable of oxidizing organic substrates by hydrogen atom abstraction, since the excited singlet state of these molecules is n-π^* in character. AQ derivatives (**15** and **16**, Chart 1.5) intercalate into DNA and cleave DNA through hydrogen abstraction.

However, if the AQ is present in excess relative to intercalation sites, spontaneous sequence-neutral cleavage of the DNA results.[30]

The preferential binding of monosubstituted AQ derivatives to DNA by intercalation limits their ability to abstract hydrogen atoms from deoxyribose due to rapid electron transfer from the nucleobases, which form the intercalation site, requiring saturation of the intercalation sites before H-abstraction by non-intercalated AQ can occur. However, AQ, (**15** and **16**, Chart 1.5), binds to DNA in one of the grooves or by electrostatic association with the backbone phosphates.[31] It has been observed that mode of their interaction has profound effect on the photochemical reaction with DNA. Laser studies of AQ derivatives **15** and **16** showed that rates of electron transfer from the nucleobases to AQ decreased by ca. 50-fold when compared to AQ bound through intercalative mode. Spontaneous sequence-neutral cleavage occurs even when AQ is present at non-saturating concentrations. Thus, it can be concluded that mode of binding in DNA can play a vital role in the cleavage mechanism of photocleavage agents.

In addition, Nielsen and co-workers[32] reported the photocleavage activity of a series of acridine-linked nitrobenzamides and Shibuya and colleagues[33] have demonstrated the photoactivity of nitro substituted oligopyrroles, which mimic the chemistry of netropsin. Recently, Saito and co-workers[34] reported the DNA photocleavage properties of a family of nitro-substituted naphthalimide derivatives. The authors propose that the oxidation reaction is due to photoinduced hydrogen abstraction from the methyl of the thymine by the excited state nitro

group. In summary, the nitro-substituted compounds are capable of cleaving DNA photochemically and that the nitro group likely abstracts hydrogen atoms from the deoxyribose, leading to spontaneous cleavage, or from the thymine methyl group, resulting in piperidine-dependent T-selective cleavage. Jeon and co-workers[35] report that the 4'-bromo-2'-fluoroacetophenone (**17**, Chart 1.5) and 2'-bromo-4'-fluoroacetophenone derivatives upon irradiation function as DNA cleaving agents putatively through the generation and reaction of phenyl radicals. 2'-Bromo-4'-fluoroacetophenones revealed higher DNA cleaving activity than 4'-bromo-2'-fluoroacetophenone derivatives, supposedly induced by the higher reactivity of the phenyl radical generated from 2'-bromo-4'-fluoroacetophenones. The attachment of a minor groove binding moiety to bromofluoroacetophenone results in increased strand scission of DNA mainly in sequence selective manner.

1.5.1.3. DNA Cleavage Induced by Hydroxyl Radical Generators

One of the well known DNA cleaving agents is the hydroxyl radical, which abstracts hydrogen atom from deoxyribose to give sugar radicals.[2b] Several methods exist for production of hydroxyl radicals, the simplest of which involves irradiation of hydrogen peroxide with UV light, leading to O-O bond homolysis. MacGregor showed that[36] irradiation of 100 mM H_2O_2 in the presence of DNA results in spontaneous, sequence-neutral cleavage of DNA. Saito and co-workers[37] reported the production of hydroxyl radicals by the irradiation of naphthalenediimide hydroperoxide (**18**, Chart 1.6) and characterized the

hydroxyl radicals by DMPO trapping and ESR spectroscopic studies. Further, photonicking of supercoiled plasmid DNA by this hydroperoxide was found to be inhibited by 1 mM sodium benzoate, consistent with hydroxyl radical mediated cleavage mechanism. When the cleavage selectivity was studied with radiolabelled restriction fragments, damage was found to occur with higher selectivity at 5'-G of GG sites and required piperidine treatment. This observation with the restricted fragment is inconsistent with the hydroxyl radical mediated damage, unless the compounds bind to DNA sequence selectively.

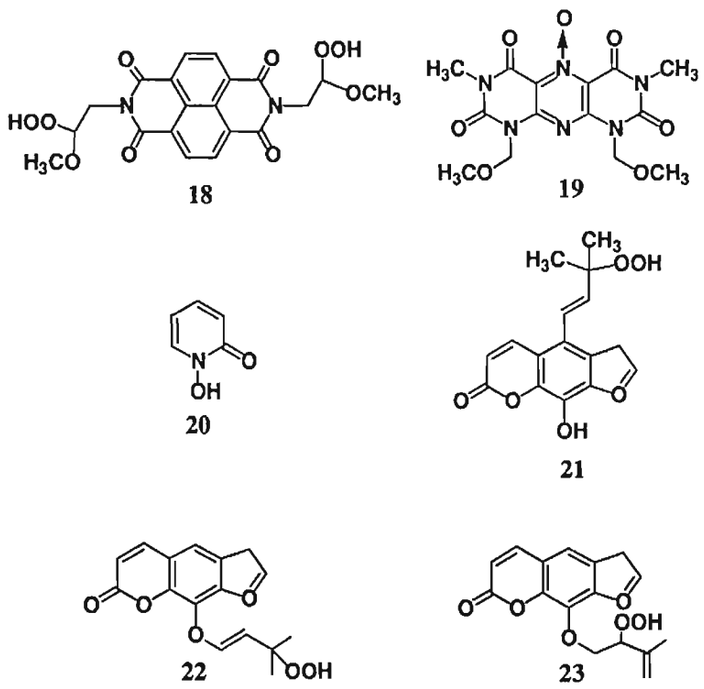

Chart 1.6

Other compounds that are known to produce hydroxyl radicals are the heterocyclic N-oxide derivatives[38] (**19**), N-hydroxypyridones (**20**) and

furocoumarin hydroperoxides (**21-23**) (Chart 1.6).[39] For example, irradiation of N-oxide in water results in the production of 2 equivalents of hydroxyl radicals per N-oxide precursor, but radicals are not produced if the irradiation is performed in acetonitrile. The N-oxide (**19**) was able to photonick plasmid DNA in a process that could be inhibited by the radical scavenger DMSO. However, production of hydroxyl radicals in the presence of DNA was not demonstrated. Furocoumarin hydroperoxide (Chart 1.6) (**21**) upon photoactivation with UV light, cleave plasmid DNA by *in situ* generation of hydroxyl radicals.[39] The analysis of DNA damage by employing various endonucleases indicated that the damage profiles are similar to that of γ–radiation induced damage. The damage was inhibited by hydroxyl radical quenchers such as *tert*-butanol and DMSO and the involvement of hydroxyl radicals in these reactions was further confirmed by isolation of products and also by trapping with phenol, adamantane and DMPO.[40]

An alternative source of hydroxyl radicals is through superoxide dismutase reaction, producing hydrogen peroxide and oxygen (eq 1.1). The hydrogen peroxide then can undergo homolysis in the presence of UV light or after

$$2O_2^{\bullet -} + 2H^+ \longrightarrow H_2O_2 + 2O_2 \qquad (1.1)$$

reduction by metal ions (Fenton reaction)[13] to produce hydroxyl radicals. Thus, any agent that is capable of reducing oxygen to superoxide can produce hydroxyl radicals and the radical of transient metals.[41] There are many examples of natural compounds[42] which photocleave DNA by processes which are partially inhibited

by radical scavangers. These photocleavers are also susceptible to inhibition by the enzyme catalase, which decomposes hydrogen peroxide to water and oxygen. Superoxide dismutase (SOD) detects superoxide in the reaction by catalysing the reaction indicated in the equation 1.1 *i.e.* hydrogen peroxide production can be faster in the presence of SOD than in its absence. Thus, inhibition of DNA cleavage by SOD without catalase means that superoxide plays a significant and complex role in the cleavage mechanism than serving as a precursor to hydrogen peroxide.

1.5.2. Photoactivated Cleaving Agents Selective for Oxidation of Nucleobases in DNA

Cleavage of DNA strand as a result of chemical reactions initially occurring on the nucleobase usually requires a second reaction step such as heat, alkali, or enzymatic treatment to effect strand scission.[2c] Hence, compounds that react with the nucleobases of DNA will not be inducing spontaneous cleavage in comparison with systems that react with sugar residues. This class of photocleavage agents function by three distinct processes: (i) direct electron transfer from the nucleobase to the excited state of the photocleaver; (ii) triplet energy transfer from the excited photocleaver to molecular oxygen producing singlet oxygen, which then reacts with nucleobases and (iii) formation of an adduct with the nucleobase. Figure 1.5 shows the reaction of a nucleobase, for example, guanine with singlet oxygen, hydroxyl radicals and ionizing radiation/electron acceptors. Hydroxyl

radicals ($HO^{\bullet}$) are very short lived and react with sugar and nucleobases. The oxidation potentials and reactivities of the four nucleobases vary over a wide range, with guanine being the most easily oxidized as well as the most reactive towards singlet oxygen.[12,43] The adduct formation on the other hand occurs with

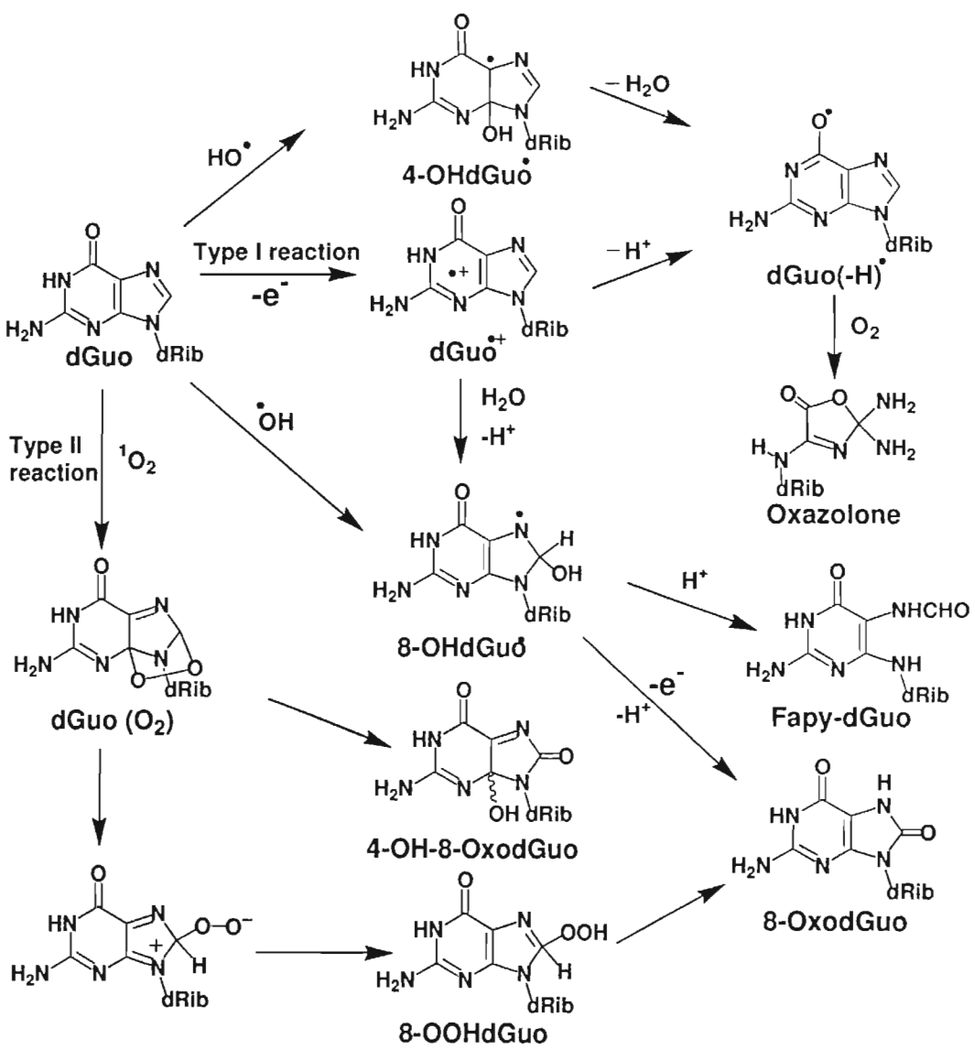

Figure 1.5. Structures and general scheme for oxidative modification of deoxyguanosine (dGuo) through different mechanisms.

different selectivities, depending on the reaction mechanism. With nucleobases they add to the double bond thereby generating piperidine dependent cleavage sites. Superoxide radical anion formed *in situ* by electron transfer mechanisms does not react directly with DNA to produce damage, but reacts through an iron-catalyzed process to yield hydroxyl radicals (Fenton reaction).[13]

1.5.2.1. Singlet Oxygen Generators

Electronically excited compounds that undergo efficient intersystem crossing to the triplet state and have sufficiently high triplet energy can generate singlet oxygen by energy transfer to molecular oxygen. Singlet oxygen is a highly reactive species that preferentially adds to guanine.[43,44] The resulting oxidized guanine is sensitive to piperidine treatment which induces a strand scission.[33] Performing experiments in D_2O rather than in H_2O can lead to a substantial increase in the cleavage efficiency since the lifetime of singlet oxygen is significantly longer in D_2O as compared to H_2O.[45]

Numerous systems have been reported to cleave DNA involving singlet oxygen mechanism. These include dioxetanes (**24**),[46] porphyrins (**25** and **26**),[47] fullerenes,[48] psoralens (**27**)[49] and ruthenium complexes (Chart 1.7). Adam and co-workers[46] demonstrated that dioxetanes (**24**), particularly, 3-(hydroxymethyl)-3,4,4-trimethyl-1,2-dioxetane (HTMD), is an efficient photooxidant of 2'-deoxyguanosine (dGuo) on thermal activation in dark. These molecules constitute excellent chemical tools to study photobiological processes without the use of light. The HTMD on thermal

activation generates triplet excited state of ketones, which *in situ* produces singlet oxygen through energy transfer. Singlet oxygen then reacts with dGuo to give the typical type II photooxidation products such as 8-oxodGuo and 4-OH-8-oxodGuo (Figure 1.5). A 3-fold increment in 8-oxodGuo product formation was observed in D_2O when compared to water indicating thereby the involvement of singlet

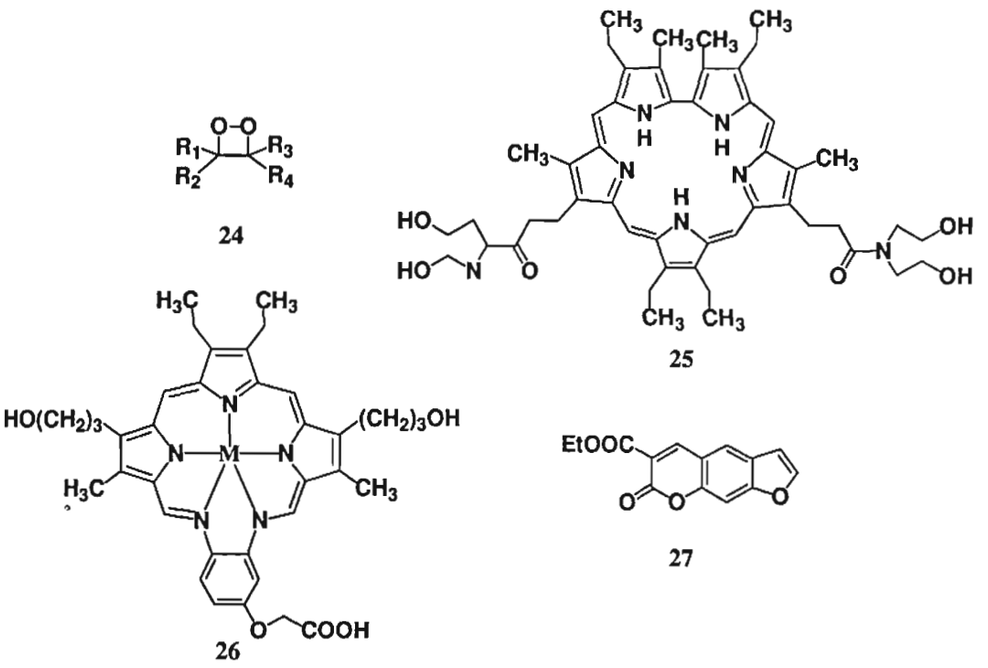

Chart 1.7

oxygen in these reactions. By employing 1,2-dioxetanes as chemical source for electronically excited ketones ("*photobiology without light*"), numerous studies have been carried to explore the biological importance of these molecules.

Porphyrins are well known singlet oxygen generators and cleave DNA selectively at guanine residues.[47] Magda, Sessler and co-workers[48] reported the photocleavage activity of several expanded porphyrins (**25** and **26**, Chart 1.7).

These compounds were found to initiate photonicking of supercoiled plasmid DNA upon irradiation at wavelengths above 700 nm. Sodium azide strongly inhibited the cleavage, which is indicative of a singlet oxygen mechanism in these reactions. The significance of this work lies in the use of long wavelength of irradiation, which is essential for *in vivo* photodynamic therapy applications. Porphyrins can also be used to probe nonduplex structures in nucleic acids. Tetracationic porphyrins[50] (Chart 1.7) for example, were found to bind with high selectivity at a DNA three way junction, then initiate photocleavage at guanine residues adjacent to the junction.

Helene and co-workers[51] demonstrated that irradiation of 3-carbethoxy-psoralen (**27**) in the presence of DNA and followed by piperidine treatment resulted in selective cleavage at GG sites with modest preference for 5'-G. When the experiments were carried out in D_2O, an enhancement in cleavage yield was observed, suggesting the involvement of singlet oxygen. Thus, while the cleavage pattern was inconsistent with a singlet oxygen process, the mechanistic experiments were. Detailed studies indicated that both singlet oxygen and electron transfer pathways were operative in the case of 3-carbethoxypsoralene.

1.5.2.2. DNA Photocleavage Through Electron Transfer Mechanism

Recently, a number of small molecules that oxidize DNA by photoinduced electron transfer mechanism have been reported. The most important systems include ethidium bromide (**28**), riboflavin[52] (**29**), naphthalimides and

anthraquinone derivatives (**30**)[30,31] (Chart 1.8). A unique feature of the cleavage induced by these systems is that it predominates at the 5'G of the GG step with a ratio of approximately 5:1. Oxidation of guanine by an excited state photocleaver (P) produces the G-radical cation and the P radical anion as shown in equation 1.2.

$$P^{*} + G \longrightarrow P^{\bullet -} + G^{\bullet +} \qquad (1.2)$$

The subsequent reactivity of $G^{\bullet +}$ is complex and highly dependent on the secondary structure of the DNA, leading to both 8-OxodG and oxazolone decomposition products (Figure 1.5).[53,54] 8-OxodG is detected in conjunction with photocleavage at G by electron transfer agents, but Cullis and co-workers questioned whether this lesion is the one which is actually cleaved by piperidine treatment or is merely incidental.[55] Photocleavage of B-form DNA by electron-transfer agents is highly selective for guanines but can be distinguished from that of singlet oxygen based on the difference in the efficiency of cleavage at different G sites. In particular, guanines located on the 5'-side of at least one other G are strongly preferred over all other cleavage sites. Kawanishi and co-workers reported that irradiation of riboflavin (**29**) (Chart 1.8) with UV light in the presence of DNA led to piperidine dependent cleavage at the 5'-G of GG steps.[52] 8-OxodG was detected as a byproduct of the chemistry. An electron transfer mechanism was suggested but the 5'-preference for the cleavage could not be explained.

Saito and co-workers[56] performed mechanistic experiments for understanding the factors leading to cleavage at GG sites and particularly preference for the cleavage at the 5'-G of the GG steps. The quantum yield for cleavage of the hexamer duplex 5'-TTGGTA-3'.5'-TACCAA-3' by lysine-naphthalimide was determined to be 3 x 10^{-4} with a 8:2 preference for the 5'-G.

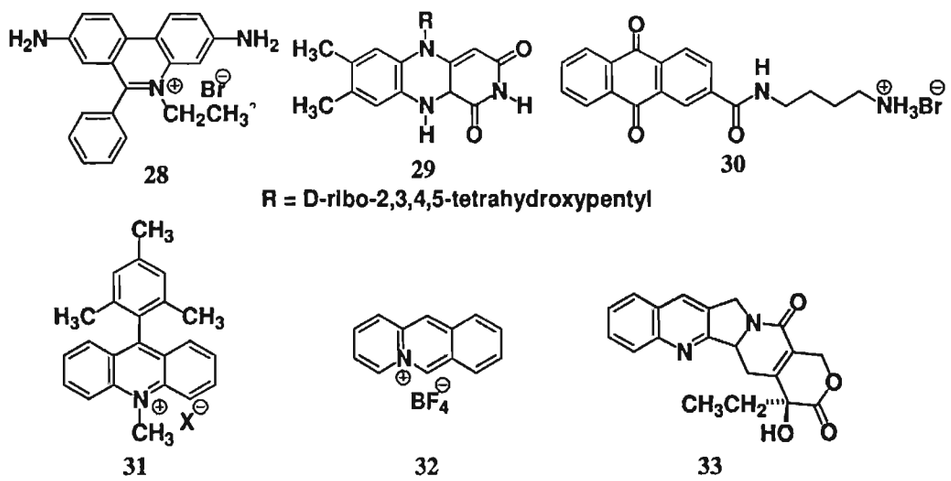

Chart 1.8

Laser experiments demonstrated the production of imide radical anion with the same microsecond time scale kinetics as quenching of the imide triplet state, providing evidence for a photoinduced electron transfer reaction. *Ab initio* calculations have been used to explain the intriguing selectivity for cleavage at GG steps by electron transfer agents. Results of calculations of all 10 of the possible stacked base paired dinucleotide steps revealed that GG steps were by far the most easily oxidized of the 10 and that the highest occupied molecular orbital (HOMO) for GG was localized almost exclusively on the 5'-G, both in the neutral and radical cation forms.

Schuster and co-workers[30] reported that the anthraquinone derivative (**15**) (Chart 1.5) cleaves DNA exclusively through electron transfer mechanism. In addition to other experimental evidence, they have made use of laser spectroscopy to understand the mechanism. AQ in the presence of DNA produced a radical anion of **30** by electron transfer from a nucleobase within 20 ps after excitation with a laser pulse, effectively precluding reaction by other pathways. This radical anion subsequently decayed by approximately 30% over the next 100-200 ps and is then stable for several microseconds, until it transfers an electron to oxygen, thereby producing superoxide radical anion and recycling of AQ.

One of the key components to successful cleavage of DNA by an electron transfer mechanism is inhibiting the exergonic back electron transfer.[5a,57] To circumvent the back electron transfer, Kochevar and co-workers[58] have adopted a co-sensitizer approach. The photosensitization involving the co-sensitizer that is bound far away from the sensitizer is expected to inhibit the back electron transfer and thereby increase the DNA modifications. For example, ethidium bromide (**28**, Chart 1.8), which is a very good intercalator and viologen, a groove binder were simultaneously bound to duplex and then irradiated with visible light to selectively excite ethidium bromide. Ethidium chromophore does not react appreciably with DNA by electron transfer, but it can be oxidized by the surface bound viologen producing the ethidium radical cation and the viologen radical cation. The oxidized ethidium can then accept an electron from one of the nucleobases in DNA, retarding back electron transfer. Meanwhile, the reduced viologen can give

the electron to oxygen, further separating the hole from the electron. This process led to the G-selective cleavage of duplex DNA. Recently, Fukuzumi and co-workers[59] reported the direct detection of nucleotide radical cations through the photoinduced electron-transfer mediated oxidation of DNA bases by charge-separated state of 9-mesityl-10-methylacridinium ion, resulting in efficient DNA cleavage in the absence of oxygen.

Ihmels and co-workers investigated various photoprocesses of the photoactivated acridizinium salts (**32**) in the presence of DNA and evaluated their relevance for the subsequent DNA damage. Under aerobic conditions, triplet sensitization leads to formation of $^1O_2$, which causes oxidative base modifications in DNA. Under anaerobic conditions, an electron transfer reaction predominates resulting in hydroxyl radicals, which abstract hydrogen atoms from the DNA backbone and induces a direct strand cleavage. It has also been observed that the intercalated acridizinium salt undergoes initially photoinduced electron transfer reaction with the DNA bases; however, due to the fast back electron transfer processes, the contribution from the excited state of the intercalated dye was found to be negligible to the overall DNA damage induced by this system. Camptothecin (CPT) (**33**) is an anticancer drug that inhibits topoisomerase I (Topo I), an enzyme closely linked to cell division, by forming a ternary DNA-CPT-Topo I complex. However, Valko and co-workers[60] have argued against this hypothesis. They have demonstrated that the photoactivation of CPT in the absence of Topo I generates

significant amount of oxidative DNA damage due to the generation of free radicals and formation of such free radicals were confirmed through ESR studies.

1.5.3. Photoactivated DNA Cleaving Agents Selective for DNA Sequences

DNA double helix can be subjected to several sequence restrictions and upon interacting with a third strand of oligonucleotide can lead to the formation of DNA triple helix.[1b] This feature has been exploited as a potential strategy for regulating gene expression. Association of a third strand with a duplex is thermodynamically weaker and kinetically a slower process than the duplex formation itself. Their instability under normal physiological conditions is a critical limitation that restricts the use of triplex DNA under *in vivo* conditions. Various approaches are being explored to improve their stability. Since triplex formation allows small molecules to recognize and associate specifically with selective sequences of duplex DNA, there have been efforts to develop ligands, which can discriminate between duplex and triplex DNA helices.

Oligonucleotides can recognize single- and double-stranded nucleic acid targets by forming Watson-Crick base paired duplexes or Hoogsteen base paired triplexes, respectively.[1b] There are two advantages for tethering a photocleaver to an oligonucleotide: (i) depending on the cleavage mechanism, the opportunity exists for sequence-specific cleavage of the nucleic acid target, and (ii) restricting

the photocleavage agent to one (or only a few) binding sites can greatly facilitate elucidation of the cleavage mechanism.

Helene and co-workers reported the G-selective photocleavage by porphyrin-oligonucleotide conjugates (**34** and **35**, Chart 1.9).[61] DNA oligomers consisting of seven consecutive thymine residues and a porphyrin photosensitizer located on either 3'- or 5'-end of these conjugates were synthesized by solid-phase methods. Hybridization of the oligomers with a DNA 27mer single-strand containing an A7 recognition site and irradiation with visible light led to extensive cross-linking of the two strands. Further treatment with piperidine led to a significant decrease in the amount of cross-linked material and the appearance of

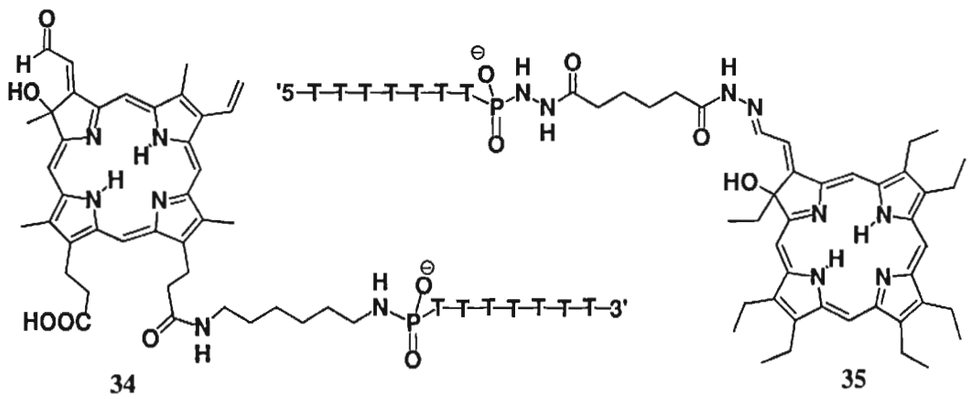

Chart 1.9

cleavage bands particularly at guanine sites. Significant cleavage bands were found in the direction where the porphyrin was expected to be positioned (i.e. 5'-end for the 3'-linked porphyrin and vice versa) and the intensity of the cleavage was greater at site G that is closest to the porphyrin chromophore. The

directionality and base selectivity of the cleavage are consistent with production of singlet oxygen by the excited porphyrin chromophore and its reaction with DNA within the vicinity of the porphyrin. Similarly, Sessler and co-workers[62] reported the enhanced cleavage selectivity with the expanded porphyrins linked to various oligonucleotide sequences.

There are also reports that fullerene C_{60} cleaves DNA selectively at site G by singlet oxygen. Miyata and co-workers[63] reported the photocleavage activity of C_{60} and acridine-C_{60} conjugate (**36**, Chart 1.10). It was observed that the irradiation of C_{60} led to about 25% conversion of supercoiled DNA to nicked form within one hour at 35-40 ^{0}C. The acridine-C_{60} conjugate, on the other hand, showed a stronger DNA cleaving activity which was attributed to the intercalating affinity of the acridine moiety and generation of singlet oxygen within the matrix. However, a recent study by Foote and co-workers questioned this mechanism through C_{60} linked oligonucleotide (**38**, Chart 1.10).[64] In such systems, they observed photocleavage primarily at G residues, but neither enhancement in D_2O nor inhibition by azide, was observed. On the other hand, eosin-oligonucleotide (**39**, Chart 1.10) conjugate showed G-selective cleavage, but in this case, the cleavage was enhanced by D_2O and inhibited by azide, as expected for singlet oxygen mediated cleavage. It seems unlikely that D_2O and azide would have such different effects if singlet oxygen was involved in the cleavage induced by C_{60} and eosin derivatives. These results clearly indicate that the cleavage mechanism induced by C_{60} involves both electron transfer processes as well as singlet oxygen. γ-Cyclodextrin-bicapped C_{60}

(C_{60}/γ-CD) (**37**, Chart 1.10),[65] on the other hand, shows an efficient DNA cleaving-activity in the presence of NADH (β-nicotinamide adenine dinucleotide, reduced form) in an O_2-saturated aqueous solution under visible-light irradiation. No significant DNA cleavage has been observed without NADH under similar experimental conditions. Though singlet oxygen ($^1O_2$) formation has been established through ESR studies, but the detailed results using various additives indicate that neither triplet excited state of C_{60}/γ-CD nor $^1O_2$ is involved in the DNA damage induced by C_{60}/γ-CD.

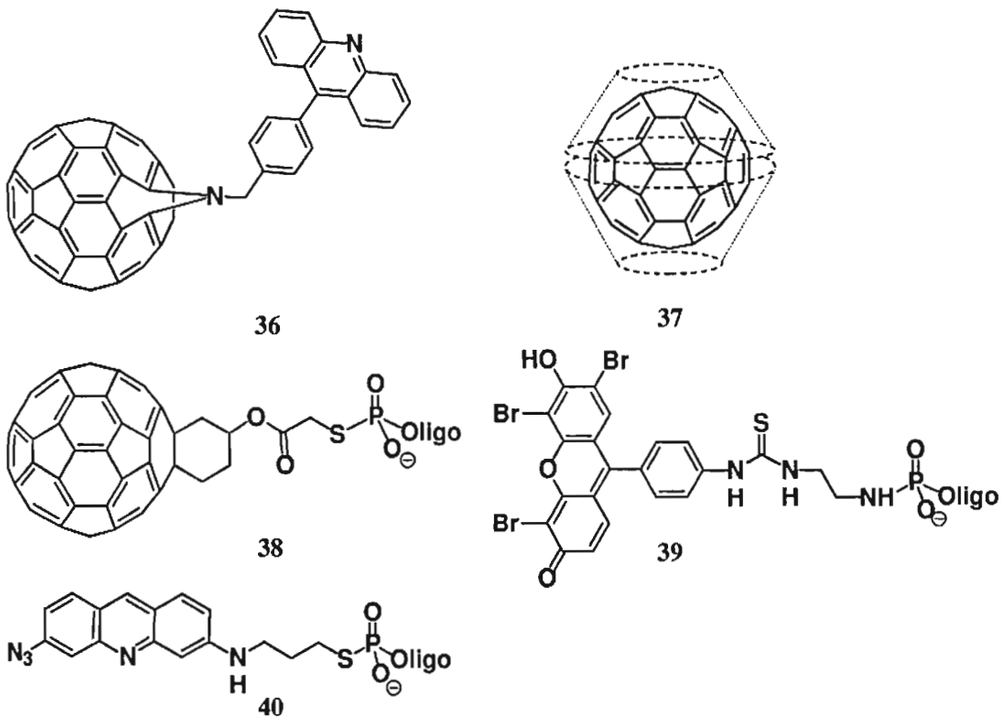

Chart 1.10

Hybridization of azidoproflavine derivative (**40**, Chart 1.10) linked to a oligonucleotide T_9 sequence with its complementary sequence in a 2:1

stoichiometry, yields triple-stranded structure.[66] Irradiation of this triple helix led to photocross-linking as well as piperidine dependent strand breaks at both ends of the target region, indicating that two T_9 strands bind in opposite directions. However, the addition of this conjugate to a duplex of $A_9.T_9$ sequence and followed by irradiation led to the piperidine dependent cleavage on both strands of the duplex, but significantly only at one end of the recognition site. These results demonstrate that T_9 strand binds to the duplex target through one preferred orientation, namely the parallel alignment to the third A_9 strand, indicating the importance of orientation of triple helices in the damage induction.

1.6. Objectives of the Present Investigation

Since photoactivated DNA cleaving agents possess significant practical advantages over the reagents that cleave under thermal conditions, one of our objectives was to design bifunctional molecules that cleave DNA purely through photoinduced electron transfer mechanism. Our strategy was to construct molecules in which both an intercalating functionality and the electron acceptor moiety are connected by a flexible linker chain. The intercalator was so chosen as to act as a sensitizer with absorption in the UVA region ($\lambda > 360$ nm) and is capable of transferring electrons, upon excitation to the acceptor moiety. The important productive reaction in such systems is the photoinduced one electron oxidation of DNA, which subsequently results in the cleavage of DNA. In this context, we have recently reported DNA binding and cleaving efficiencies of a few acridinium and

bisacridinium systems and conjugates consisting of acridine chromophore as sensitizer and the viologen moiety as co-sensitizer.[67,68] These molecules exhibited high affinity for DNA and induced DNA damage that is characteristic of an electron transfer mechanism involving two different pathways (Figure 1.6). One of these pathways follows the oxidation of DNA by the excited state of acridine (path A); whereas the other one involves the oxidation of DNA by the charge separated

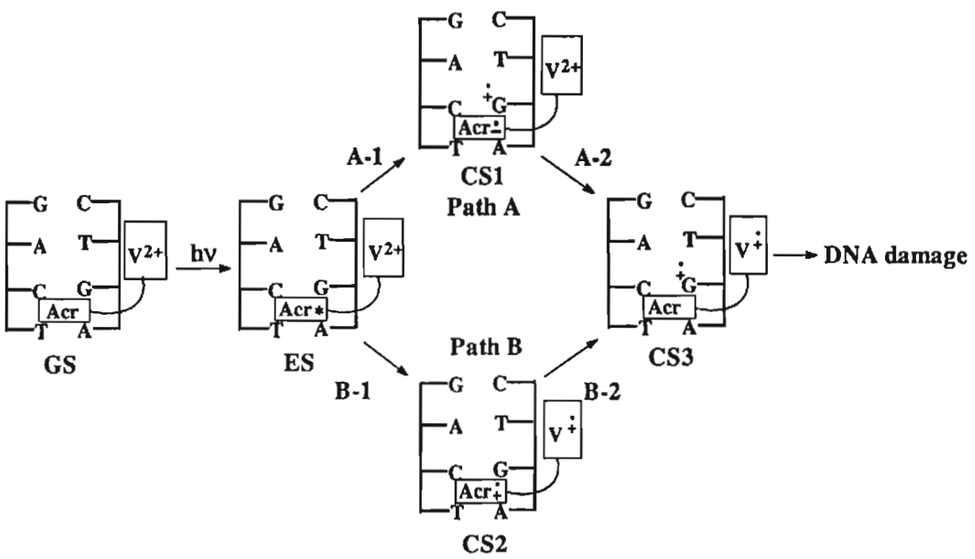

Figure 1.6. Schematic representation of pathways A and B for the oxidative DNA damage induced by the photoactivated viologen linked acridine derivatives (Acr = Acridine, V = Viologen moiety, GS = Ground state complex, ES = Excited state complex, CS = Charge-separated state).

viologen linked acridine (path B). Eventhough both these pathways lead to the oxidation of DNA, back-electron transfer from the excited acridine to DNA involved in the former pathway reduces the efficiency of the DNA damage.

Progress in this area would require new strategies to reduce the back electron transfer between the donor-acceptor dyads and DNA bases and for the efficient oxidation of DNA through co-sensitization mechanism.

In the present investigation, we have designed a new series of novel bifunctional conjugates consisting of intercalating pyrene chromophore as a sensitizer and the viologen moiety as an electron acceptor cum co-sensitizer. Both the sensitizer and cosensitizer can bind with DNA through non-covalent interactions and the binding affinity in these systems can be tuned by varying the length of the linking spacer group. Similarly, the spacer group so varied that it can also control the electron transfer processes between the sensitizer and cosensitizer. Another objective of our investigations was to evaluate how efficiently these molecules interact with various nucleosides and DNA and cleave DNA upon photoexcitation.

We have investigated the interactions of these bifunctional molecules with nucleosides, calf thymus DNA and polyoligonucleotides through photophysical and biophysical techniques and investigated their efficiency of plasmid DNA cleavage employing various restriction enzymes. Yet another objective of our investigations has been to evaluate the cytotoxicity of the bifunctional conjugates in the dark as well as under irradiation conditions so that they can have potential biological applications. It was also our interest to investigate the interaction of a few viologen linked acridine derivatives containing aliphatic and aromatic spacer groups with organized media. In this context, we have examined the photophysical properties of these systems in presence of β-cyclodextrin, evaluated the intramolecular electron

transfer processes and characterized the inclusion complexes through various photophysical, electrochemical, chiroptical and microscopic techniques.

1.7. References

1. (a) Armitage, B. *Chem. Rev.* **1998**, *98*, 1171-1200. (b) David, S. S.; Williams, S. D. *Chem. Rev.* **1998**, *98*, 1221-1261. (c) Kuimelis, R. G.; McLaughlin, L. W. *Chem. Rev.* **1998**, *98*, 1027-1044. (d) Trawick, B. N.; Daniher, A. T.; Bashkin, J. K. *Chem. Rev.* **1998**, *98*, 939-960. (e) Oivanen, M.; Kuusela, S.; Lonnberg, H. *Chem. Rev.* **1998**, *98*, 961-990. (f) Schuster, G. B. *Acc. Chem. Res.* **2000**, *33*, 253-260.

2. (a) Sigman, D. S.; Mazumdar, A.; Perrin, D. M. *Chem. Rev.* **1993**, *93*, 2295-2316. (b) Pogozelski, W. K.; Tullius, T. D. *Chem. Rev.* **1998**, *98*, 1089-1107. (c) Burrows, C. J.; Muller, J. G. *Chem. Rev.* **1998**, *98*, 1109-1151. (d) McMillin, D. R.; McNett, K. M. *Chem. Rev.* **1998**, *98*, 1201-1219.

3. (a) Dervan, P. B. *Science* **1986**, *232*, 464-471. (b) Thuong, N. T.; Helene, C. *Angew. Chem. Int. Ed. Engl.* **1993**, *32*, 666-690. (c) Sigman, D. S.; Bruice, T. W.; Mazumdar, A.; Sutten, C. L. *Acc. Chem. Res.* **1993**, *26*, 98-104.

4. (a) Gemmen, G. J.; Millin, R.; Smith, D. E. *Proc. Natl. Acad. Sci. USA* **2006**, *103*, 11555-15560. (b) Nielsen, P. E. *J. Mol. Recognit.* **1990**, *3*, 1-25.

5. (a) Kochevar, I. E.; Dunn, D. A. *Bioorg. Photochem.* **1990**, *1*, 273-315. (b) Paillous, N.; Vicendo, P. *J. Photochem. Photobiol. B.* **1993**, *20*, 203-209.

6. (a) Lehninger, A. L. In *Principles of Biochemistry*; CBS Publishers and Distribution: New Delhi, 1984. (b) Saenger, W. In *Principles of Nucleic Acid Structure*; Springer Verlag: New York, 1984.

7. Watson, J. D.; Crick, F. H. C. *Nature* **1953**, *171*, 737-738.

8. (a) Dickerson, R. E.; Drew, H. R.; Connor, B. N.; Wing, R. M.; Fratini, A. V.; Kapka, M. L. *Science* **1982**, *216*, 475-485. (b) Dickerson, R. E. *Adv. Enzymol.* **1992**, *211*, 67-111.

9. (a) In *Nucleic Acids in Chemistry and Biology*; Blackburn, G. M., Gait, M. J., Eds.; Oxford University Press: Oxford, 1996, pp 285-324. (b) Cadet, J.; Vigny, P. In *Bioorganic Photochemistry, Photochemistry and the Nucleic Acids*; Morrison, H. Ed.; John Wiley and Sons: New York, 1990, Vol. 1, pp 1-272.

10. (a) Brown, D. M. In *Basic Principles of Nucleic Acids Chemistry*; Ts'o, P. O. P. Ed.; Academic Press: London, 1974, Vol. 2, pp 2-90.

11. (a) Cadet, J.; Vigny, P. In *Bioorganic Photochemistry. Photochemistry and the Nucleic acids*; Morrison, H. Ed.; John Wiley and Sons: New York, 1990, Vol. 1, pp 1-272. (b) Helene, C. In *From Photochemistry to Photobiology*; Favre, A.; Tyrrell, R.; Cadet, J. Eds.; Elsevier: Amsterdam, 1987, pp 3-22.

12. Marnett, L. J.; Burcham, P. C. *Chem. Res. Toxicol.* **1993**, *6*, 771-785.

13. Walling, C. *Acc. Chem. Res.* **1975**, *8*, 125-132.

14. (a) Jovanovich, S. V.; Simic, M. G. *J. Phys. Chem.* **1986**, *90*, 974-979. (b) Steenken, S. *Chem. Rev.* **1989**, *89*, 503-520.

15. Nielsen, P. E.; Jeppensen, C.; Buchardt, O. *FEBS Lett.* **1988**, *235*, 122-124.

16. (a) Nielsen, P. E. *Nucleic Acids Res.* **1992**, *20*, 2735-2730. (b) Mellegard, N. E.; Rasmussan, P. B. Valentin-Hansen, P.; Nielsen, P. E. *J. Biol. Chem.* **1993**, *268*, 17471-17477.

17. Sitlani, A.; Long, E. C.; Pyle, A. M.; Barton, J. K. *J. Am. Chem. Soc.* **1992**, *114*, 2302-2312.

18. Shields, T. P.; Barton, J. K. *Biochemistry* **1995**, *34*, 15037-15048.

19. Chang, C. –H.; Meares, C. F. *Biochemistry* **1982**, *21*, 6332-6334.

20. Saito, I.; Morii, T.; Sugiyama, H.; Matsuura, T.; Meares, C. F.; Hecht, S. M. *J. Am. Chem. Soc.* **1989**, *111*, 2307-2308.

21. (a) Breiner, K. M.; Daugherty, M. A.; Oas, T. G.; Thorp, H. H. *J. Am. Chem. Soc.* **1995**, *117*, 11673-11679. (b) Kalsbeck, W. A.; Groover, N.; Thorp, H. H. *Angew. Chem. Int. Ed. Engl.* **1991**, *30*, 1517-1518.

22. Eppley, H. J.; Lto, S. M.; Elington, A. D.; Zaleski, J. M. *Chem. Commun.* **1999**, 2405-2406.

23. Maurer, T. D.; Kraft, B. J.; Lato, S. M.; Ellington, A. D.; Zaleski, J. M. *Chem. Commun.* **2000**, 69-70.

24. (a) Mohler, D. L.; Downs, J. R.; Hurely-Predecki, A. L.; Sallman, J. R.; Gannett, P. M.; Shi, X. *J. Org. Chem.* **2005**, *70*, 9093-9102. (b) Mohler, D. L.; Barnhardt, E. K.; Hurley, A. L. *J. Org. Chem.* **2002**, *67*, 4982-4984.

25. Chen, C.-T.; Lin, J.-S.; Kuo, J.-H.; Weng, S.-S.; Cuo, T.-S.; Lin, Y.-W.; Cheng, C.-C.; Huang, Y.-C.; Yu, J.-K.; Chou, P.-T. *Org. Lett.* **2004**, *6*, 4471-4474.

26. Sakamoto, F.; Sumiya, T.; Fujita, M.; Tada, T.; Tan, X. S.; Suzuki, E.; Okura, I.; Fujii, Y. *Chem. Lett.* **1998**, 1127-1128.

27. (a) Nicolaou, K. C.; Dai, W. M.; Taay, S. C.; Estevez, V. A.; Wrasidln, W. *Science*, **1992**, *256*, 1172-1178. (b) Goldberg, I. H. *Acc. Chem. Res.* **1991**, *24*, 191-198.

28. Xu, Y. -J.; Zhen, Y. -S.; Goldberg, I. H. *J. Am. Chem. Soc.* **1997**, *119*, 1133-1134.

29. Wender P. A.; Touami, S. M.; Alayrac, C.; Philip, U. C. *J. Am. Chem. Soc.* **1996**, *118*, 6522-6523.

30. Armitage, B.; Yu, C.; Devadoss, C.; Schuster, G. B. *J. Am. Chem. Soc.* **1994**, *116*, 9847-9859.

31. Breslin, D. T.; Coury, J. E.; Anderson, J. R.; Mc Fail-Isom, L.; Kan, Y.; Williams, L. D.; Bottomley, L. A.; Schuster, G. B. *J. Am. Chem. Soc.* **1997**, *119*, 5043-5044.

32. Nielsen, P. E.; Jeppensen, C.; Egholm, M.; Buchardt, O. *Biochemistry* **1988**, *27*, 6338-6343.

33. Nishiwaki, E.; Lee, H.; Matsumoto, T.; Toyooka, K.; Sakurai, H.; Shibuya, M. *Tetrahedron Lett.* **1990**, *31*, 1299-1302.

34. Saito, I.; Takayama, M.; Kawanishi, S. *J. Am. Chem. Soc.* **1995**, *117*, 5590-5591.

35. (a) Wender, P. A.; Jeon, R. *Bioorg. Med. Chem. Lett.***2003**, *13*, 1763-1766. (b) Wender, P. A.; Jeon, R. *Org. Lett.* **1999**, *1*, 2117-2120.

36. Mc Gregor, R. B. Jr. *Anal. Biochem.* **1992**, *204*, 324-327.

37. Matsugo, S.; Kawanishi, S.; Yamamoto, K.; Sugiyama, H.; Matsuura, T.; Saito, I. *Angew. Chem. Int. Ed. Engl.* **1991**, *30*, 1351-1353.

38. Sako, M.; Nagai, K.; Maki, Y. *J. Chem. Soc. Chem. Commun.* **1993**, 750-751.

39. Epe. B.; Haring, M.; Ramaiah, D.; Stopper, H.; Abou-Elzahab, M. M.; Adam. W.; Saha-Moller, C. R. *Carcinogenesis* **1993**, *14*, 2271-2276.

40. Adam, W.; Cadet, J.; Dall'Acqua, F.; Epe, B.; Ramaiah, D.; Saha-Moller, C. R. *Angew. Chem. Int. Ed. Engl.* **1995**, *34*, 107-110.

41. Kamioka, H.; Suzuki, M.; Tamiya, E.; Karabe, I. *J. Mol. Catal.* **1989**, *54*, 1-7.

42. (a) Zou, W.; An, J. -Y.; Jiang, L. J. *J. Photochem. Photobiol. B.* **1996**, *33*, 73-78. (b) Routaboul, C.; Serpentini, C. -L.; Msika, P.; Cesarini, J. -P.; Paillous, N. *Photochem. Photobiol.* **1995**, *62*, 469-475. (c) Artuso, T.; Bernadou, J.; Meunier, B.; Piette, J.; Paillous, N. *Photochem. Photobiol.* **1991**, *54*, 205-213.

43. Cadet, J.; Teoule, R. *Photochem. Photobiol.* **1978**, *28*, 661-667.

44. Revanat, J. –L.; Berger, M.; Bernard, F.; Langlois, R.; Quellett, R.; van Lier. J. E.; Cadet, J. *Photochem. Photobiol.* **1992**, *55*, 809-814.

45. (a) Rodgers, M. A. J.; Snowden, P. T. *J. Am. Chem. Soc.* **1982**, *104*, 5541-5543. (b) Merkel, P. B.; Kearns, D. R. *J. Am. Chem. Soc.* **1972**, *94*, 1029-1031-1030.

46. Adam, W.; Saha-Moller, C. R.; Schonberger, A. *J. Am. Chem. Soc.* **1997**, *119*, 719-723.

47. Croke, D. T.; Perrouault, L.; Sari, M. A.; Battioni, J. P.; Mansuy, D.; Helene, C.; Le Doan, T. *J. Photochem. Photobiol. B.* **1993**, *18*, 41-50.

48. Magda, D.; Wright, M. M.; Miller, R. A.; Sessler, J. L.; Sansom, P. I. *J. Am. Chem. Soc.* **1995**, *117*, 3629-3630.

49. Woo, J.; Hopkins, P. B. *J. Am. Chem. Soc.* **1991**, *113*, 5457-5459.

50. Nussbaum, J. M.; Newport, M. E. A.; Mackie, M.; Leontis, N. B. *Photochem. Photobiol.* **1994**, *59*, 515-528.

51. Sage, E.; le Doan, T.; Boyer, V.; Helland, D. E.; Kittler, L.; Helene, C.; Moustacchi, E. *J. Mol. Biol.* **1989**, *209*, 297-314.

52. Ito, K.; Inoue, S.; Yamamoto, K.; Kawanishi, S. *J. Biol. Chem.* **1993**, *268*, 13221-13227.

53. (a) Cadet, J.; Vigny, P. In *Bioorganic Photochemistry. Photochemistry and the Nucleic acids*; Morrison, H. Ed.; John Wiley and Sons: New York, 1990, Vol. 1, pp 1-272. (b) Helene, C. In *From Photochemistry to*

Photobiology; Favre, A.; Tyrrell, R.; Cadet, J. Eds.; Elsevier: Amsterdam, 1987, pp 3-22.

54. Angelov, D.; Spassky, A.; Berger, M.; Cadet, J. *J. Am. Chem. Soc.* **1997**, *119*, 11373-11380.

55. Cullis, P. M.; Malone, M. E.; Merson-Davies, L. A. *J. Am. Chem. Soc.* **1996**, *118*, 2775-2781.

56. Saito, I.; Takayama, M.; Sugiyama, H.; Nakatani, K.; Tsuchida, A.; Yamamoto, M. *J. Am. Chem. Soc.* **1996**, *118*, 7063-7068.

57. Kochevar, I. E.; Dunn, D. A. In *Bioorganic Photochemistry. Photochemistry and the Nucleic Acids*; Morrison, H. Ed.; John Wiley and Sons: New York, 1990, Vol. 1, pp 273-315.

58. Dunn, D. A.; Lin, V. H.; Kochevar, I. E. *Biochemistry* **1992**, *31*, 11620-11625.

59. Okhubo, K.; Yukimoto, K.; Fukuzumi, S. *Chem. Commun.* **2006**, 2504-2506.

60. Brezova, V.; Valko, V.; Breza, M.; Morris, H.; Telser, J.; Dvoranova, D.; Kaiserova, K.; Varecka, L.; Mazur, M.; Leibfritz, D. *J. Phys. Chem. B* **2003**, *107*, 2415-2425.

61. Le Doan, T.; Praseuth, D.; Perroualt, L.; Chassignol, M.; Thoung, N. T.; Helene, C. *Bioconjugate Chem.* **1990**, *1*, 108-113.

62. Magada, D.; Wright, M. M.; Miller, R. A.; Sessler, J. L.; Sansan, P. I. *J. Am. Chem. Soc.* **1996**, *117*, 3629-3630.

63. Yamakoshi, Y. N.; Yagani, T.; Sueyoshi, S.; Miyata, N. *J. Org. Chem.* **1995**, *61*, 7236-7237.

64. An, Y. –Z.; Chen, C. –H. B.; Anderson, J. L.; Sigmon, D. S.; Foote, C. S.; Rubin, Y. *Tetrahedron* **1996**, *52*, 5179-5189.

65. Nakanishi, I.; Fukuzumi, S.; Konishi, T.; Okhubo, K.; Fujitsuka, M.; Ito, O.; Miyata, N. *J. Phys. Chem. B* **2002**, *106*, 2372-2380.

66. Le Doan, T.; Perrouault, L.; Praseuth, D.; Habhoub, N.; Decout, J. –L.; Thoung, N. T.; Lhomme, J.; Helene, C. *Nucleic Acids Res.* **1987**, *15*, 7749-7760.

67. (a) Eldho, N. V.; Joseph, J.; Ramaiah, D. *Chem. Lett.* **2001**, 438-439. (b) Kuruvilla, E.; Joseph, J.; Ramaiah, D. *J. Phys. Chem. B* **2005**, *109*, 21997-22002. (c) Joseph, J.; Kuruvilla, E.; Achuthan, A. T.; Ramaiah, D.; Schuster, G. B. *Bioconjugate Chem.* **2004**, *15*, 1230-1335.

68. (a) Joseph, J.; Eldho, N. V.; Ramaiah, D. *Chem. Eur. J.* **2003**, *9*, 5926-5935. (b) Joseph, J.; Eldho, N. V.; Ramaiah, D. *J. Phys. Chem. B* **2003**, *107*, 4444-4450.

Chapter 2

SYNTHESIS AND STUDY OF PHOTOPHYSICAL PROPERTIES OF A FEW VIOLOGEN LINKED PYRENES

2.1. Abstract

With the objective of developing efficient DNA oxidizing agents, a new series of viologen linked pyrene conjugates having different number of methylene spacer units (n) was synthesized and their interactions with nucleosides have been investigated through photophysical and laser flash photolysis techniques. The viologen linked pyrene derivatives **1** (n = 1), **2** (n = 7) and **3** (n = 12) exhibited characteristic fluorescence emission of the pyrene chromophore centered around 380 nm, but with significantly reduced yields, when compared to the model compound, **4**. The fluorescence quenching observed in these systems is explained through an electron transfer mechanism based on calculated favorable change in free energy (ΔG_{ET} = -1.59 eV) and redox species characterized through laser flash photolysis studies. Intramolecular electron transfer rate constants (k_{ET}) were calculated from the observed fluorescence yields and singlet lifetime of the model compound and are found to decrease with increasing spacer length. As per the calculated change in free energy values for the electron-transfer reaction between

nucleobases and the pyrene derivatives, we observed negligible quenching of fluorescence of the viologen-linked pyrenes with the addition of the nucleobases. Photoactivation of these systems initiate electron transfer from the singlet excited state of the pyrene chromophore to the viologen moiety followed by an electron transfer from either guanosine or DNA to the oxidized pyrene. This reaction results in the formation of stable charge separated species such as radical cations of guanosine or DNA and reduced viologen as characterized by laser flash photolysis studies and subsequently the oxidized DNA modifications. These novel systems are soluble in buffer media, stable under irradiation conditions and oxidize guanosine and DNA efficiently and selectively through co-sensitization mechanism and hence can be useful as photoactivated DNA cleaving agents.

2.2. Introduction

Design of functional molecules that bind selectively to DNA and are capable of modifying duplex or single stranded DNA is an active area of research that has important biochemical and medicinal applications.[1] Several molecules, which induce DNA modifications by various mechanisms, have been reported in the literature.[2] Among these, the photoactivated DNA oxidizing agents have been found to possess significant practical advantages over the reagents that cleave DNA under thermal conditions.[3] An interesting aspect of these agents is that they allow the reaction to be controlled spatially and temporally by combining all of the components of the reaction mixture before the irradiation. Excitation of the reaction

mixture with an appropriate light source initiates the reaction, which continues until the light is shut off.[4,5] The ability to control light in both spatial and temporal sense would be advantageous for various biological applications.

By absorption of light, these reagents are known to modify DNA through different mechanisms, including the electron-transfer reaction, generation of diffusible and non-diffusible reactive intermediates, and H-atom abstraction.[3-6] In the latter two processes, selectivity of the DNA cleavage is rather difficult to attain, as these reactions are generally non-specific, while the former mechanism is shown to have base selectivity. A large number of simple organic as well as inorganic sensitizers have been reported, which oxidize DNA through photoinduced electron transfer mechanism.[7,8] However, most of these sensitizers were found to be less efficient due to the existence of efficient back electron transfer between the resultant oxidized DNA and the reduced sensitizer. To overcome the drawback of the back electron transfer process associated with such systems, a few examples based on co-sensitization mechanism have been developed.[9,10] These systems consists of a sensitizer, which is also an intercalator, transfers an electron upon excitation to a co-sensitizer (electron acceptor), bound on the surface of DNA. The photosensitization involving the co-sensitizer that bound far away from the sensitizer is expected to inhibit the back electron transfer and thereby increase the DNA modifications. However, in reality, only a marginal improvement in DNA oxidation was observed using these systems owing to the complications with respect to the concentration, distance and DNA binding affinities of the sensitizer and co-sensitizer. Therefore,

molecules that exhibit considerable DNA binding affinity and specificity in cleavage are yet to be achieved.

Recently, we have reported DNA binding and cleaving efficiencies of a few bifunctional conjugates consisting of acridine as sensitizer and the viologen moiety as co-sensitizer.[11] These molecules exhibited high affinity for DNA and induced DNA damage that is characteristic of an electron transfer mechanism involving two different pathways. One of these pathways follows the oxidation of DNA by the excited state of acridine; whereas the other one involves the oxidation of DNA by the charge separated viologen linked acridine. Eventhough both these pathways lead to the oxidation of DNA, back-electron transfer from the excited acridine to DNA involved in the former pathway reduces the efficiency of the DNA damage. Progress in this area would require new strategies to control the sequence of electron transfer reactions between the donor-acceptor dyads and DNA bases and for the efficient oxidation of DNA through co-sensitization mechanism.

In this context, we have designed a new series of donor-acceptor conjugates, which can strongly bind to DNA and in principle, can oxidize DNA selectively through co-sensitization mechanism (Figure 2.1). We chose pyrene, a known intercalator, as the electron donor, whereas the viologen moiety, a groove binder as the electron acceptor. These molecules were designed on the basis of theoretically calculated change in free energy values for the electron transfer and photophysical studies. The present Chapter deals with the synthesis and photophysical properties of a few novel bifunctional viologen linked pyrene and

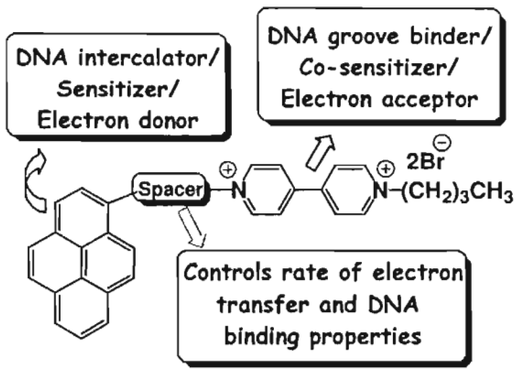

Figure 2.1. Schematic representation of the co-sensitization strategy adopted for the design of photoactivated DNA cleaving agents.

anthracene conjugates (Figure 2.2) including inter- and intramolecular electron transfer reactions and their interactions with nucleosides. Our results demonstrate that the pyrene moiety in these molecules constitutes an interesting variation and plays a major role in controlling the electron transfer pathways, which ultimately lead to the efficient photoxidation of DNA.

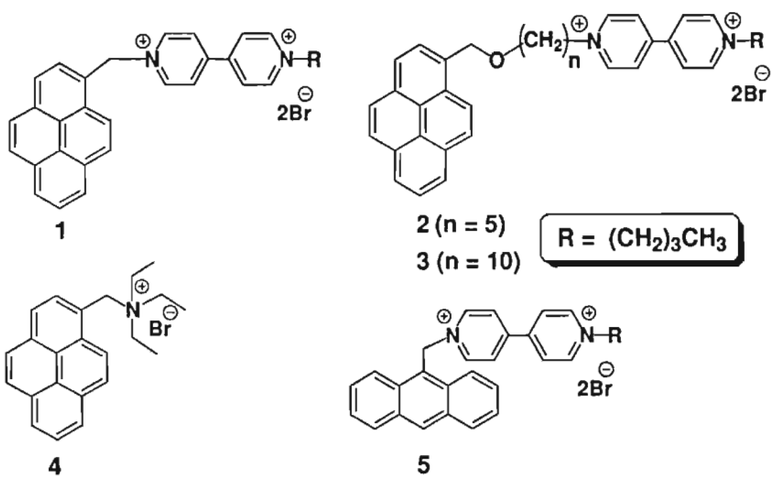

Figure 2.2. Structures of the viololen linked pyrene and anthracene conjugates used for the present investigation.

2.3. Results

2.3.1. Synthesis of a Few Bifunctional Conjugates

The synthesis of the viologen linked pyrene conjugates **1-3** and the model derivative **4** was achieved as shown in Schemes 2.1 and 2.2. 1-Pyrene-carboxaldehyde was prepared in 91% yield through modified Villsmeier-Hack reaction of pyrene with N-methylformanilide and phophonylchloride and was then reduced with sodium borohydride to yield 84% of 1-(hydroxymethyl)pyrene (**8**). Subsequently, 1-(bromomethyl)pyrene (**9**) was synthesized in 82% yield by the reaction of 1-(hydroxymethyl)pyrene with phosphorus tribromide. The synthesis of the model derivative **4** was achieved in 45% yield through the S_N2 reaction of the compound **9** with dry triethylamine, while with 1-butyl-4,4'-bipyridinium bromide gave the viologen linked pyrene conjugate **1** in 29% yield.

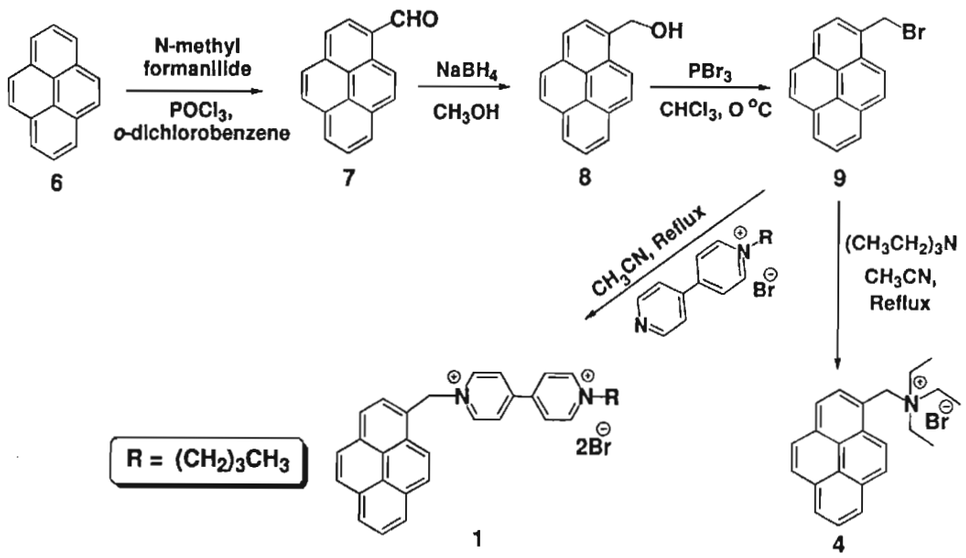

Scheme 2.1

The synthesis of the bromoalkylpyrenes **10** and **11** was achieved in moderate yields through the bromoalkylation of 1-(hydroxymethyl)pyrene (**8**) with the corresponding α,ω–dibromoalkane using sodium hydride in dry THF as shown in Scheme 2.2. The S_N2 reaction of **10** and **11** with 1-butyl-4,4'-bipyridinium bromide gave 53% and 42%, respectively, of the viologen linked pyrene conjugates **2** and **3**.

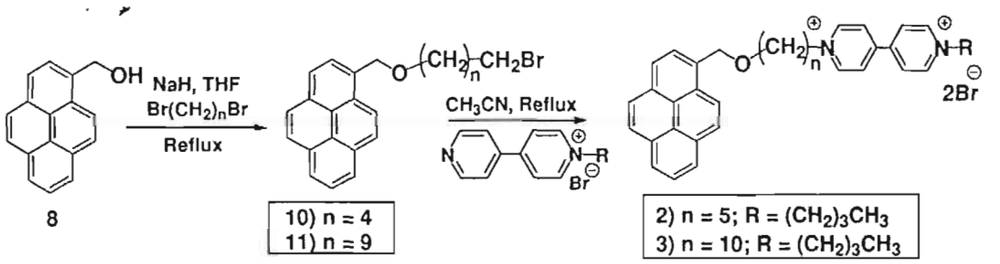

Scheme 2.2

The synthesis of the viologen linked anthracene conjugate **5** was achieved as per the Scheme 2.3. 9-Anthracenecarboxaldehyde was reduced using sodium borohydride to yield 90% of 9-(hydroxymethyl)anthracene (**13**). The reaction of **13** with phosphorus tribromide gave 9-(bromomethyl)anthracene (**14**) in 87% yield. The viologen linked anthracene conjugate **5**, on the other hand, was obtained in 26% yield through the S_N2 reaction of **14** with 1-butyl-4,4'-bipyridinium bromide. These bifunctional conjugates and the model derivative were purified and characterized on the basis of analytical results and spectral evidence. ^{1}H NMR spectrum of the viologen linked pyrene **1** in DMSO-d_6, for example, showed peaks corresponding to the quarternized methylene groups at δ4.69 and 6.82, whereas

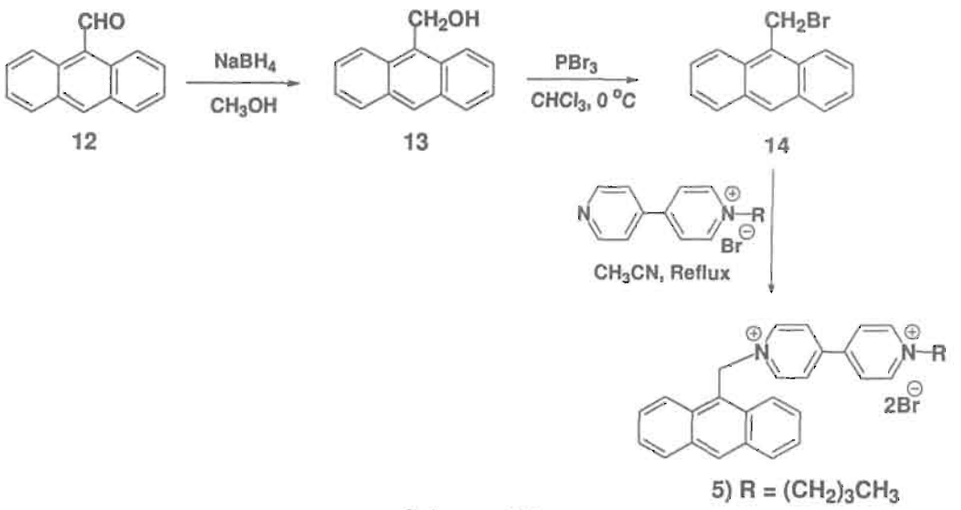

Scheme 2.3

the aliphatic protons corresponding to the butyl group appeared as multiplets in the region between δ 0.90 and 1.97. While the aromatic protons corresponding to the pyrene and the viologen moieties appeared as multiplets in the region between δ 7.5 and 9.85. On the other hand, the higher conjugates **2** and **3** showed a single peak corresponding to both the quarternized methylene groups at δ 4.69, whereas the aliphatic protons corresponding to the spacer and butyl groups appeared as multiplets in the region between δ 0.94 and 3.64. ^{1}H NMR spectrum of the model compound **4** in DMSO-d_6, showed a multiplet corresponding to the methyl groups at δ 1.25 and peaks corresponding to the quarternized methylene groups at δ 3.35 and 5.31, whereas the aromatic protons corresponding to the pyrene moiety appeared as multiplets in the region between δ 8.17 and 8.73.

The ^{13}C spectrum of **1** showed five sp^3 carbons appearing at δ 13.8, 19.2, 33.2, 52.7 and 61.8 corresponding to the four carbons of *n*-butyl group and one

methylene carbon. The other aromatic carbons appeared in the region between δ 109.9 and 146.2. Similarly, the ^{13}C spectra of the higher homologues **2** and **3** showed twelve and eleven sp^3 carbons, respectively, corresponding to the four carbons of *n*-butyl group and methylene carbons present in the spacer groups. On the other hand, the ^{13}C spectrum of the model compound **4** showed three sp^3 carbons corresponding to the two carbons of ethyl groups and one methylene carbon corresponding to the spacer. The mass spectra of the viologen linked pyrene derivatives **1-3** gave a molecular ion peak in each case corresponding to M^+Br^-, indicating that one of the bromide ions is closely associated with the organic ligand (M^+). Similarly, the mass spectrum of the viologen linked anthracene derivative **5** showed the molecular ion peak corresponding to M^+Br^-.

2.3.2. Photophysical Properties

Figure 2.3 shows the absorption spectra of the viologen linked pyrene conjugates **1-3**, the model compound **4** and the viologen linked anthracene conjugate **5** in 10 mM phosphate buffer containing 2 mM NaCl. The viologen linked pyrene conjugates **1-3** and the model compound **4** in 10 mM phosphate buffer showed characteristic absorption spectra with a maximum at 344 nm, corresponding to the pyrene chromophore. The absorption spectra of these derivatives in buffer can be described as the sum of the absorption bands of the pyrene chromophore and viologen (MV^{2+}) moiety. There is no evidence for any ground-state charge-transfer interaction existing between the pyrene and viologen

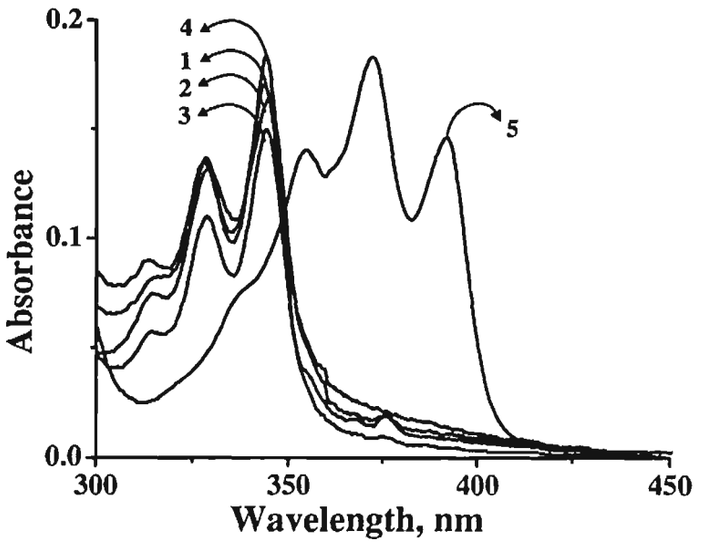

Figure 2.3. Absorption spectra of **1** (0.56 x 10^{-5} M), **2** (0.55 x 10^{-5} M), **3** (0.5 x 10^{-5} M), model compound **4** (0.51 x 10^{-5} M) and **5** (0.73 x 10^{-5} M) in phosphate buffer (10 mM, pH 7.4) containing 2 mM NaCl.

moieties in these systems. The absorption properties of the viologen linked pyrene conjugates in buffer are summarized in Table 2.1. Similarly, the viologen linked anthracene conjugate **5** in 10 mM phosphate buffer showed characteristic absorption spectrum with a maximum at 372 nm, corresponding to the anthracene chromophore, indicating thereby that no ground-state charge-transfer interactions exist between anthracene and viologen moieties present in this system.

Figure 2.4 shows the fluorescence emission spectra of **1-3** and the model compound **4** in buffer. All these compounds show structurally similar fluorescence spectra characteristic of the pyrene chromophore with a maximum around 380 nm. The fluorescence quantum yields of the viologen linked pyrene derivatives were calculated and are found to be two orders of magnitude less than that of the model

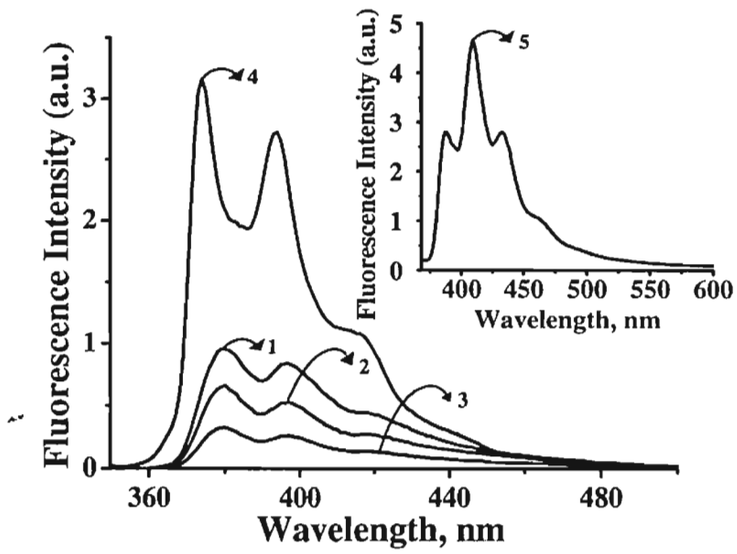

Figure 2.4. Fluorescence emission spectra of **1-3** (Multiplied by a factor of 25 for clarity) and model compound **4** in buffer. Excitation wavelength, 340 nm. Inset shows the fluorescence emission spectrum of **5**. Excitation wavelength, 360 nm.

compound **4** (Table 2.1). For example, the model derivative **4** exhibited a emission quantum yield of Φ_f = 0.32, whereas significantly lower values of Φ_f = 0.0021, 0.0044 and 0.0058, respectively, were observed for the bifunctional derivatives **1-3**. Inset of Figure 2.4 shows the fluorescence emission spectrum of **5** in buffer. This conjugate showed fluorescence spectrum characteristic of the anthracene chromophore with a maximum around 410 nm with a significantly lower fluorescence quantum yield value of Φ_f = 0.001, as compared to the 9-(hydroxymethyl)anthracene (Φ_f = 0.3).

In order to understand the excited state properties of the viologen linked pyrene derivatives, we have carried out picosecond time-resolved fluorescence

Table 2.1. Absorption (λ_{ab}) and fluorescence (λ_{em}) properties of viologen linked pyrene derivatives **1-3** and model derivative **4** in phosphate buffer (10 mM, pH 7.4)[a]

Compound	λ_{ab}, nm ε, $M^{-1}cm^{-1}$	λ_{em}, nm Φ_f[a] x 10^2	k_{ET}[b], s^{-1}	τ, ns
1	344 (22650)	380 (0.21±0.01)	3.2 x 10^9	9.6 (37%) 1.7 (27%) 0.2 (36%)
2	344 (19170)	380 (0.44±0.07)	1.5 x 10^9	18.2 (62%) 2.5 (27%) 0.44 (11%)
3	344 (28730)	380 (0.58±0.09)	1.1 x 10^9	38.8 (63%) 5.2 (27%) 0.3 (10%)
4	344 (24090)	374 (32±0.1)	-	118.8 (100%)

[a] The data are the average of more than two independent experiments and the error is ca. ±5%. [b] Intramolecular electron transfer rate constants are determined using the fluorescence lifetime of the model derivative **4** in buffer (τ = 118.8 ns).

studies in buffer, using the single photon counting technique. Figure 2.5 shows the fluorescence lifetime decay profiles of the viologen linked pyrene derivatives **1-3** and the model compound **4**. The viologen linked pyrene derivatives exhibited triexponential fluorescence decay, while the model compound showed monoexponential decay in buffer. For example, the conjugate **1**, showed three components in buffer with lifetimes of 9.6 ns (37%), 1.7 ns (27%) and 0.2 ns (36%). With increasing in spacer length between the pyrene and viologen

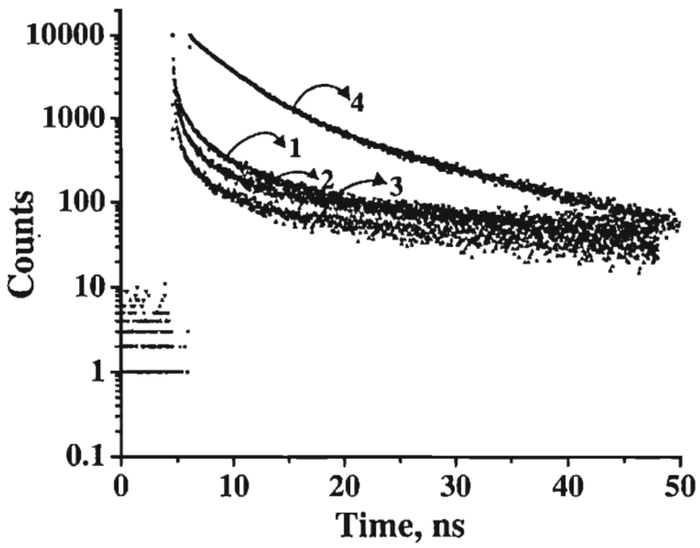

Figure 2.5. Time-resolved fluorescence emission spectra of **1-3** and the model compound **4** in buffer. Excitation wavelength, 335 nm and emission monitored at 380 nm.

moieties, we observed enhancement in lifetimes of the long lived species by ca. 2-fold for the conjugate **2** and ca. 4-fold for the conjugate **3.** On the other hand, the lifetime of the short lived species remained unchanged with increasing in spacer length. In contrast, the model derivative **4** exhibited monoexponential decay with a lifetime of 118.8 ns. The fluorescence lifetimes of the viologen linked pyrene systems **1-3** and the model compound **4** are summarized in the Table 2.1.

2.3.3. Electron Transfer Studies

In order to understand the efficiency of the viologen linked pyrene conjugates as photoactivated DNA cleaving agents, it is important to know the

electron transfer ability of the photoactivated pyrene moiety to the viologen moiety in addition to their absorption and fluorescence properties. In this context, the feasibility of photoinduced electron transfer between the individual units i.e. the 1-(hydroxymethyl)pyrene and methyl viologen was evaluated through photophysical studies and theoretical calculations. Fluorescence emission spectrum of 1-(hydroxymethyl)pyrene (Figure 2.6.) in methanol showed a

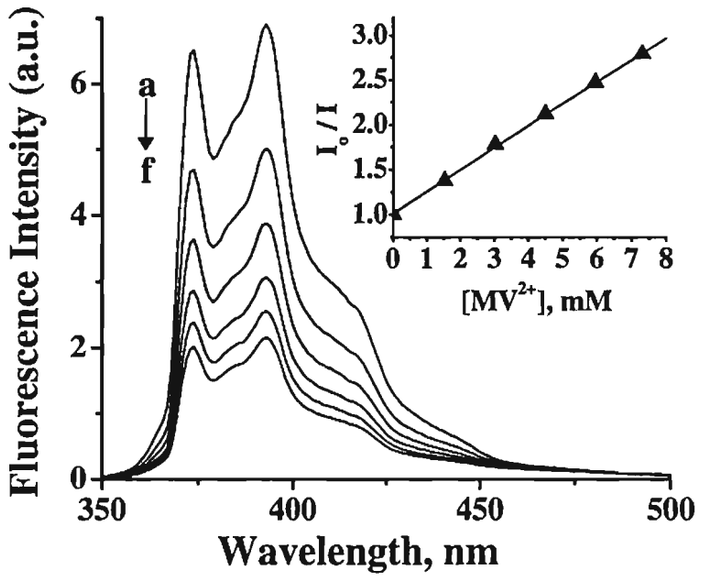

Figure 2.6. Effect of viologen (MV^{2+}) concentration on the fluorescence spectra of 1-(hydroxymethyl)pyrene (5.86×10^{-4} M) in methanol. [MV^{2+}] (a) 0, (b) 1.53, (c) 3.02, (d) 4.46, (e) 5.89 and (f) 7.28 mM. Inset shows the corresponding Stern-Volmer plot. Excitation wavelength, 340 nm.

significant quenching with increasing concentration of MV^{2+}. From the titration data, the bimolecular quenching rate constant (k_q), was calculated and is found to be 2×10^9 M^{-1} s^{-1}. To understand the mechanism of fluorescence quenching and to characterize the transient intermediates involved, we have carried out laser flash

photolysis studies under different conditions. For example, Figure 2.7 shows the transient absorption spectrum obtained immediately after laser excitation (355 nm, pulse width 20 ns) of 1-(hydroxylmethyl)pyrene in methanol and in the presence of MV^{2+}. On the basis of quenching experiments with molecular oxygen, the transient species having absorption maximum at 450 nm and lifetime of 3 μs could be assigned to the radical cation of the pyrene chromophore. As per the literature evidence,[12] the other transient with two absorption maxima at 395 and 610 nm could be due to the reduced viologen radical cation. Interestingly, the reduced viologen radical cation thus formed is found to be quite stable in methanol under

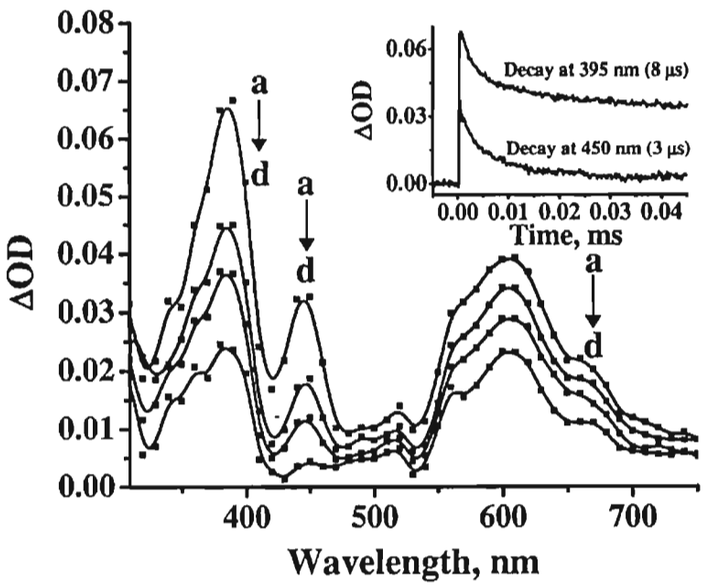

Figure 2.7. Transient absorption spectra of 1-(hydroxymethyl)pyrene (5 x 10^{-5} M) in the presence of viologen (MV^{2+}, 5 x 10^{-5} M) in methanol recorded at a) 7, b) 10, c) 20 and d) 55 ms after 355 nm laser excitation. The inset shows the decay of the pyrene radical cation at 450 nm and the decay of the reduced viologen radical cation at 395 nm.

argon atmosphere. The inset of Figure 2.7 shows the decay of the radical cation of pyrene moiety and the decay of the reduced viologen radical cation, under argon saturated conditions. In support of the experimental observations, we calculated change in free energy for the electron transfer reaction using redox potentials and singlet excited state energy of the pyrene chromophore[13] and is found to be ΔG_{ET} = -1.59 eV in the aqueous medium.

In the case of DNA modifications induced by the electron transfer mechanism, the oxidation of DNA bases by sensitizers plays a major role.[14,15] Several molecules are known to oxidize DNA bases with varying degrees of selectivity. In order to understand the mechanism and efficacy as DNA oxidizing agents, we have investigated the bimolecular quenching properties of the viologen linked pyrene derivatives with various DNA nucleosides (Figure 2.8). With

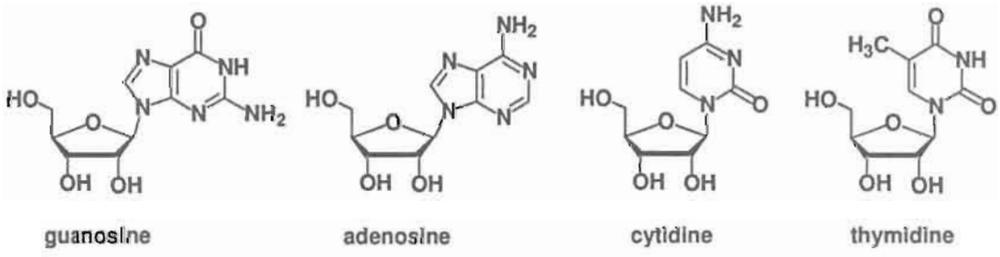

Figure 2.8. Structures of the nucleosides used for the present investigation.

increasing in concentration of nucleosides such as guanosine, adenosine, thymidine and cytidine, we observed negligible changes in the fluorescence emission spectra of **1** (Figures 2.9 and 2.10). Corresponding Stern-Volmer plots are shown in the Figure 2.11. Similar observations were made for other conjugates

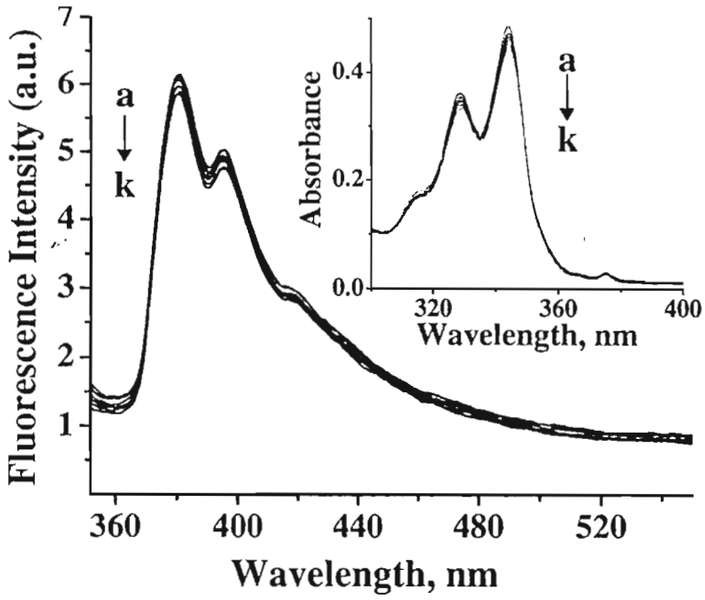

Figure 2.9. Effect of guanosine (Guo) concentration on the fluorescence emission spectra of the viologen linked pyrene **1** (1.48×10^{-5} M) in phosphate buffer (10 mM, pH 7.4) containing 2 mM NaCl. [Guo] (a) 0, (b) 0.16, (c) 0.32, (d) 0.47, (e) 0.63, (f) 0.78, (g) 0.93, (h) 1.08, (i) 1.225, (j) 1.369 and (k) 1.512 mM; excitation wavelength 340 nm. Inset shows the corresponding changes in the absorption spectra.

2 and **3**. Figure 2.12 shows the effect of guanosine in the time-resolved fluorescence emission of **1** in buffer. We observed negligible change in the lifetimes of **1** in the presence of the guanosine. Similar observations were made with nucleosides such as adenosine, cytidine and thymidine and also with the viologen linked pyrene derivatives such as **2** and **3** in the presence of various nucleosides. To understand the effect of chromophore, we have carried out the investigation on the interaction of various nucleosides with the viologen linked anthracene conjugate **5**. With increasing in concentration of nucleosides such as

guanosine, adenosine, thymidine and cytidine, we observed negligible changes in the fluorescence emission spectra of **5** (Figure 2.13), which is in agreement with the results obtained in the case of the viologen linked pyrene conjugates. In contrast, the titration with strong electron donors, such as triethanolamine, led to the significant fluorescence quenching (ca. 2-fold) of the viologen linked pyrene derivative **1** (Figure 2.14). From the corresponding Stern-Volmer plot (inset of Figure 2.14), we obtained a high rate of electron transfer k_{ET} = 1 x 10^{10} $M^{-1}s^{-1}$ for the reaction between triethanolamine and the viologen linked pyrene conjugate **1**.

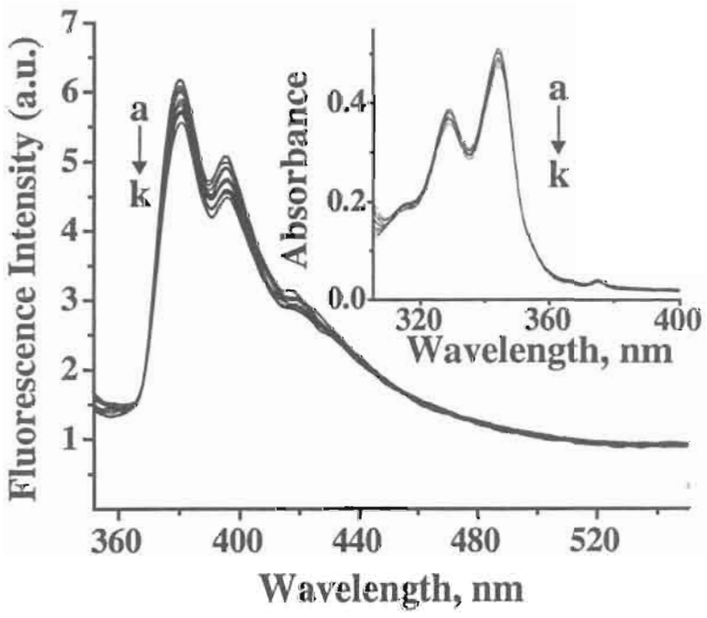

Figure 2.10. Effect of adenosine (Ade) concentration on the fluorescence emission spectra of the viologen linked pyrene **1** (1.48 × 10^{-5} M) in phosphate buffer (10 mM, pH 7.4) containing 2 mM NaCl. [Ade] (a) 0, (b) 0.16, (c) 0.32, (d) 0.47, (e) 0.63, (f) 0.78, (g) 0.93, (h) 1.08, (i) 1.225, (j) 1.369 and (k) 1.512 mM; excitation wavelength 340 nm. Inset shows the corresponding changes in the absorption spectra.

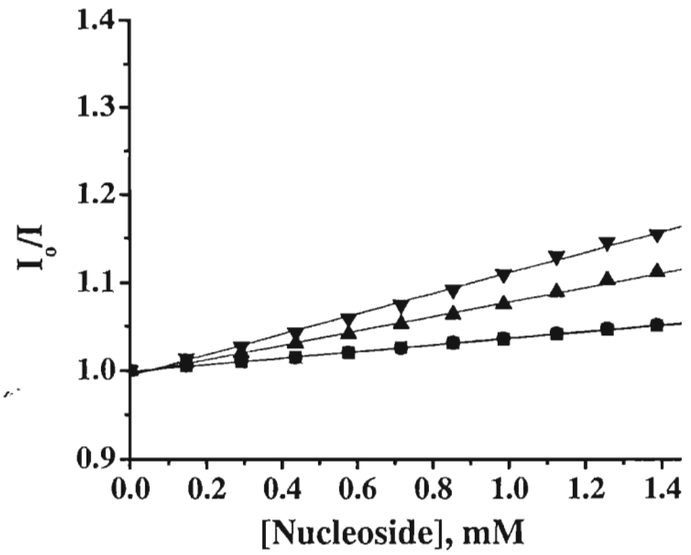

Figure 2.11. Stern-Volmer plot for the quenching of **1** (1.48×10^{-5} M) by guanosine (▼), adenosine (▲), cytidine (●) and thymidine (■). Excitation wavelength, 340 nm.

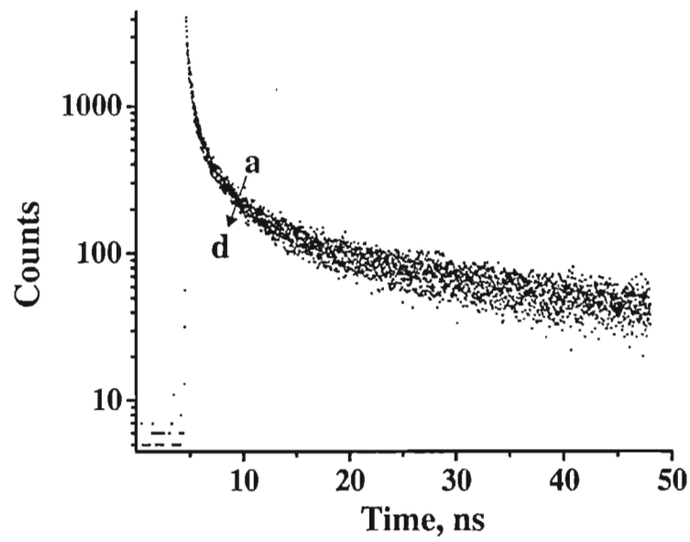

Figure 2.12. Time-resolved fluorescence decay of **1** (1.48×10^{-5} M) in buffer with increasing concentration of guanosine. [Guo] (a) 0, (b) 0.47, (c) 0.93 and (d) 1.512 mM; excitation wavelength 335 nm and emission monitored at 380 nm.

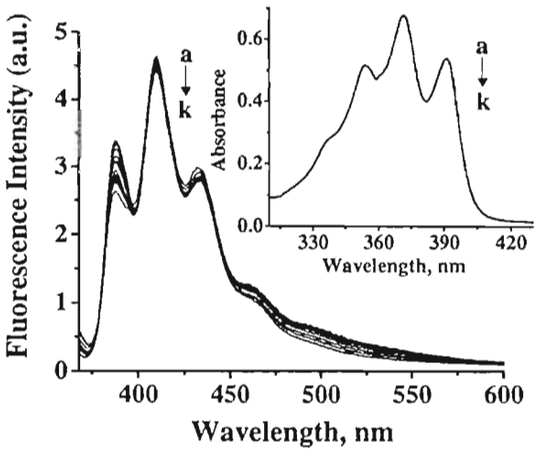

Figure 2.13. Effect of guanosine (Guo) concentration on the fluorescence emission spectra of the derivative **5** (1.48×10^{-5} M) in phosphate buffer (10 mM, pH 7.4) containing 2 mM NaCl. [Guo] (a) 0, (b) 0.16, (c) 0.32, (d) 0.47, (e) 0.63, (f) 0.78, (g) 0.93, (h) 1.08, (i) 1.225, (j) 1.369 and (k) 1.512 mM; excitation wavelength 360 nm. Inset shows the corresponding changes in the absorption spectra.

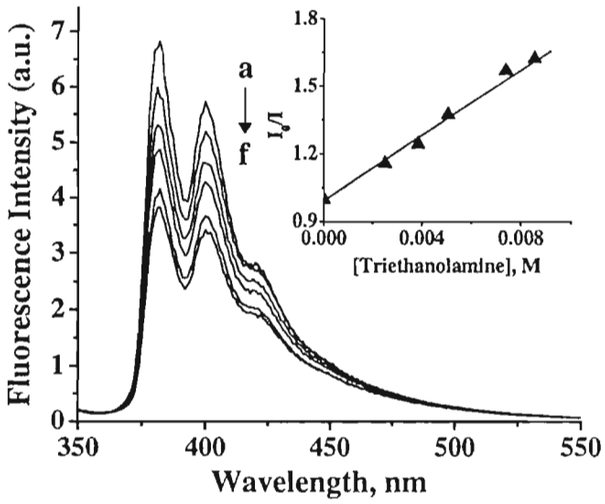

Figure 2.14. Effect of triethanolamine concentration on the fluorescence emission spectra of the derivative **1** (1.48×10^{-5} M) in phosphate buffer (10 mM, pH 7.4) containing 2 mM NaCl. [Triethanolamine] (a) 0, (b) 2.50, (c) 3.85, (d) 5.06, (e) 7.40 and (f) 8.54 mM; excitation wavelength 340 nm. Inset shows the corresponding Stern-Volmer plot.

2.3.4. Oxidation of Guanosine and DNA

To evaluate the potential use of the viologen linked pyrene conjugates as photoactivated DNA cleaving agents, we have carried out laser flash photolysis experiments under different conditions to characterize the transient intermediates involved in these systems. The direct excitation of the viologen linked pyrene conjugates (355 nm, pulse width 20 ns) in buffer or methanol did not show any transients. However, in the presence of an external donor such as guanosine or CT DNA, characteristic transient absorptions due to the redox species were observed. For example, Figure 2.15 shows the transient absorption spectrum obtained on laser excitation of **1** in methanol and in the presence of guanosine (1 mM). This

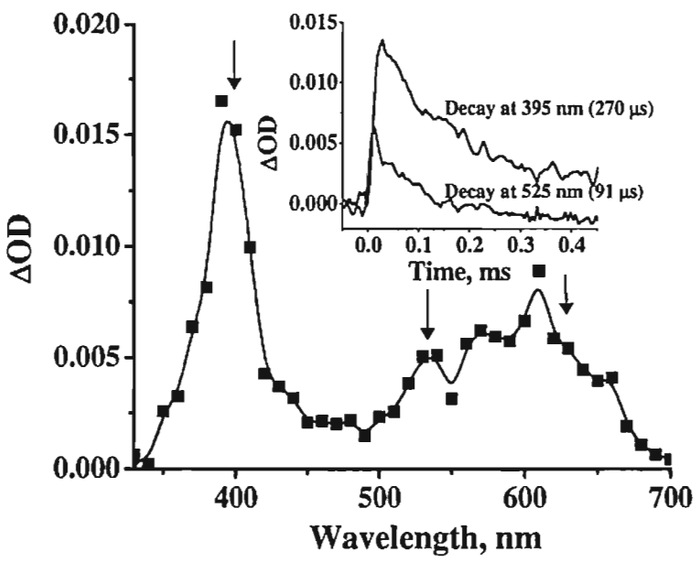

Figure 2.15. Transient absorption spectrum of **1** (3.6×10^{-5} M) in the presence of guanosine (1 mM) in methanol recorded at 2 μs after 355 nm laser excitation. The inset shows the decay of the reduced viologen radical cation at 395 nm and the guanosine radical cation at 525 nm.

spectrum exhibited three absorption maxima at 395, 525 and 610 nm and consisted of two transient species as shown in the inset of Figure 2.15. The first transient with two maxima at 395 and 610 nm exhibited first-order decay with a rate constant of 3.6 x 10^3 s^{-1}, which could be assigned to the reduced viologen radical cation.[12] Whereas, the second transient species with absorption maximum at 525 nm, exhibited first-order decay with a rate constant of 1.1 x 10^4 s^{-1}. As per the literature evidence,[14] the latter species could be due to the formation of the guanosine radical cation. Similar transients were obtained with the viologen linked pyrene conjugates **2** and **3**. In contrast, the model derivative **4** in the presence of guanosine in methanol showed transient absorption at 420 nm with a decay rate constant of 2.3 x 10^4 s^{-1}

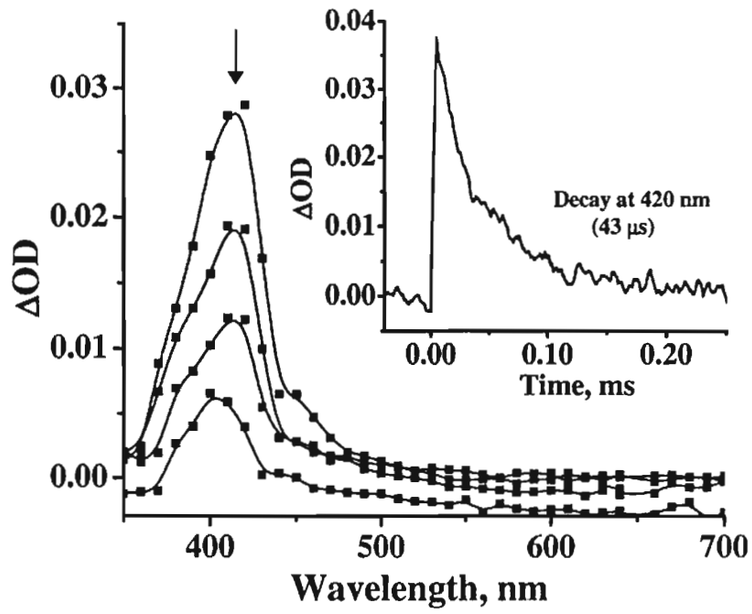

Figure 2.16. Transient absorption spectra of **4** (2.8 x 10^{-5} M) in the presence of guanosine (1 mM) in methanol recorded at, a) 13, b) 26, c) 50 and d) 91 μs after 355 nm laser excitation. The inset shows the decay of the triplet excited state of **4** at 420 nm.

(Figure 2.16). On the basis of quenching experiments with molecular oxygen, this transient species could be assigned to triplet excited state of the pyrene chromophore. No transient absorption corresponding to the guanosine radical cation at 525 nm was observed with the model compound **4**. Figure 2.17 shows the transient absorption spectrum obtained on laser excitation of **3** in the presence of DNA (0.68 mM) in phosphate buffer (10 mM, pH 7.4) containing 10% methanol. As in the case of guanosine, the spectrum consisted of two transient species. The transient absorption with two maxima at 395 and 610 nm, corresponding to the radical cation of viologen exhibited first-order decay rate constant of $3.0 \times 10^5\ s^{-1}$

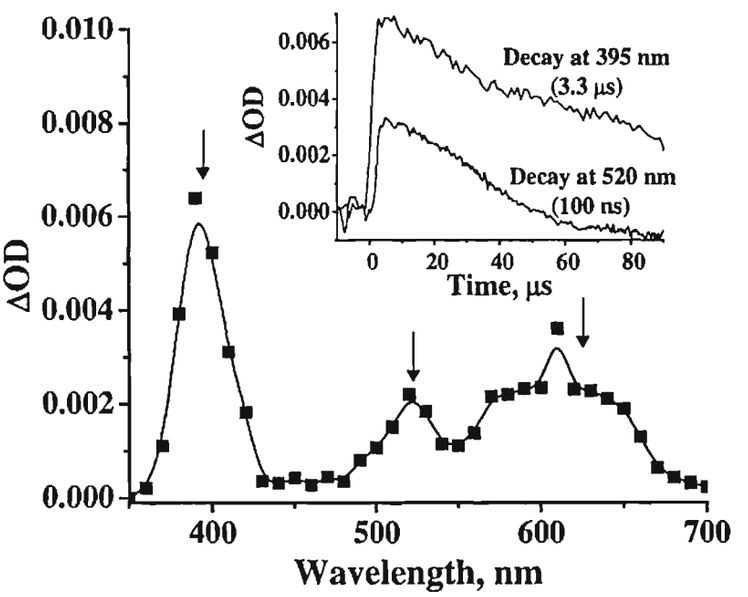

Figure 2.17. Transient absorption spectrum of **3** (2.5×10^{-4} M) in the presence of calf thymus DNA (0.68 mM) in 9:1 phosphate buffer (10 mM, pH 7.4) /methanol mixture recorded at 5 μs after 355 nm laser excitation. The inset shows the decay of the reduced viologen radical cation at 395 nm and the DNA radical cation at 520 nm.

with a lifetime of 3.3 μs. The other transient with absorption maximum at 520 nm exhibited first order decay rate of 8.9 x 10^6 s^{-1} with a lifetime of 0.1 μs. This species could be assigned to the formation of the radical cation of DNA wherein the radical center is located at the guanine moiety in DNA, as per the literature reports.[14] The formation of the radical cations of both reduced viologen and DNA in the presence of CT DNA indicates that the photoactivated viologen linked pyrene conjugates are capable of oxidizing DNA efficiently.

2.4. Discussion

The photophysical studies of the novel bifunctional viologen linked pyrene derivatives **1-3** indicate that they exhibit low fluorescence quantum yields when compared to the model compound **4**. The observed values demonstrate that the interaction between pyrene and viologen moieties is maximum for the conjugate **1** with n = 1 and, which decreases with increasing in spacer length (n = 7 and 12). The calculated change in free energy values and the formation of the radical cation of the pyrene chromophore and reduced viologen moiety indicate that the excited state of the pyrene chromophore is an efficient electron donor to the viologen moiety. The observed rate of electron transfer value of k_{ET} = 3.2 x 10^9 s^{-1} for **1** (n = 1), and ca. 3-times lower value of k_{ET} = 1.1 x 10^9 s^{-1}, for **3** (n = 12), indicate that the rate of intramolecular electron transfer reaction decreases with increasing in spacer length (Table 1) in these systems.

Nanosecond time-resolved fluorescence studies establish that model compound **4** with a lifetime of 118.8 ns exists as single conformer, whereas viologen linked pyrene derivatives **1-3** exist in different conformations in which the viologen moiety has different orientations with respect to the pyrene plane. The long lived component with a lifetime in the range of 9-40 ns could be attributed to the extended conformer of these derivatives with largest distance between the pyrene and viologen moieties present in these derivatives. As expected the lifetime of the extended conformer is found to increase with increasing spacer length. On the other hand, the short component with lifetimes in the range of 0.2-0.4 ns could be attributed to the folded conformer where pyrene and viologen moieties undergo an efficient interaction.

As per the calculated change in free energy values for the electron transfer reaction between nucleobases and the pyrene derivatives (ΔG_{ET} = -0.03, 0.13, 0.33 and 0.46 eV, respectively for G, A, C and T),[15] we observed negligible quenching of fluorescence of the viologen linked pyrene derivatives with the addition of the nucleobases.[16-18] This clearly demonstrates that the viologen linked pyrene derivatives, under investigation, can neither be reduced nor oxidized by the nucleobases directly. Furthermore, change in free energy values for the electron transfer reaction between nucleobases and the anthracene moiety were calculated and are found to be ΔG_{ET} = -0.13, 0.00, 0.18 and 0.28 eV, respectively for G, A, C and T. Interestingly, we observed negligible quenching of fluorescence of the viologen linked anthracene with the addition of the nucleobases, which is in support

of the results obtained in the case of the viologen linked pyrene conjugates. However, a strong electron donor such as triethanolamine is quite efficient in reducing these derivatives as evidenced from the fluorescence quenching observed when triethanolamine was added. This is in good agreement with the thermodynamically predicted change in free energy values for electron transfer from triethanolamine to singlet excited state of the pyrene chromophore (ΔG_{ET} = -0.33 eV). In the case of the viologen linked pyrene derivatives, the rate of charge separation k_{ET} and the rate of charge recombination are expected to be fast, and hence the reduced viologen radical cation could not be observed by a nanosecond laser flash photolysis technique. However, in the presence of external donors such as guanosine and DNA, we observed the formation of the radical cations of both guanosine and reduced viologen. This can be attributed due to the reduced rate of charge recombination (k_{CR} = 1.1 x 10^4 s^{-1}) in the case of the charge-separated species formed in the presence of the guanosine, whereas in the presence of DNA in buffer, we observed relatively a higher rate of charge recombination (k_{CR} = 8.9 x 10^6 s^{-1}).

Considering the electron transfer processes in the presence of DNA, two pathways can be proposed for the oxidation of DNA by the viologen linked pyrenes (Figure 2.18). Of these two pathways, path A involves the first electron transfer from the DNA bases to the excited state of the pyrene chromophore, followed by transfer of an electron from the pyrene radical anion to the viologen moiety. This pathway can be ruled out in the case of the viologen linked pyrene conjugates because of the calculated unfavorable change in free energy values for such an

electron transfer reaction and the observed negligible fluorescence quenching with various nucleobases. On the other hand, path B involving the first electron transfer from the excited state of the pyrene chromophore to the viologen moiety, followed

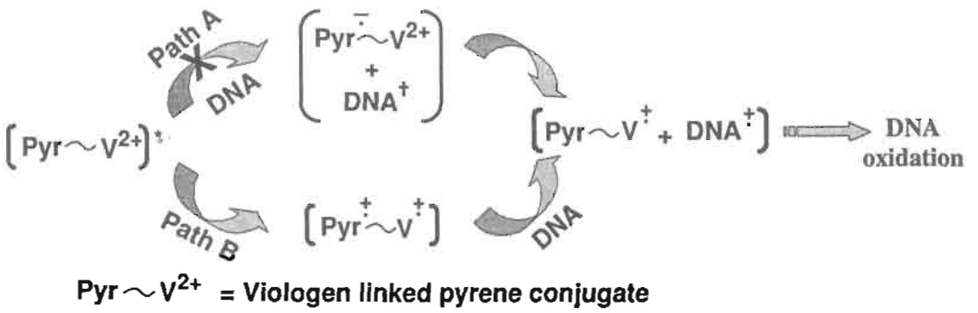

Figure 2.18. Schematic representation of the DNA oxidation pathways induced by the photoactivated bifunctional viologen linked pyrene conjugates.

by second electron transfer from the DNA base (preferably from guanine) to the radical cation of the pyrene is expected to be the exclusive pathway for the oxidation of DNA by these systems. This interpretation is in agreement with the (i) theoretically calculated favorable change in free energy values (ΔG = -1.59 eV), (ii) the observation of efficient fluorescence quenching by the viologen moiety and (iii) formation of the radical cations of both reduced viologen and guanosine in presence of the sacrificial donors such as guanosine and DNA. Interestingly, the first electron transfer reaction in path B leads to the formation of radical cations of both pyrene and viologen moieties, which then lead to the formation of the charge separated radical cations of both DNA and reduced viologen moiety. The radical cation of DNA thus formed leads to the DNA damage and eventually cleavage of DNA.

2.5. Conclusions

In conclusion, we observed that the pyrene chromophore in the case of the viologen linked bifunctional systems **1-3** constitutes an interesting variation, which controls electron transfer pathways for the oxidation of DNA. Theoretically calculated favorable change in free energy values, negligible fluorescence quenching with various nucleobases and formation of the radical cations of both reduced viologen and DNA confirm that these systems undergo first electron transfer exclusively from the excited state of the pyrene chromophore to the viologen moiety. Subsequently, a second electron transfer occurs from the DNA bases (preferably guanosine) to the radical cation of the pyrene, which results in the formation of the charge separated radical cations of both DNA and reduced viologen moiety. These novel bifunctional systems, which are stable in aqueous medium and efficient in oxidizing guanosine and DNA can have potential use as photoactivated DNA cleaving agents that function purely through the co-sensitization mechanism.

2.6. Experimental Section

2.6.1. General Techniques

All melting points are uncorrected and were determined on a Mel-Temp II melting point apparatus.[19,20] An Elico pH meter was used for pH measurements. The electronic absorption spectra were recorded on a Shimadzu UV-VIS-NIR

spectrophotometer. Fluorescence spectra were recorded on a SPEX-Fluorolog F112X spectrofluorimeter. The fluorescence quantum yields were determined by using optically matched solutions. Quinine sulphate (Φ_f = 0.54) in 0.1 N H_2SO_4 was used as the standard.[21] The quantum yields of fluorescence were calculated using the equation 2.1, where, A_s and A_u are the absorbance of standard and

$$\Phi_u = \frac{A_s F_u n_s^2}{A_u F_s n_u^2} \Phi_s \qquad (2.1)$$

unknown, respectively. F_u and F_s are the areas of fluorescence peaks of the unknown and standard and n_s and n_u are the refractive indices of the standard and unknown solvents, respectively. Φ_s and Φ_u are the fluorescence quantum yields of the standard and unknown.

Fluorescence lifetimes were measured using a IBH Picosecond single photon counting system. The fluorescence decay profiles were deconvoluted using IBH data station software V2.1, fitted with monoexponential decay and minimizing the χ^2 values of the fit to 1 ± 0.1. The quenching rate constant k_q was calculated by employing Equations (2.2) and (2.3), where I_0 and I are the

$$I_0/I = 1 + K_{SV}[Q] \qquad (2.2)$$

$$K_{SV} = K_q \times \tau_0 \qquad (2.3)$$

fluorescence intensities in the absence and presence of quencher (Q), K_{sv} the Stern-Volmer constant, and τ_0 the singlet lifetime of 1-(hydroxylmethyl)pyrene in the absence of quencher.

From the relative fluorescence quantum yields of the viologen linked pyrene derivatives and fluorescence lifetime of the model derivative **4**, an estimate of the rate constant of electron transfer process k_{ET} can be made by using Equation 2.4, where Φ_{ref} and Φ are the relative fluorescence quantum yields of the model

$$k_{ET} = [(\Phi_{ref} / \Phi) - 1] / \tau_{ref} \qquad (2.4)$$

compound **4** and the viologen linked pyrene derivative, respectively, and τ_{ref} is the fluorescence lifetime of the model compound **4**. Laser flash photolysis experiments were carried out in an Applied Photophysics Model LKS-20 Laser Kinetic Spectrometer using the third harmonic (355 nm) of a Quanta Ray GCR-12 series pulsed Nd:YAG laser. ^{1}H and ^{13}C NMR spectra were measured on a 300 MHz Bruker advanced DPX spectrometer. The concentrations of DNA solutions were determined by using the average value of 6600 M^{-1} cm^{-1} for the extinction coefficient of a single nucleotide at 260 nm.[22]

2.6.2. Materials

Pyrene, N-methylformanilide, phosphonylchloride, 4,4'-bipyridine, 1,5-dibromopentane, 1,10-dibromodecane, 1-bromobutane, triethanolamine, guanosine, adenosine, thymidine and cytidine (all from Aldrich), calf thymus DNA (Pharmacia Biotech, USA) were obtained and used as received. 1-Butyl-4,4'-bipyridinium bromide was obtained in 95% yield by the reaction of 4,4'-bipyridine with 1-bromobutane in the molar ratio of 3:1 in dry acetonitrile.[11]

Petroleum ether used was the fraction with bp 60-80 °C and doubly distilled water was used for all the experiments.

2.6.3. Synthesis of 1-[(pyren-1-yl)methyl]-1'-N,N',N''-triethylammonium bromide (4)

N-methylformanilide (25 mmol) was dissolved in *o*-dichlorobenzene (5 mL) and the solution was stirred and maintained at 20-25 °C, during the addition of $POCl_3$ (45 mmol) for 2 h. Pyrene (25 mmol) was then added and the mixture stirred at 90-95 °C for 2 h. The resulting deep red solution on cooling gave a precipitate which was collected, hydrolyzed with water and extracted with benzene. The organic layer was separated and the solvent was removed under vacuum. The product thus obtained was chromatographed on silica gel using hexane to give 1-pyrenecarboxaldehyde (91%), after recrystallization from methanol, mp 123-126 °C (mixture mp)[23]: ^{1}H NMR ($CDCl_3$, 300 MHz) δ 7.81-8.14 (9H, m, aromatic), 10.16 (1H, CHO); ^{13}C NMR ($CDCl_3$, 75 MHz) δ 123.4, 125.2, 125.7, 126.8, 127.0, 127.1, 128.5, 129.1, 129.8, 130.7, 131.8, 132.7, 134.3, 136.4, 138.4, 140.1, 198.2.

To an ice cold solution of 1-pyrenecarboxaldehyde (2.2 mmol) in 50 mL dry methanol, sodium borohydride (2.8 mmol) was added and the resulting mixture was stirred for 1 h. Excess sodium borohydride was washed with ice cold water and methanol was evaporated under reduced pressure. The aqueous layer was extracted with dichloromethane and removal of solvent under reduced

pressure gave a white solid which was chromatographed on silica gel using a mixture of ethyl acetate and hexane (1:19) to give 84% of 1-(hydroxymethyl)pyrene, mp 123-124 ^{0}C (mixture mp)[23]: ^{1}H NMR ($CDCl_3$, 300 MHz) δ 5.40 (2H, d, J = 5.28 Hz), 7.98-8.21 (9H, m, aromatic), 8.37 (1H, d, J = 9.23 Hz); ^{13}C NMR ($CDCl_3$, 75 MHz) δ 63.84, 122.9, 124.7, 125.3, 125.9, 126.0, 127.4, 127.5, 127.9,130.8.

To an ice cold solution of 1-(hydroxymethyl)pyrene (0.65 mmol) in 35 mL of dry chloroform, phosphorus tribromide (0.21 mmol) was added and the resulting solution was stirred for 12 h. Reaction mixture was neutralized with saturated sodium bicarbonate solution. The organic layer was separated and evaporated under reduced pressure to give 82% of 1-(bromomethyl)pyrene, after recrystallization from chloroform, mp 136-137 ^{0}C (mixture mp)[23]: ^{1}H NMR ($CDCl_3$, 300 MHz) δ 5.25 (2H, s), 8.06-8.13 (5H, m), 8.20-8.26 (3H, m), 8.39 (1H, d, J = 9.2 Hz); ^{13}C NMR ($CDCl_3$, 75 MHz) δ 32.2, 122.8, 124.8, 125.6, 126.2, 127.3, 127.7, 127.9, 128.2. Anal. Calcd for $C_{17}H_{11}Br$: C, 69.17; H, 3.76. Found: C, 69.31; H, 3.57.

To a solution of 1-(bromomethyl)pyrene (0.65 mmol) in dry acetonitrile (30 mL), triethylamine (0.65 mmol) was added and stirred for 12 h at room temperature. The precipitated product was filtered and dried under vacuum, to give 45% of the model compound **4**, which was recrystallized from a mixture (6:4) of methanol and ethyl acetate, mp 184-185 °C: ^{1}H NMR (DMSO-d_6, 300 MHz) δ 1.25-1.29 (9H, m),

3.35-3.42 (6H, m), 5.31 (2H, s), 8.17-8.73 (9H, m); ^{13}C NMR (DMSO-d_6, 75 MHz) δ 7.8, 52.7, 58.3, 121.0, 122.0, 122.9, 124.2, 125.4, 125.7, 126.1, 126.5, 128.3, 128.4, 129.3, 130.1, 130.9, 131.7; HRMS (ESI) Calcd for $C_{23}H_{26}BrN$: 396.3633. Found: 396.3639. Anal. Calcd for $C_{23}H_{26}BrN$: C. 69.70; H, 6.61; N, 3.53. Found: C, 69.59; H, 6.83; N, 3.71.

2.6.4. Synthesis of 1-[(pyren-1-yl)methyl]-1'-butyl-4,4'-bipyridinium dibromide (1)

To a solution of 1-(bromomethyl)pyrene (0.6 mmol) in dry acetonitrile (50 mL), 1-butyl-4,4'-bipyridinium bromide (0.6 mmol) was added and stirred at room temperature for 12 h. Precipitated product was filtered and dried to give 29% of the viologen linked pyrene conjugate **1**, which was recrystallized from a mixture (7:3) of methanol and ethyl acetate, mp 286-290 °C: ^{1}H NMR (DMSO-d_6, 300 MHz) δ 0.90-0.95 (3H, t, J = 7.4Hz), 1.29-1.33 (2H, m), 1.93-1.97 (2H, m), 4.69 (2H, t, J = 7.1Hz), 6.82 (2H, s), 8.17-8.75 (9H, m), 8.58-9.51 (8H, m); ^{13}C NMR (DMSO-d_6, 75 MHz) δ 13.8, 19.2, 33.2, 52.7, 61.8, 109.9, 115.4, 122.8, 124.1, 125.9, 126.6, 126.7, 126.8, 127.3, 127.4, 127.5, 127.7, 129.1, 129.5, 129.8, 130.6, 131.2, 146.2; HRMS (ESI) Calcd for $C_{31}H_{28}BrN_2$: 508.4715. Found: 508.4711. Anal. Calcd for $C_{31}H_{28}Br_2N_2$: C, 63.28; H, 4.80; N, 4.76. Found: C, 63.14; H, 4.69; N, 4.86.

2.6.5. Synthesis of {N-(butyl)-N'-[5-(1-pyrenylmethoxy)pent-1-yl]}-4,4'-bipyridinium dibromide (2)

To a stirred suspension of sodium hydride (19 mmol) in dry THF (10 mL) under reflux condition was added a solution of 1-(hydroxymethyl)pyrene (1 mmol) and 1,5-dibromopentane (5 mmol) over a period of 30 min in dry THF (20 mL). The reaction mixture was refluxed for 24 h and excess sodium hydride was quenched with water. The organic layer was extracted with dichloromethane. Removal of the solvent under reduced pressure gave the product, which was purified by recrystallization from a mixture (2:8) of ethyl acetate and hexane to give 5-bromopentyl-1-methylpyrene ether (53%), mp 83-84 °C: ^{1}H NMR ($CDCl_3$, 300 MHz) δ 1.20-1.80 (6H, m), 3.34-3.38 (2H, m), 3.59-3.63 (2H, m), 5.21 (2H, s), 7.98-8.38 (9H, m); ^{13}C NMR ($CDCl_3$, 300 MHz) δ25.0, 29.0, 32.6, 33.7, 70.1, 76.6, 115.8, 123.5, 125.5, 125.2, 125.9, 126.9, 127.4, 127.6.

To a solution of 5-bromopentyl-1-methylpyrene ether (0.5 mmol) in dry acetonitrile (30 mL), 1-butyl-4,4'-bipyridinium bromide (0.5 mmol) was added and stirred for 12 h at room temperature. Precipitated product was filtered and dried in vacuum oven, which was then recrystallized from a mixture (7:3) of methanol and ethyl acetate to give the viologen linked pyrene conjugate **2** (32%), mp 216-217 °C: (DMSO-d_6, 300 MHz) δ0.94-2.08 (13H, m), 3.60-3.64 (2H, m), 4.69 (4H, s), 5.17 (2H, s), 8.01-9.37 (17H, m); ^{13}C NMR (DMSO-d_6, 75 MHz) δ 13.8, 19.2, 22.8, 28.0, 29.0, 30.6, 30.9, 33.1, 60.7, 61.2, 69.8, 70.8, 123.0, 124.0, 125.0, 125.7, 125.8,

126.8, 126.9, 126.9, 127.1, 127.4, 127.5, 127.7, 127.9, 130.9, 131.1, 145.8, 146.1; HRMS (ESI) Calcd for $C_{36}H_{38}N_2OBr$: 594.6038. Found: 594.6032. Anal. Calcd for $C_{36}H_{38}Br_2N_2O$: C, 64.10; H, 5.68; N, 4.15. Found: C, 64.19; H, 5.91; N 4.02.

2.6.6. Synthesis of {N-(butyl)-N'-[10-(1-pyrenylmethoxy)dec-1-yl]}-4,4'-bipyridinium dibromide (3)

To a stirred suspension of sodium hydride (19 mmol) in dry THF (10 mL) under reflux condition was added a solution of 1-(hydroxymethyl)pyrene (1 mmol) and 1,10 dibromodecane (5 mmol) over a period of 30 min in dry THF (20 mL). The reaction mixture was refluxed for 24 h and excess sodium hydride was quenched with water. The organic layer was extracted with dichloromethane. Removal of the solvent under reduced pressure gave the product, which was purified by recrystallization from a mixture (2:8) of ethyl acetate and hexane to give 10-bromodecyl-1-methylpyrene ether (42%), mp 54-55 °C: ^{1}H NMR ($CDCl_3$, 300 MHz) δ 1.20-1.80 (16H, m), 3.35-3.40 (2H, m), 3.58-3.62 (2H, m), 5.21 (2H, s), 8.01-8.40 (9H, m); ^{13}C NMR ($CDCl_3$, 75 MHz) δ25.0, 25.8, 26.2, 28.7, 29.2, 29.4, 29.9, 32.6, 33.7, 70.1, 76.6, 115.8, 123.5, 125.5, 125.2, 125.9, 126.9, 127.4, 127.7.

To a solution of 10-bromodecyl-1-methylpyrene ether (0.5 mmol) in dry acetonitrile (30 mL), 1-butyl-4,4'-bipyridinium bromide (0.5 mmol) was added and stirred for 12 h at room temperature. Precipitated product was filtered and dried in vacuum oven, which was then recrystallized from a mixture (7:3) of methanol and

ethyl acetate to give the viologen linked pyrene conjugate **3** (29%), mp 217-218 °C: ^{1}H NMR (DMSO-d_6, 300 MHz) δ 1.15-2.08 (23H, m), 3.55-3.59 (2H, m), 4.65-4.69 (4H, m), 5,17 (2H, s), 8.09-9.33 (17H, m); ^{13}C NMR (DMSO-d_6, 75 MHz) δ 12.5, 18.1, 24.7, 25.0, 27.6, 27.9, 28.1, 28.6, 29.9, 31.9, 60.3, 69.0, 69.7, 122.9, 123.3, 123.4, 123.9, 124.5, 125.6, 125.9, 126.6, 126.5, 126.7, 128.0, 128.9, 129.7, 131.6, 145.0, 146.0, 148.0; HRMS (ESI) Calcd for $C_{41}H_{48}N_2OBr$: 664.7367. Found: 664.7360. Anal. Calcd for $C_{41}H_{48}Br_2N_2O$: C, 66.13; H, 6.50; N, 3.76. Found: C, 66.29; H, 6.33; N, 3.89.

2.6.7. Synthesis of 1-[(anthr-9-yl)methyl]-1'-butyl-4,4'-bipyridinium dibromide (5)

To an ice cold solution of 9-anthracenecarboxaldehyde (2.2 mmol) in 50 mL dry methanol, sodium borohydride (2.8 mmol) was added and the resulting mixture was stirred for 1 h. Excess sodium borohydride was washed with ice cold water (or ice) and methanol was evaporated under reduced pressure. The aqueous layer was extracted with dichloromethane and removal of solvent under reduced pressure gave a white solid which was chromatographed on silica gel using a mixture of ethyl acetate and hexane (1:19) to give 9-(hydroxymethyl)anthracene (90%), mp 162-164 ^{0}C (mixture mp)[23]: ^{1}H NMR ($CDCl_3$, 300 MHz) δ 5.40 (2H, d, J = 5.28), 7.48-7.53 (2H, m), 7.62-7.67 (2H, m), 8.05 (2H, d, J = 9.23 Hz), 8.31 (2H, d, J = 8.71 Hz); ^{13}C NMR ($CDCl_3$, 75 MHz) δ 26.9, 123.5, 125.4, 126.8, 129.1, 129.2, 129.7, 131.5.

To an ice cold solution of 9-(hydroxymethyl)anthracene (0.65 mmol) in 35 mL of dry chloroform, phosphorus tribromide (0.21 mmol) was added and the resulting solution was stirred for 12 h. Reaction mixture was neutralized with saturated sodium bicarbonate solution. The organic layer was separated and evaporated under reduced pressure to give 87% of 9-(bromomethyl)anthracene, after recrystallization from chloroform, mp 136-137 ^{0}C (mixture mp)[23] : ^{1}H NMR ($CDCl_3$, 300 MHz) δ 5.55 (2H, s), 7.48-7.53 (2H, m), 7.62-7.67 (2H, m), 8.04 (2H, d, J = 9.23 Hz), 8.31 (2H, d, J = 8.71 Hz); ^{13}C NMR ($CDCl_3$, 75 MHz) δ 26.9, 123.5, 125.4, 126.8, 129.1, 129.2, 129.7, 131.5.

To a solution of 9-(bromomethyl)anthracene (0.6 mmol) in dry acetonitrile (50 mL), 1-butyl-4,4'-bipyridinium bromide (0.6 mmol) was added and stirred at room temperature for 12 h. Precipitated product was filtered and dried to give 29% of the viologen linked anthracene derivative **5**, which was recrystallized from a mixture (7:3) of methanol and ethyl acetate, mp 289-290 °C: ^{1}H NMR (DMSO-d_6, 300 MHz) δ 0.88 (3H, t, J = 7.4Hz), 1.28-1.29 (2H, m), 1.89-1.91 (2H, m), 4.67 (2H, t, J = 7.4Hz), 7.08 (2H, s), 7.61-9.33 (17H, m); ^{13}C NMR (DMSO-d_6, 75 MHz) δ 13.3, 18.7, 32.7, 56.1, 60.5, 121.6, 123.3, 125.8, 126.7, 126.9, 128.4, 129.6; HRMS (FAB) Calcd for $C_{29}H_{28}BrN_2$: 484.4501. Found: 484.4495. Anal. Calcd for $C_{29}H_{28}Br_2N_2$: C, 61.72; H, 5.00; N, 4.96. Found: C, 61.54; H, 4.89; N, 4.86.

2.7. References

1. (a) Waring, M. J. In *Drug Action at the Molecular Level*; Roberts, G. K., Ed.; Macmillan, London, 1977, pp. 167-189. (b) Lambert, B.; LePecque, J.–B. In *DNA-Ligand Interactions*: *From Drugs to Proteins*; Guschlbauer, W., Saenger, W. Eds.; Plenum, New York, 1986, p 141. (c) Pullman, B.; Jortner, J. In *Molecular Basis of Specificity in Nucleic Acid-Drug Interactions*, *Vol. 1* ; CRC Press, Ann Arbor, MI, 1993; (d) Bischofberger, N.; Shea, R. G. In *Nucleic Acid Targeted Drug Design*; Propst, C. L., Perun, T. J. Eds.; Dekker, New York, 1992, pp. 579-612. (e) *Small Molecule DNA and RNA Binders*; Demeunynck, M., Bailly, C., Wilson, W. D. Eds.; Wiley-VCH, Weinheim, 2003.

2. (a) Tidd, D. M. In *Molecular Aspects of Anticancer Drug-DNA Interactions*, Vol.1: Neidle, S., Waring, M. Eds.; CRC, Boca Raton, FL, 1993, pp. 272-300. (b) Arkin, M. R.; Stemp, E. D. A.; Turro, C.; Turro, N. J.; Barton, J. K. *J. Am. Chem. Soc.*, **1996**, *118*, 2267-2274. (c) Nielsen, P. E. *Bioconjugate Chem.* **1991**, 2, 1-12. (d) Rajski, S. R.; Williams, R. M. *Chem. Rev.* **1998**, *98*, 2723-2796. (e) Brun, A. M.; Harriman, A. *J. Am. Chem. Soc.* **1994**, *116*, 10383-10393. (f) Nakatani, K.; Sando, S.; Saito, I. *J. Am. Chem. Soc.* **2000**, *122*, 2172-2177. (g) Adam, W.; Cadet, J.; Dall' Acqua, F.; Epe, B.; Ramaiah, D.; Saha-Moller, C. R. *Angew. Chem. Int. Ed. Engl.* **1995**, *34*, 107-110. (h) Duarte, V.; Gasparutto, D.; Yamaguchi, L. F.;

Ravanat, J.-L.; Martinez, G. R.; Madeiros, M. H. G.; Di Mascio, P.; Cadet, J. *J. Am. Chem. Soc.* **2000**, *122*, 12622-12628. (i) Ravanat, J. –L.; Mascio, P. D.; Martinez, G. R.; Medeiros, M. H. G.; Cadet, J. *J. Biol. Chem.* **2000**, *275*, 40601-40604.

3. (a) Schuster, G. B. *Acc. Chem. Res.* **2000**, *33*, 253-260. (b) Breslin, D. T.; Schuster, G. B. *J. Am. Chem. Soc.*, **1996**, *118*, 2311-2319. (c) Armitage, B.; Yu, C.; Devadoss, C.; Schuster, G. B. *J. Am. Chem. Soc.* **1994**, *116*, 9847-9859.

4. (a) Bohne, C.; Faulhaber, K.; Giese, B.; Hafner, A.; Hofmann, A.; Ihmels, H.; Kohler, A.-K.; Pera, S.; Scheider, F.; Sheepwash, M. A. L. *J. Am. Chem. Soc.* **2005**, *127*, 76-85. (b) B. Giese, *Acc. Chem. Res.* **2000**, *33*, 631-636. (c) Meggers, E.; Beyerle, M. E. M.; Giese, B. *J. Am. Chem. Soc.* **1998**, *120*, 12950-12955.

5. (a) Armitage, B. *Chem. Rev.* **1998**, *98*, 1171-1200. (b) Kochevar, I. E.; Dunn, D. A. In *Bioorganic Photochemistry. Photochemistry and the Nucleic Acids*; Morrison, H. Ed.; John Wiley and Sons: New York, 1990, Vol. 1, pp 273-315.

6. (a) Pogozelski, W.; Tullius, T. *Chem. Rev.* **1998,** *98,* 1089-1107. (b) Burrows, C. J.; Muller, J. G. *Chem. Rev.* **1998**, *98*, 1109-1152.

7. (a) Johnston, D. H.; Thorp, H. H. *J. Phys. Chem.* **1996**, *100,* 13837-13843. (b) Fu, P. K. -L.; Bradley, P. M.; van Loyen, D.; Durr, H.; Bossmann, S. H.; Turro, C. *Inorg. Chem.* **2002**, *41*, 3808-3810.

8. (a) Choi, S.; Cooley, R. B.; Hakemian, A. S.; Larrabee, Y. C.; Bunt, R. C.; Maupas, S. D.; Muller, J. G.; Burrows, C. J. *J. Am. Chem. Soc.* **2004**, *126*, 591-598. (b) Fromherz, P.; Rieger, B. *J. Am. Chem. Soc.* **1986**, *108*, 5361-5362.

9. Dunn, D. A.; Lin, V. H.; Kochevar, I. E. *Biochemistry*, **1992**, *31*, 11620-11625.

10. (a) Rogers, J. E.; Weiss, S. J.; Kelly, L. A. *J. Am. Chem. Soc.* **2000**, 122, 427-436. (b) Le, T. P.; Rogers, J. E.; Kelly, L. A. *J. Phys. Chem. A* **2000**, *104*, 6778-6785. (c) Rogers, J. E.; Le, T. P.; Kelly, L. A. *Photochem. Photobiol.* **2001**, *73*, 223-229.

11. (a) Joseph, J.; Eldho, N. V.; Ramaiah, D. *Chem. Eur. J.* **2003**, *9*, 5926-5935. (b) Eldho, N. V.; Joseph, J.; Ramaiah, D. *Chem. Lett.* **2001**, 438-439. (c) Joseph, J.; Eldho, N. V.; Ramaiah, D. *J. Phys. Chem. B* **2003**, *107*, 4444-4450.

12. Watanabe, T.; Honda, K. *J. Phys. Chem.* **1982**, *86*, 2617-2619.

13. (a) Oxidation potential of pyrene = 1.28 V, reduction potential of viologen = -0.45 V and singlet energy of pyrene = 3.32 V; see reference Murov, S. L.; Carmichael, I.; Hug, G. L. In *Handbook of Photochemistry II*nd *Edition,* Marcel Dekker, Inc., New York, 1993. (b) Rehm, D.; Weller, A. *Ber. Bunsenges Phys. Chem.* **1969**, *73*, 834-836. c) Weller, A. Z. *Phys. Chem.* **1982**, *133*, 93-98.

14. (a) Candeias, L. P.; Steenken, S. *J. Am. Chem. Soc.* **1989**, *111*, 1094-1099. (b) Okhubo, K.; Yukimoto, K.; Fukuzumi, S. *Chem. Commun.* **2006**, 2504-2506.

15. (a) Zahavy, E.; Fox, M. A. *J. Phys. Chem. B* **1999**, *103*, 9321-9327. (b) Reduction potential of pyrene, Py/Py^{-} = -2.09 V; oxidation potentials of nucleobases dG^{+}/dG = 1.29 V, dA^{+}/dA = 1.42 V, dC^{+}/dC = 1.60 V, dT^{+}/dT = 1.70 V; reduction potentials of nucleobases dG/dG^{-} = -2.52 V, dA/dA^{-} = -2.28 V, dC/dC^{-} = -2.11 V, dT/dT^{-} = -1.94 V, dU/dU^{-} = -1.83 V as per the reference Steenken, S.; Telo, J. P.; Novais, H. M.; Candeias, L. P. *J. Am. Chem. Soc.* **1992**, *114*, 4701-4709.

16. (a) Trifonov, A.; Raytchev, M.; Bucharov, I.; Rist, M.; Barbaric, J.; Wagenknecht, H.-A.; Fiebig, T. *J. Phys. Chem. B.* **2005**, *109*, 19490-19495. (b) Wagenknecht, H.-A. *Angew. Chem. Int. Ed.* **2003**, *42*, 2454-2460.

17. (a) Seidel, C. A. M.; Schulz, A.; Sauer, H. M. *J. Phys. Chem.* **1996**, *100*, 5541-5553. (b) Telser, J.; Cruickshank, K. A.; Morrison, L. E.; Netzel, T. L.; Chan, C.-K. *J. Am.Chem. Soc.* **1989**, *111*, 7226-7232. (c) Mann, J. S.; Shibata, Y.; Meehan, T. *Bioconjugate Chem.* **1992**, *3*, 5544-5558.

18. Crean, C.; Geacintov, N. E.; Shafirovich, V. *Angew. Chem. Int. Ed.* **2005**, *44*, 5057-5060.

19. (a) Neelakandan, P. P.; Hariharan, M.; Ramaiah, D. *Org. Lett.* **2005**, *7*, 5765-5768. (b) Arun, K. T.; Ramaiah, D. *J. Phys. Chem. A* **2005**, *109*, 5571-5578. (c) Arun, K. T.; Epe, B.; Ramaiah, D. *J. Phys. Chem. B* **2002**,

106, 11622-11627. (d) Neelakandan, P. P.; Hariharan, M.; Ramaiah, D. *J. Am. Chem. Soc.* **2006**, *128*, 11334-11335. (e) Jisha, V. S.; Arun, K. T.; Hariharan, M.; Ramaiah, D. *J. Am. Chem. Soc.* **2006**, *128*, 6024-6025.

20. (a) Kuruvilla, E.; Joseph, J.; Ramaiah, D. *J. Phys. Chem. B* **2005**, *109*, 21997-22002. (b) Joseph, J.; Kuruvilla, E.; Achuthan, A. T.; Ramaiah, D.; Schuster, G. B. *Bioconjugate Chem.* **2004**, *15*, 1230-1235.

21. Roshal, A. R.; Organero, J. A.; Douhal, A. *Chem. Phys. Lett.* **2003**, *379*, 53-59.

22. Baguley, B. C.; Falkenhaug, E.-M. *Nucleic Acids Res.* **1978**, *5*, 161-171.

23. Bayer, O. In *Methoden der Organischen Chemie-Vierte Auflage,* Vol. 1: Muller, S., Ed.; Georg Thieme Verlag, Stuttgart, Germany, 1954, p 34.

Chapter 3

DNA BINDING AND PHOTOACTIVATED DNA CLEAVING PROPERTIES OF A FEW VIOLOGEN LINKED PYRENES

3.1. Abstract

DNA binding and *in vitro* photobiological properties of a few selected bifunctional viologen-linked pyrene conjugates have been investigated using calf thymus DNA, supercoiled PM2 DNA and synthetic oligonucleotides. The DNA binding studies through photophysical, chiroptical, viscometric, electrochemical and thermal denaturation techniques demonstrate that these systems undergo effective DNA intercalation with association constants (K_{DNA}) in the range 1.1-2.6 x 10^4 M^{-1}. The efficiency and mechanism of DNA cleavage induced by these systems was analyzed using cell-free DNA in the presence and absence of additives and scavengers. Irradiation of supercoiled DNA from bacteriophage PM2 (PM2 DNA, 10^4 kbp) in the presence of these derivatives showed spacer length dependent DNA damage that is sensitive to formamidopyrimidine-DNA glycosylase (Fpg). This damage was found to increase with increasing in irradiation time as well as the concentration of the probe. The presence of the additives such as superoxide dismutase, catalase and D_2O showed negligible

influence on the extent of DNA damage. The viologen linked pyrene derivatives, under investigation, were found to be non-toxic in the dark but interestingly exhibited significant photocytotoxicity in L1210 murine leukemia cells. Results of these investigations clearly demonstrate that the spacer group in these systems constitutes an interesting variation which controls the efficiency of DNA binding and photoactivated DNA cleaving properties of the bifunctional derivatives. These bifunctional conjugates which are highly soluble in aqueous medium, exhibit significant cytotoxicity and DNA cleavage upon photoexcitation and hence can have potential phototherapeutic applications.

3.2. Introduction

The study of DNA binding and cleaving properties of small molecules is important in the design of probes and more efficient drugs, that are targeted to DNA.[1-7] Several aromatic hydrocarbons and related systems have been reported to be highly carcinogenic, and the carcinogenicity of these molecules, in general, has been attributed to their activity at the DNA level.[8-15] When molecules bind with DNA, number of modes of interactions are possible such as electrostatic, groove binding and intercalative interactions.[1-7,16-17] Alkali metal ions are electrostatically attracted to the phosphate backbone of DNA and prefer electrostatic binding, whereas transition metal ions may coordinate with the nitrogen atoms of the nucleobases.[18] Since the interior of the double helix is fairly hydrophobic due to the π-electron cloud of the nucleotide bases, planar aromatic heterocyclic compounds prefer intercalative binding interactions

with DNA, where the probe molecule is inserted between the base pairs.[19] These different kinds of interactions can have varying effects on the ground and excited state properties of the guest molecules. For example, the photophysical studies of 3,6-diaminoacridine[20] bound to DNA show increase in lifetimes and fluorescence quantum yields when bound to AT-rich DNA, while significantly reduced values were observed in the case presence of GC-rich sequences. The fluorescence quenching of the probe by GC-sequences through electron transfer mechanism has been suggested to be the reason for the observed differences, however; in both these cases the acridine chromophore undergoes intercalative interactions with DNA.

As described in the Chapter 2 of the thesis, the photophysical properties including laser flash photolysis studies and interactions of the viologen linked pyrenes with various nucleosides indicate that these bifunctional molecules can be used as photoactivated DNA cleaving agents. In this context, it was our interest to investigate how efficiently these bifunctional molecules interact with DNA and cleave DNA upon photoexciation. This chapter describes the DNA binding as well as in vitro photobiological properties including cytotoxicity of a few selected viologen linked pyrenes **1-3** (Figure 3.1). Interactions of the viologen linked pyrene derivatives with DNA have been carried out using various photophysical, electrochemical and biophysical techniques. On the other hand, DNA cleaving properties of the viologen linked pyrene conjugates have been evaluated through

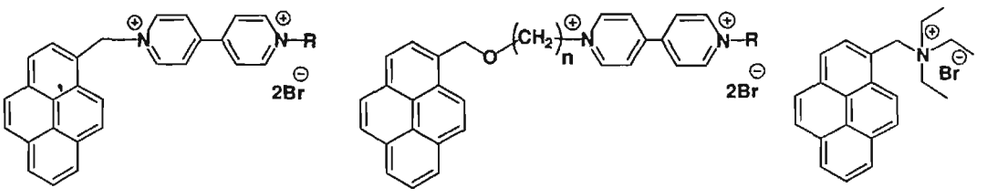

1) R = $(CH_2)_3CH_3$ 2 (n = 5) 3 (n = 10) R = $(CH_2)_3CH_3$ 4

Figure 3.1. Structure of the pyrene derivatives used for the present investigation.

DNA relaxation assay and employed various restriction enzymes. These bifunctional conjugates showed efficient interaction with DNA through intercalation and exhibited significant DNA modifications that are sensitive to formamidopyrimidine glycosylase (Fpg). Results of these investigations demonstrate that the presence of spacer group and viologen moiety imparts amphiphilicity to these derivatives and thereby enhances their cellular uptake and efficiency as DNA cleaving agents. These novel derivatives are found to preferentially localize in the cytoplasm thereby induce cytotoxicity only upon photoexcitation and hence can have potential use in therapeutical applications.

3.3. Results

3.3.1. DNA Binding Properties

To understand how efficiently the viologen linked pyrene conjugates interact with DNA, we investigated their DNA binding properties using absorption,

fluorescence, thermal denaturation, viscometry, circular dichroism (CD) and cyclic voltammetry (CV) techniques. As shown in Figure 3.2, the addition of DNA to a solution of the compound **1** (n = 1) resulted in gradual decrease in absorbance at 345 nm, corresponding to the pyrene chromophore. The maximum hypochromism

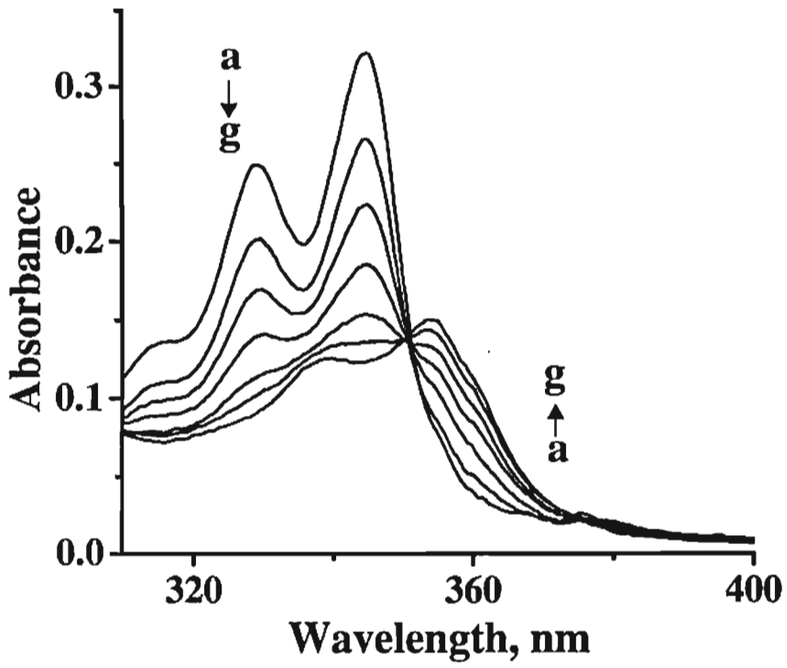

Figure 3.2. Absorption spectra of **1** (1.1 x 10^{-5} M) in the presence of CT DNA in phosphate buffer (10 mM, pH 7.4) containing 2 mM NaCl. [DNA] (a) 0, b) 0.012, (c) 0.021, (d) 0.034, (e) 0.045, (f) 0.056 and (g) 0.08 mM.

(~50%) was observed at 0.08 mM of DNA and with formation of a new band at 355 nm. The corresponding fluorescence spectra are shown in the Figure 3.3, which showed negligible changes with increase in concentration of DNA. Half-reciprocal analysis[21] of the absorbance changes gave a linear plot (Figure 3.4) with an intrinsic binding constant (K_{DNA}) of 1.1±0.05 x 10^4 M^{-1} and the binding site size of

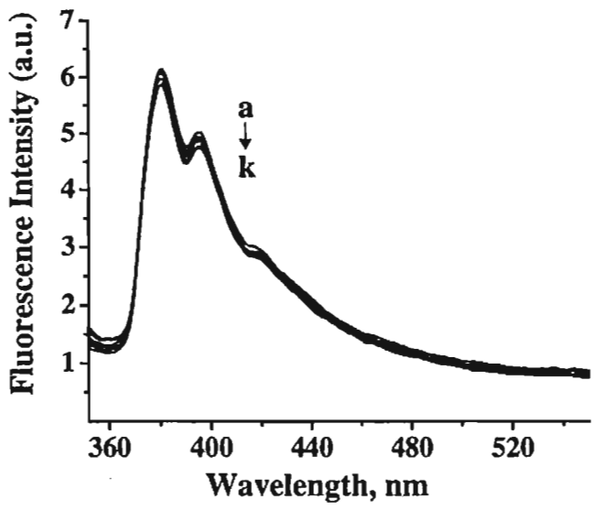

Figure 3.3. Fluorescence emission spectra of **1** (1.1 x 10^{-5} M) in the presence of CT DNA in phosphate buffer (10 mM, pH 7.4) containing 2 mM NaCl. [DNA] (a) 0, b) 0.012, (c) 0.021, (d) 0.034, (e) 0.045, (f) 0.056 and (g) 0.08 mM. Excitation wavelength, 351 nm.

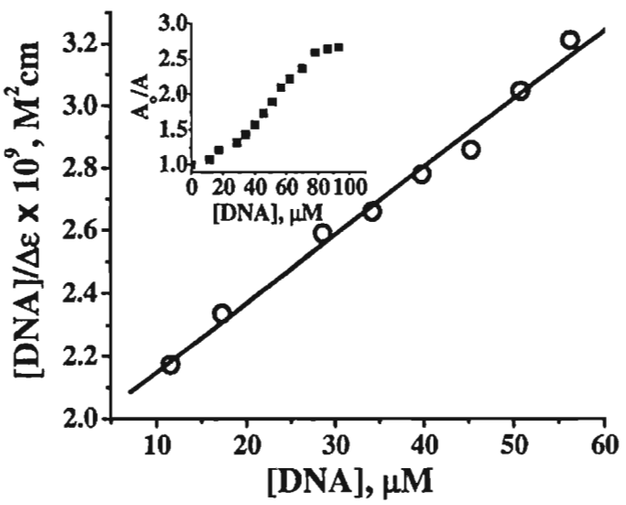

Figure 3.4. Half-reciprocal plot for the binding of **1** with CT DNA in phosphate buffer (10 mM, pH 7.4) containing 2 mM NaCl. Inset shows the saturation of absorption changes at 345 nm with increase in DNA concentration.

1.4±0.2 for the compound **1**. A gradual decrease in the absorption intensity of **1** was observed (inset of Figure 3.4), which reached saturation at a high concentration of DNA (0.08 mM). Similar changes in absorption and fluorescence spectra were obtained in the case of the higher conjugates **2** and **3** and the model compound **4** (Figures 3.5-3.7). The binding analysis gave intrinsic binding constants of 1.9, 2.3 and 2.6 x 10^4 M^{-1} and binding site sizes of 1.7±0.2, 1.8±0.3 and 1.9±0.3, for the derivatives **2**, **3** and **4**, respectively. Table 3.1 summarizes the DNA binding properties of the viologen linked pyrene derivatives **1-3** and the model compound **4**.

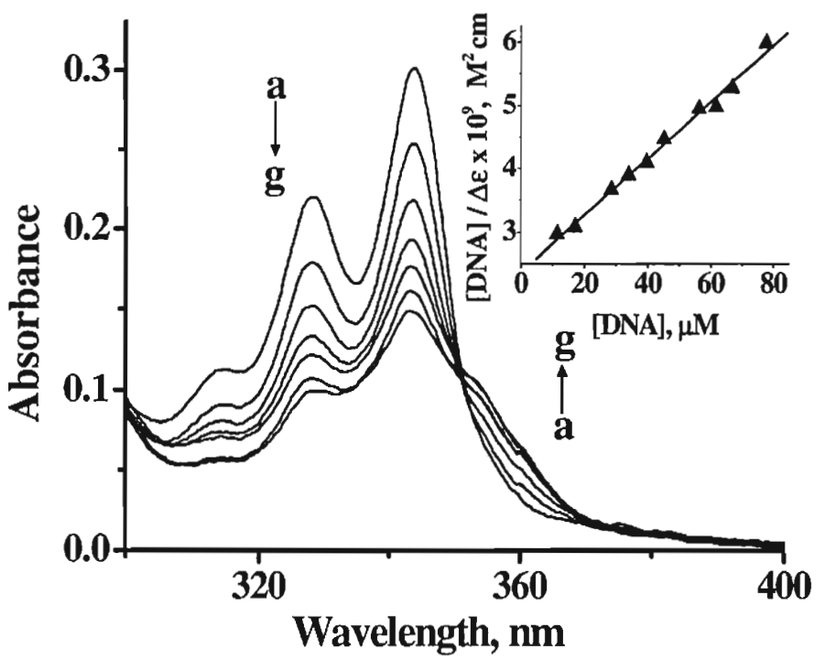

Figure 3.5. Absorption spectra of **2** (1.05 x 10^{-5} M) in the presence of CT DNA in phosphate buffer (10 mM, pH 7.4) containing 2 mM NaCl. [DNA] (a) 0, b) 0.015, (c) 0.017, (d) 0.029, (e) 0.034, (f) 0.039 and (g) 0.045 mM. Inset shows the corresponding half- reciprocal plot.

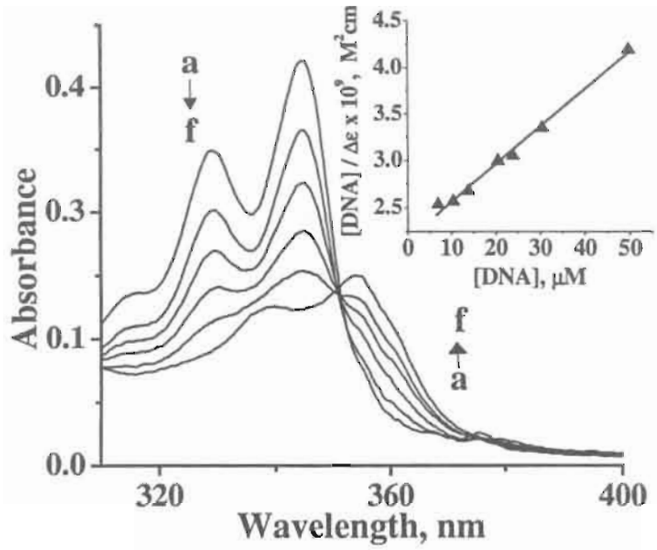

Figure 3.6. Absorption spectra of **3** (2 x 10^{-5} M) in the presence of CT DNA in phosphate buffer (10 mM, pH 7.4) containing 2 mM NaCl. [DNA] (a) 0, (b) 0.010, (c) 0.014, (d) 0.024, (e) 0.031 and (f) 0.049 mM. Inset shows the corresponding half-reciprocal plot.

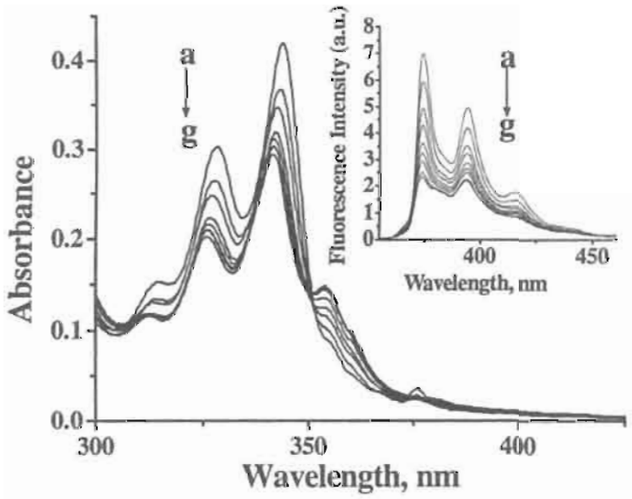

Figure 3.7. Absorption spectra of **4** (1.8 x 10^{-5} M) in the presence of CT DNA in phosphate buffer (10 mM, pH 7.4) containing 2 mM NaCl. [DNA] (a) 0, (b) 0.023, (c) 0.035, (d) 0.046, (e) 0.069, (f) 0.079 and (g) 0.091 mM. Inset shows the corresponding changes in fluorescence spectra; excitation wavelength 351 nm.

Table 3.1. DNA binding (K_{DNA}) properties and binding site sizes (n) of conjugates 1-3 and model compound 4 in phosphate buffer (10 mM, pH 7.4)[a]

Compound	K_{DNA}[b], M^{-1}	n[c]	T_m, °C[d]
1	1.1×10^4	1.4±0.2	60
2	1.9×10^4	1.7±0.2	63
3	2.3×10^4	1.8±0.3	66
4	2.6×10^4	1.9±0.3	67

[a] The data are the average of more than two independent experiments and the error is ca. ±5%.[b] Calculated as reported in reference (21). [c] Binding site size. [d] Thermal denaturation temperature of a duplex DNA1.DNA2 in phospahet buffer (10 mM, pH 7.4). DNA1: 5'-CGT GGA CAT TGC ACG GTA C-3'; DNA2: 5'-GTA CCG TGC AAT GTC CAC G-3'.

Ionic strength of the medium plays a major role in determining the mode of ligand-DNA interactions.[22] For example, intercalative mode of interaction exhibit negligible changes in the association constants with increasing ionic strength of the medium, whereas ligands that undergo electrostatic interactions exhibit decrease in association constant with increase in ionic strength of the medium. To evaluate the mode of binding interactions of the viologen linked pyrene conjugates with DNA, we have monitored the changes in the absorption spectrum of the conjugate **1** with increasing concentration of DNA in 10 mM phosphate buffer containing different concentrations of NaCl (Figure 3.8). Addition of DNA to a solution of **1** in 10 mM phosphate buffer containing 100 and 500 mM NaCl

resulted in gradual decrease in absorbance at 345 nm, with maximum hypochromicity (~46% and 42%, respectively) at 0.06 mM of DNA. The viologen linked conjugate **1**, which showed K_{DNA} = 1.1±0.05 x 10^4 M^{-1} in phosphate buffer

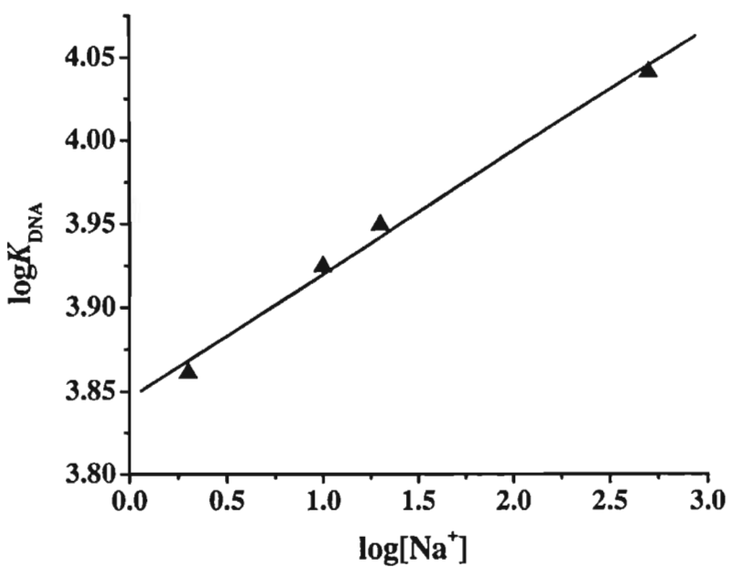

Figure 3.8. The plot of logarithm of binding constant K_{DNA} versus negative logarithm of sodium ion concentration in phosphate buffer (10 mM, pH 7.4) showing the linearity fit.

containing 2 mM NaCl, exhibited a marginal decrease in values of K_{DNA} = 0.9, 0.84 and 0.66±0.04 x 10^4 M^{-1}, respectively, at 50, 100 and 500 mM NaCl. From the values of K_{DNA} obtained for **1** at different salt concentrations, we calculated the value of counter ion release of 0.09 per molecule. The non-electrostatic contribution to the change in free energy (ΔG) of association at 300 K is calculated to be -23.1 kJM^{-1}, which is in agreement with the reported values for the intercalating dyes such as ethidium bromide.[22]

3.3.2. DNA Sequence Selective Binding Properties

With a view to understanding the binding selectivity, we have carried out the interactions of the selected viologen linked pyrene derivatives with duplexes such as poly(dA).poly(dT), poly(dG).poly(dC) and CT DNA, under different salt concentrations. Figure 3.9 shows the effect of polynucleotide such as poly(dG).poly(dC) concentration on the absorption spectra of the viologen linked

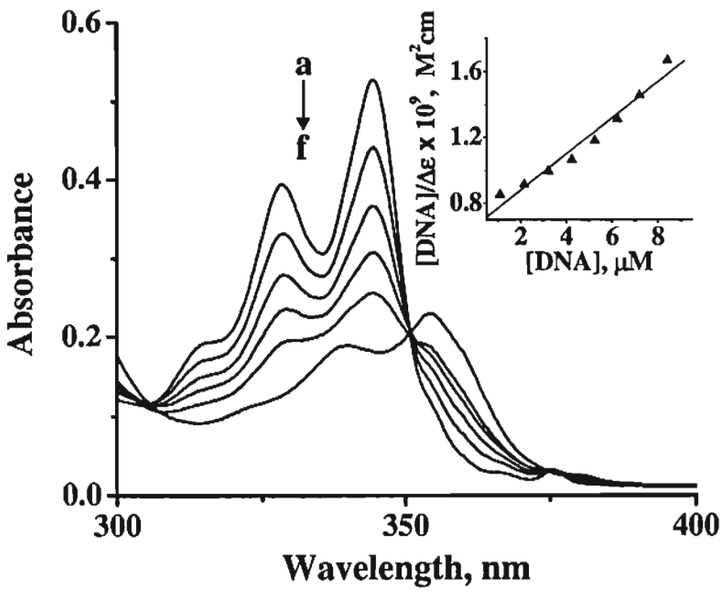

Figure 3.9. Absorption spectra of **1** (1.9 x 10^{-5} M) in the presence of poly(dG).poly(dC) in phosphate buffer (10 mM, pH 7.4) containing 2 mM NaCl. [poly(dG).poly(dC)] (a) 0, b) 0.002, (c) 0.004, (d) 0.006, (e) 0.008 and (f) 0.009 mM. Inset shows the corresponding half-reciprocal plot of **1**.

pyrene conjugate **1**, whereas the inset of Figure 3.9 shows the corresponding half-reciprocal plot. In the case of the derivative **1**, we observed significant hypochromicity with increasing in concentration of poly(dG).poly(dC), whereas

only marginal decrease in absorbance was observed with the duplex poly(dA).poly(dT) (Figure 3.10). From the half- reciprocal plots, we calculated the binding constants of the conjugate **1**, which are found to be K_{DNA} = 1.65 ± 0.06 x 10^4 M^{-1} and 0.84 ± 0.03 x 10^4 M^{-1}, respectively, for the different duplexes poly(dG).poly(dC) and poly(dA).poly(dT).

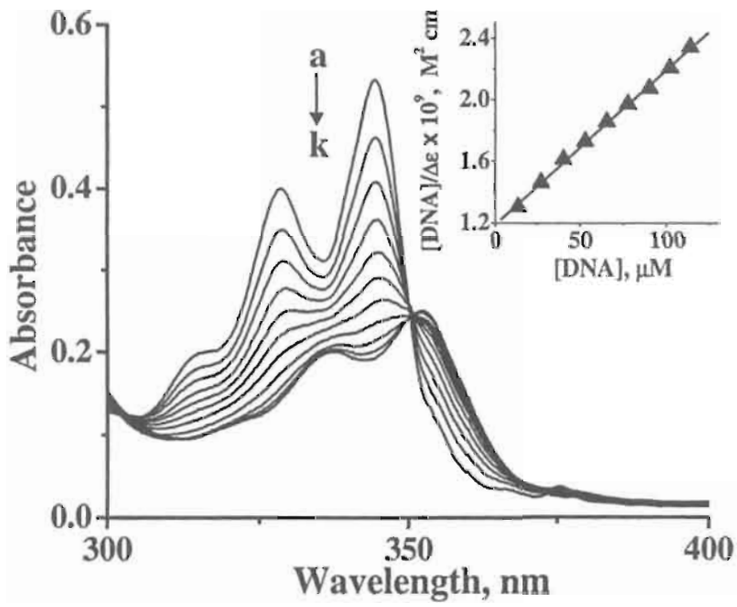

Figure 3.10. Absorption spectra of **1** (1.9 x 10^{-5} M) in the presence of poly(dA).poly(dT) in phosphate buffer (10 mM, pH 7.4) containing 2 mM NaCl. [poly(dA).poly(dT)] (a) 0, b) 0.01, (c) 0.02, (d) 0.04, (e) 0.05, (f) 0.06, (g) 0.08, (h) 0.09, (i) 0.10 and (k) 0.11 mM. Inset shows the corresponding half-reciprocal plot.

Further confirmation on the nature of interaction of the viologen linked pyrene derivatives with DNA was demonstrated using thermal denaturation, CD, viscometric and CV studies. Circular dichroism studies are useful in identifying

the binding modes of organic ligands with DNA. Binding of an achiral molecule within a chiral environment, such as DNA, can lead to the induced optical activity of the bound species.[23] Figure 3.11 shows the positively bisignated induced CD spectra of viologen linked pyrene conjugate **1** corresponding to the pyrene moiety with increasing concentration of DNA. Similar observations were made in the case of the higher viologen linked pyrene conjugates **2** and **3**.

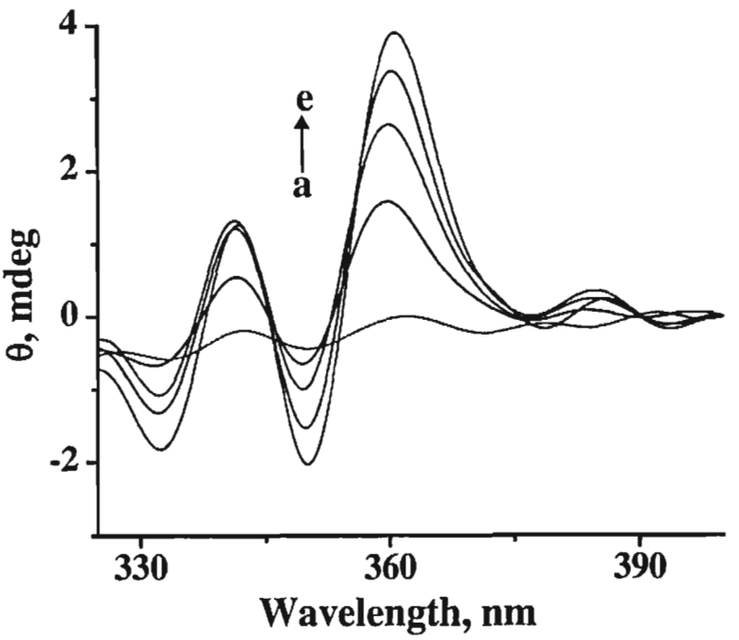

Figure 3.11. Circular dichroic (CD) spectra of CT DNA (0.9 mM) in the (a) absence and (b-e) presence of **1**. [**1**] (a) 0.0, (b) 0.09, (c) 0.17, (d) 0.26 and (e) 0.34 mM.

Viscosity of DNA is known to be sensitive to the mode of interaction of a ligand with DNA.[24] For example, if a ligand binds through intercalative interactions with DNA, it exhibits significant increase in the length of the DNA resulting in enhancement in the viscosity of DNA. To have a better understanding

of the interactions, the viscosity measurements of DNA were carried out in the presence and absence of various viologen linked pyrenes. Figure 3.12 shows the change in viscosity of DNA with the increase in addition of the viologen linked pyrene derivatives. Results indicate that the relative viscosity of DNA increases proportionally with the binding affinity of the derivatives as observed from the absorption studies. The derivative with the longer spacer length **3** showed maximum increase in the relative viscosity of DNA as compared to **1** and **2**.

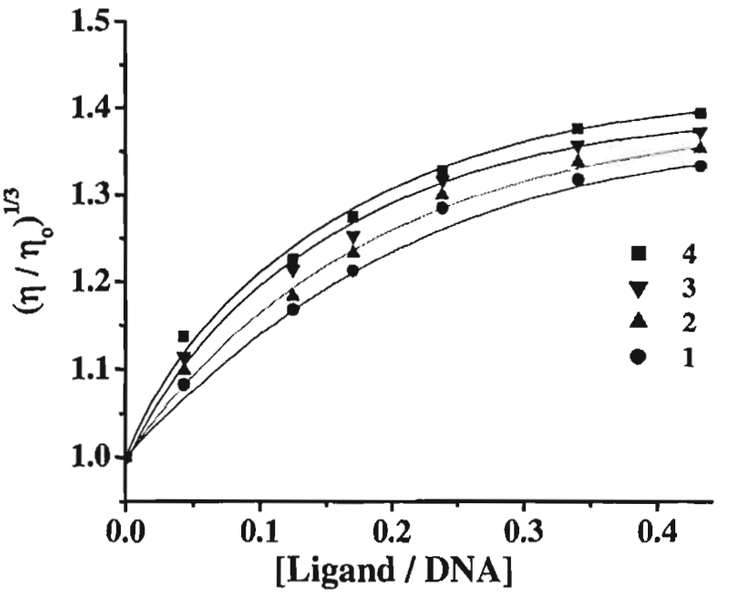

Figure 3.12. The effect of increasing concentrations of the viologen linked conjugates **1-3** and model compound **4** on the relative viscosity of CT DNA (0.88 mM) at 25 ± 0.2 ^{0}C in phosphate buffer (10 mM, pH 7.4).

Electrochemical studies of DNA-binding ligands have a potential importance in probing the DNA-ligand interactions and in electrochemical detection of DNA.[25] The complexation of a ligand within a macromolecule such as

DNA can reduce the mobility of the ligand thereby resulting in the decrease in the intensity of current. Moreover, ligands are expected to exhibit significant changes in their redox properties in the presence of DNA, which can be characteristic of their mode of binding interactions. Figure 3.13 shows the cyclic voltammograms of the conjugate **1** in the presence and absence of DNA. The conjugate **1,** shows

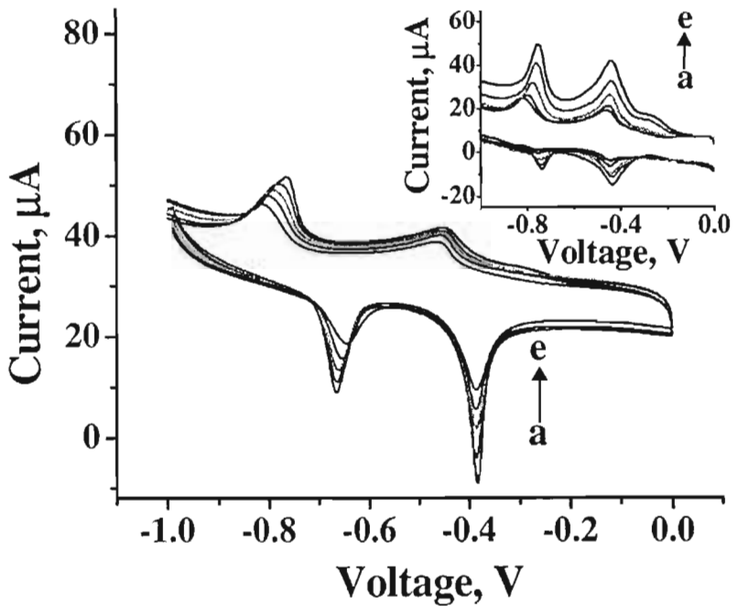

Figure 3.13. Cyclic voltammograms of **1** (0.26 mM) in 26 mM NaCl (pH 7.4) with increasing concentrations of DNA. [DNA] a) 0, b) 0.045, c) 0.09, d) 0.18 and e) 0.36 mM. Scan rate, 100 mV/s. Inset shows the corresponding square wave voltammograms.

two reversible one-electron reduction processes centered at -0.44 and -0.75 V, characteristic of the viologen moiety. In contrast, in presence of DNA, we observed an increase in the magnitude of reduction potentials by 22 and 70 mV, along with a significant decrease in current intensity of 22.7 μA (54%) and 25.1

μA (50%). The changes in the current intensity and the reduction potentials clearly indicate the formation of a strong complex between DNA and the conjugate **1**. Similar cyclic voltammograms were obtained with the higher conjugates **2** and **3** in the presence and absence of DNA.

Intercalation of the ligands with duplex DNA and interstrand crosslink formation during irradiation are known to increase the DNA melting temperature (T_m), *i.e.* the temperature at which the double helix denatures to single stranded DNA.[26] The extinction coefficient of DNA bases at 260 nm in the double helical form is much less than that of the single strand form; hence, melting of the helix leads to an increase in the absorption at this wavelength. Thus, the helix to coil transformation can be determined by monitoring the absorbance of the duplex at 260 nm as a function of temperature.[26,27] In order to understand the extent of interaction of the viologen linked pyrene conjugates with DNA, we have examined the stabilization of DNA duplex in the presence of these molecules using DNA thermal denaturation technique of duplex **DNA1.DNA2**. Figure 3.14 shows the thermal denaturation curves for the duplex **DNA1.DNA2**, in the absence and presence of the viologen linked pyrene conjugates **1-3** and the model derivative **4**. DNA melting temperature was evaluated from the corresponding first derivative plots and are summarized in the Table 3.1. The DNA duplex alone showed a melting temperature (T_m) of 53 °C without any additive, while in the presence of **1-3** and the model derivative **4**, the melting temperatures were found to be 60 °C, 63 °C, 66

°C and 67 °C, respectively, indicating significant stabilization of the duplex in the presence of these conjugates.

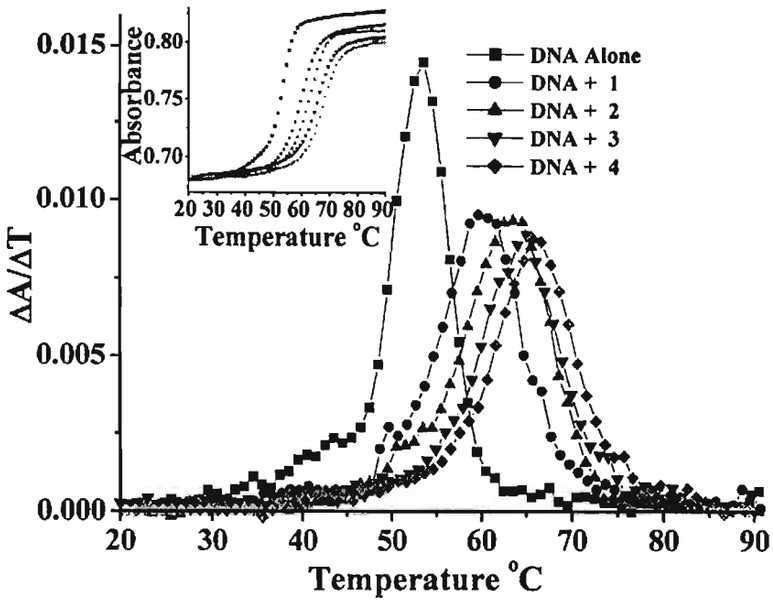

Figure 3.14. Differential thermal denaturation curves for the DNA duplex, DNA1.DNA2 in the absence (T_m = 53 °C) and presence of **1** (20 μM, T_m = 60 °C), **2** (20 μM, T_m = 63 °C), **3** (20 μM, T_m = 66 °C) and **4** (20 μM, T_m = 67 °C). DNA 1: 5'-CAC TGG CTT TTC GGT GCA T- 3'; DNA 2: 5'-ATG CAC CGA AAA GCC AGT G-3'. Inset shows the corresponding thermal denaturation curves.

3.3.3. Photoactivated DNA Cleaving Properties

Among various methods, the most convenient technique for analysis of DNA damage is the DNA relaxation assay (Figure 3.15). This assay makes use of the fact that supercoiled DNA (plasmid, bacteriophage DNA, mitochondrial DNA) (Form I) is converted by either single-strand cleavage or the incision of a repair endonuclease into a relaxed circular DNA (Form II), which migrates separately

from the supercoiled form in agarose gel electrophoresis. When several repair endonucleases are used in parallel with this technique, DNA profiles are obtained which give the relative frequencies of various endonuclease sensitive damage

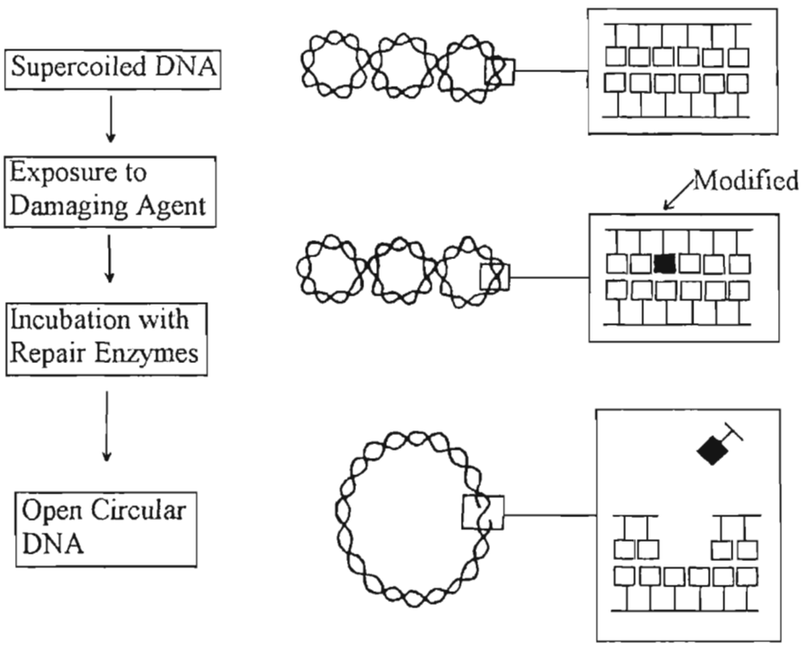

Figure 3.15. Schematic representation of transformation of supercoiled DNA to relaxed circular DNA.

and serve as fingerprints of the ultimate damaging species and also the mechanism of DNA damage.[28] However, the transformation of the supercoiled form directly to linear form (Form III) indicates the coincident-site, double strand cleavage. The supercoiled, circular and linear forms of plasmid DNA can be separated by agarose gel electrophoresis and can be easily visualized by staining with a fluorescent dye. To evaluate the biological activity and to understand the

type of modifications induced by the viologen linked pyrene conjugates, we examined the cleavage of supercoiled DNA from bacteriophage PM2 (PM2 DNA, 10^4 bp) in the presence and absence of various repair endonucleases.[29] The recognition spectrum of various enzymes is summarized in Figure 3.16.[28]

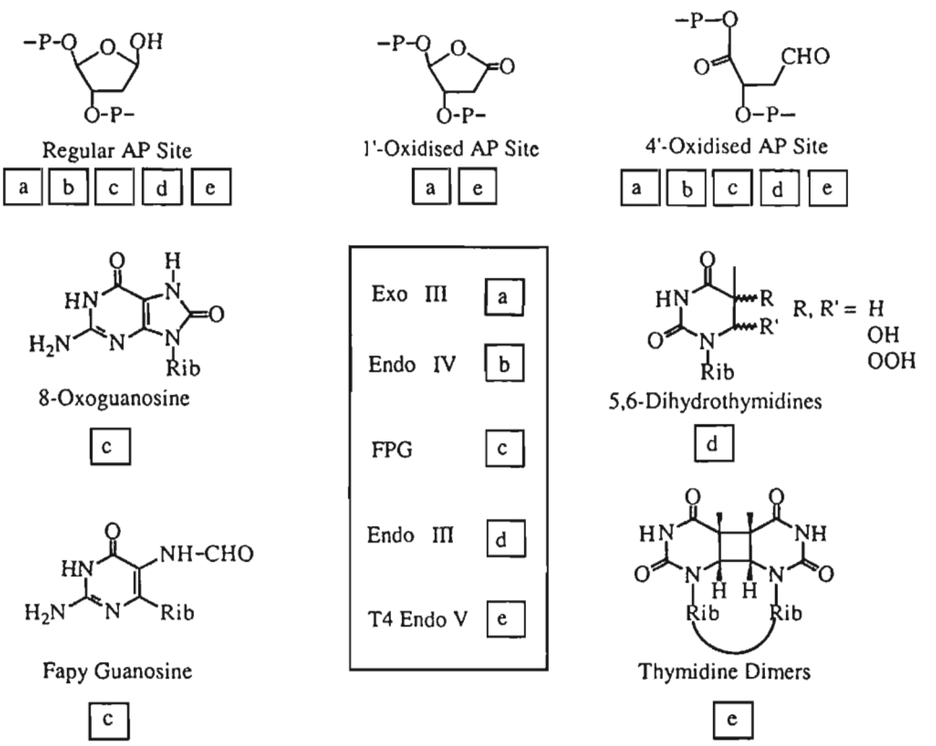

Figure 3.16. Recognition spectrum of various repair endonucleases.

Phosphate-buffered (pH 7.0), air-saturated solutions of PM2 DNA (10 μg/mL) were exposed at 0 °C to near-UV irradiation (360 nm) in the presence of various concentrations of the viologen linked pyrene derivatives **1** and **2** (Chart 3.1). Subsequently, the DNA was analyzed for the following types of modifications: (i) DNA single and double strand breaks; (ii) sites of base loss (AP sites) recognized

by exonuclease III; (iii) base modifications plus AP sites sensitive to the T4 endonuclease V; (iv) base modifications plus AP sites sensitive to the endonuclease III and (v) base modifications plus AP sites sensitive to formamidopyrimidine-DNA glycosylase (FPG protein). Figure 3.17 shows the DNA damage profiles of the viologen linked pyrenes **1** and **2**. It is evident from the damage profiles, that both these compounds induce very few AP sites and few modifications sensitive to endonuclease III, but a large number of base modifications sensitive to FPG protein. Compound **1** (n = 1) was found to be more effective (ca. 2-fold) in inducing DNA damage compared to **2** (n = 3). However, no SSBs were observed, in each case. Further, no significant DNA damage was observed either by irradiation of PM2 DNA alone or in the dark in presence of the viologen linked pyrenes **1** and **2** at the highest concentrations, thereby indicating that the damage observed is purely initiated by the photoactivated compounds.

Figure 3.18 shows the irradiation time dependent formation of single-strand breaks (SSBs) and FPG sensitive modifications induced by viologen linked pyrene conjugate **1**. The damage sensitive to FPG protein induced by **1,** increases withincreasing irradiation time. No significant increase in SSBs was observed, even after irradiation for 30 min. Figures 3.19-3.21 show the concentration dependent formation of single-strand breaks (SSBs) and FPG sensitive modifications induced by viologen linked pyrene conjugates **1-3** and for the comparison, the model compound pyrene. An increase in FPG-sensitive modifications was observed with increasing concentration of the conjugate **1**. Similar observations were made with the higher

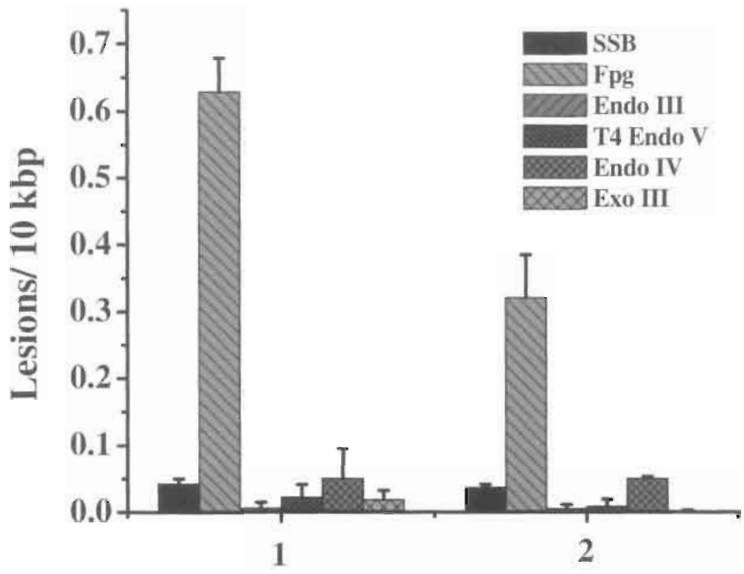

Figure 3.17. DNA damage profiles. Single strand breaks and various endonuclease-sensitive modifications induced in PM2 DNA by photoactivated viologen linked pyrene conjugates **1** (10 μM, 90 kJ m^{-2}) and **2** (10 μM, 90 kJ m^{-2}).

conjugates **2** and **3**, but with significantly reduced efficiency. The FPG modifications induced by these derivatives are found to be ca. 2 and 10-fold, respectively, lower for higher conjugates as compared to the conjugate **1** (n = 1). In contrast, the model compound pyrene alone (inset of Figure 3.21) induced no significant DNA modifications even at high concentrations (20 μM); indicating its inefficiency in inducing the DNA damage.

To test the possible role of various reactive species such as superoxide radical anion, hydrogen peroxide and singlet oxygen on the DNA damage, the generation of FPGs by the photoactivated viologen linked pyrene conjugates **1-3** was investigated in the presence of various additives and scavengers. These

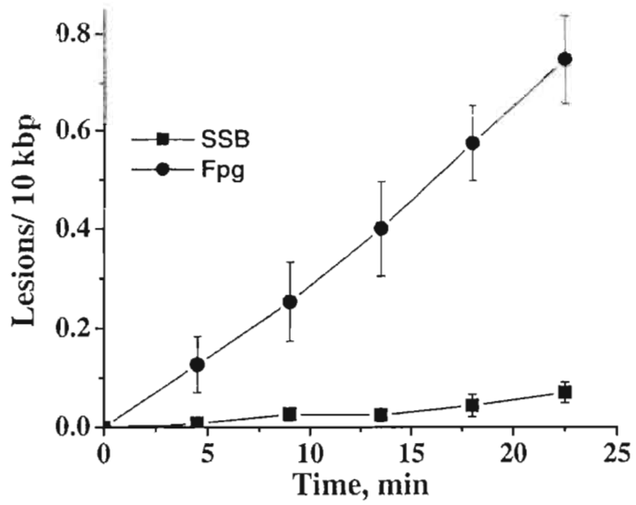

Figure 3.18. The time dependence of DNA modifications, SSB (■) and FPG (•), induced in PM2 DNA by **1** (10 μM, 0 °C) upon UV irradiation with 360 nm light (90 kJ m^{-2}).

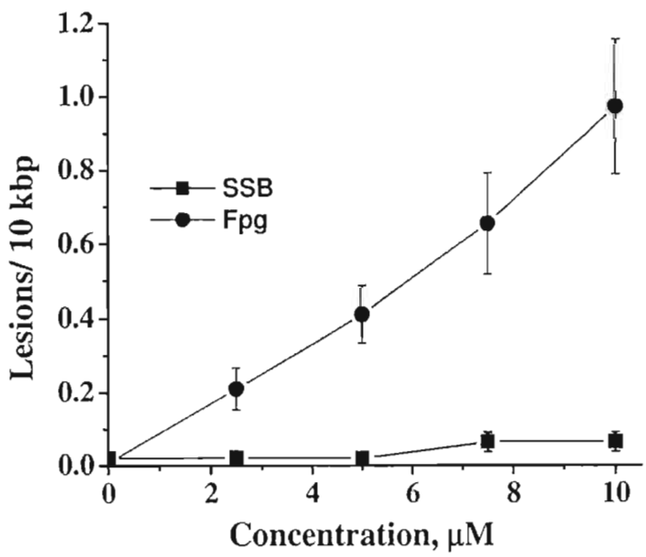

Figure 3.19. The concentration dependence of DNA modifications, SSB(■) and FPG (•), induced in PM2 DNA by **1** (0 °C) upon UV irradiation with 360 nm light (90 kJ m^{-2}).

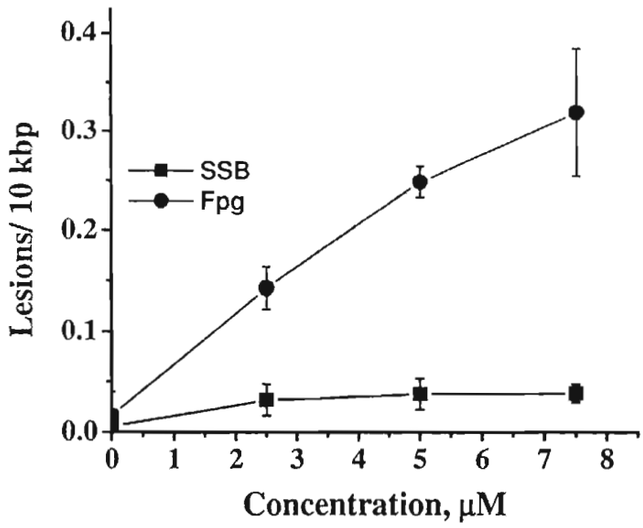

Figure 3.20. The concentration dependence of DNA modifications, SSB(■) and FPG (•), induced in PM2 DNA by **2** (0 °C) upon UV irradiation with 360 nm light (90 kJ m^{-2}).

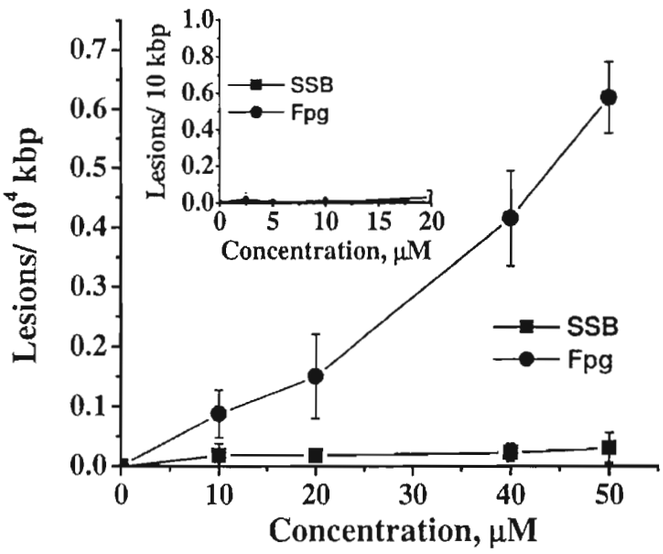

Figure 3.21. The concentration dependence of DNA modifications, SSB(■) and FPG (•), induced in PM2 DNA by **3** (0 °C) upon UV irradiation with 360 nm light (90 kJ m^{-2}). Inset shows concentration dependence of DNA modifications, SSB (■) and FPG (•), induced in PM2 DNA by pyrene (0 °C) upon UV irradiation with 360 nm light (90 kJ m^{-2}).

include catalase, superoxide dismutase and by replacing H_2O in the buffer with D_2O. For example, Figure 3.22 shows the ratio of FPG modifications induced by viologen linked pyrene conjugates **1-3** in normal and D_2O buffer media. As can be seen from Figure 3.22, no significant effect on FPG modifications was observed when H_2O was replaced by D_2O, ruling out the involvement of singlet oxygen. Superoxide dismutase is known to catalyze the reduction of superoxide radical anion to hydrogen peroxide while catalase converts hydrogen peroxide to water and molecular oxygen and hence studies with these enzymes have been very useful in understanding the involvement of superoxide radical anion and hydrogen peroxide in the DNA damage. We observed negligible effect in the FPG sensitive modifications in the presence of catalase and superoxide dismutase, indicating that

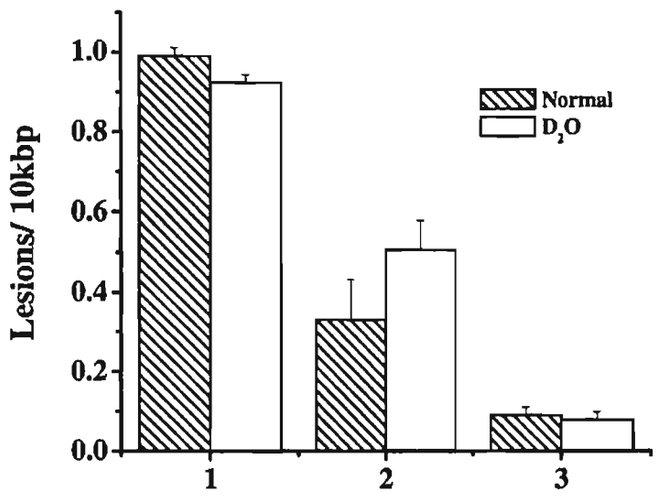

Figure 3.22. FPG sensitive modifications in D_2O buffer and H_2O buffer induced in PM2 DNA by the conjugates **1-3** (0 °C) upon UV irradiation with 360 nm light (90 kJ m^{-2}).

neither superoxide radical anion nor hydrogen peroxide are responsible for the DNA damage induced by the photoactivated viologen linked pyrene conjugates **1-3**.

3.3.4. Cellular Localization and Cytotoxicity Studies

The efficacy of photosensitization depends on the close proximity of photosensitizers and their targets. Therefore, if the targets are cells, the pharmacokinetics of photosensitizer at the cellular and subcellular level are important. The predominant localization sites for most of the photosensitizers are nucleus, cytoplasm, mitochondria and the lysosomes. Depending on the nature of the chromophore such as lipophilicity, charge and amphiphilicity, diverse patterns of cellular localization are observed.[30] To understand the site of localization of the viologen linked pyrene conjugates, we have investigated the localization of these compounds in L1210 cells employing fluorescence microscopy. Figure 3.23 shows the fluorescence microscopic image of L1210 cells in the presence of the viologen linked pyrene conjugate **1** incubated for different time intervals. Upon incubating the L1210 murine leukemia cells with the derivative **1** (10 μM) for 1 min at 37 °C, the fluorescence microscope images clearly showed the sparse fluorescence of the pyrene chromophore in the cytoplasm. This indicates that these molecules preferentially localize in the cytoplasm but not in the nucleus.[31] With increasing in time of incubation of the L1210 cells in the presence of conjugate **1**, we observed increase in the intensity of fluorescence of the pyrene chromophore in the cytoplasm and exhibited maximum intensity and reached saturation at around 30 min.

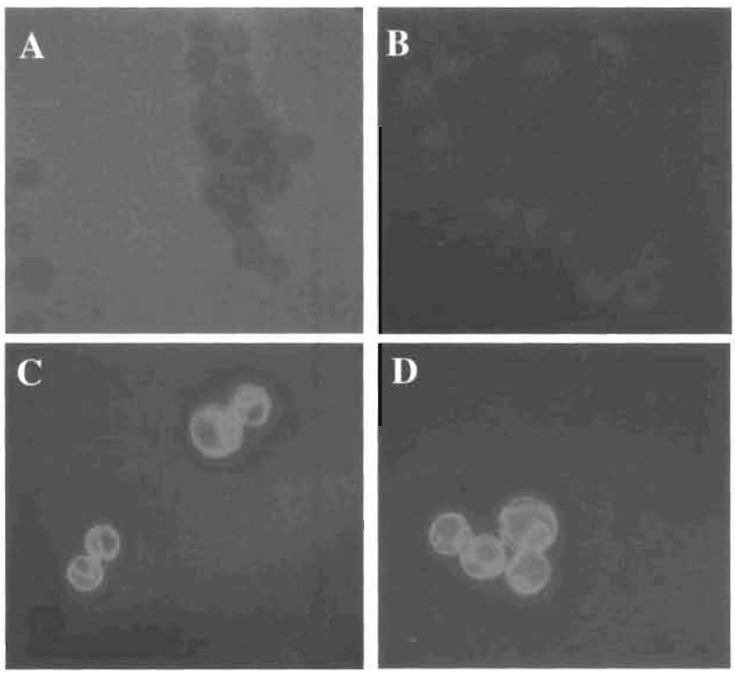

Figure 3.23. Intracellular localization of **1** (10 μM) in L1210 murine leukemia cells incubated for different time intervals at 37 °C; A) 1, B) 5, C) 15 and D) 30 min. Images were obtained using inverted fluorescence microscope.

To evaluate the potential use as phototherapeutical agents, we examined the cytotoxicity induced by various viologen linked pyrene conjugates in hematopoetic cancer cell line growing in suspension, L1210 murine leukemia cells. Experiments were carried out by exposing various concentrations of these derivatives with and without irradiation, and the percentage survival of the cells in full medium were determined subsequently after extensive washing. Figure 3.24 shows the cytotoxicity induced by the viologen linked pyrene conjugates **1** and **2**. In the presence of light, the derivative **1** reduced the number of cells, counted after

48 h, to less than 20% at concentrations as low as 20 μM. In the dark, the cell survival was found to be almost 100% at the same concentration, indicating non-toxicity of the system in the dark. The higher homologue **2** (n = 7), on the other hand, showed comparable cytotoxicity (ca. 20% survival) even at half the concentrations (10 μM), when compared to the viologen linked pyrene conjugate **1** (20 μM). These results clearly indicate that these molecules show significant toxicity only upon irradiation and that spacer length and substituents play major role in the biological activity of the viologen linked pyrenes conjugates.

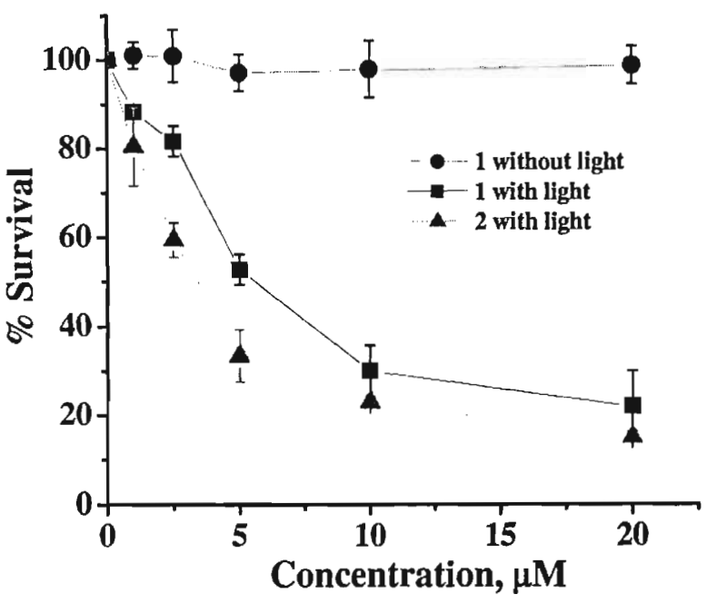

Figure 3.24. Cytotoxicity of the viologen linked pyrene conjugates **1** and **2** in L1210 murine leukemia cells. Data give the percentage cell survival counted 48h after the treatment for 22.5 min at 0 °C with various concentrations of the viologen linked pyrene conjugates with and without UV irradiation using 360 nm light (90 kJm^{-2}). Data points represent the mean of 3 independent experiments (±SD).

3.4. Discussion

Interaction of the viologen linked pyrene conjugates with CT DNA, we observed a strong hypochromic effect along with a red shift of 7 nm in the absorption spectra. This could be attributed to the π-π stacking of the pyrene chromophore between DNA bases through intercalation. This interpretation is based on the experimental evidence and literature reports.[19] The observation of negligible changes in DNA association constants of the viologen linked pyrenes upon increasing ionic strength of the medium from 2 to 500 mM and -23.1 kJ/mol of non-electrostatic contribution to the change in free energy, clearly suggests that these molecules undergo predominantly intercalative interactions with DNA.

Furthermore, the increase in values of DNA association constants with increase in spacer length of viologen linked pyrene conjugates, indicates that spacer groups separating the pyrene chromophore and viologen moiety play major role in the stabilization of such DNA-ligand complexes.[17b] This could be attributed due to the steric constraints of the viologen moiety arising from the proximity with the intercalating pyrene moiety. The observation of increase in DNA viscosity in presence of the bifunctional conjugates,[24] bisignated induced CD signal corresponding to the pyrene chromophore in the presence of DNA, decrease in the current intensity corresponding to the viologen moiety in the presence of DNA and decrease in K_{DNA} values with increasing ionic strength of the buffer confirm that *these systems undergo predominantly intercalative interaction with DNA.*

The observation of predominantly Fpg sensitive modifications in the case of the viologen linked pyrenes confirms that the photoinduced charge-separated base radical cation, once formed, results in the oxidative DNA damage. This leads to the formation of products such as 8-hydroxyguanosine and formamidopyrimidines, which are recognized by FPG protein. In addition, the observation of only Fpg selective modifications clearly demonstrates the involvement of electron transfer mechanism in the DNA damage induced by various viologen linked pyrene conjugates. The possibility of involvement of singlet oxygen and hydroxyl radical intermediates can be ruled out, since the damage profiles observed are quite different from that induced by the disodium salt of 1,4-etheno-2,3-bensoxlioxin-1,4-dipropanoic acid ($NDPO_2$), a singlet oxygen generator and ionizing radiation, which is a source of hydroxyl radicals. Furthermore, neither hydrogen peroxide nor superoxide radical anion is involved in the damage induced by these systems, since the number of Fpg modifications were not altered in the presence of superoxide dismutase and catalase or in the presence of both these enzymes. These results clearly indicate the fact that the DNA modifications induced by these molecules originate from the oxidation of guanosine, since guanine has the lowest ionization potential. Moreover, the selective oxidation of guanine in DNA can also be rationalized by the mechanism of fast hole hopping even if the initial electron transfer caused by the photoexcited viologen-linked pyrene occurs at a remote site in the DNA duplex.

The cytotoxicity studies using L1210 murine leukemia cells indicate that the viologen linked pyrene conjugates **1** and **2** exhibit efficient cytotoxicity upon photoexcitation. In contrast to the efficiency of DNA cleavage induced by these systems, the higher therapeutic index, given by the ratio of concentrations in the dark and upon irradiation, is observed for the derivative **2** (n = 7), when compared to the conjugate **1** (n = 1). This clearly indicates that spacer group such as polymethylene linker plays a major role in their cellular intake as well as their efficiency of generation of cytotoxic agents. Results of these investigations indicate that this new series of bifunctional conjugates are stable in aqueous medium, efficient in oxidizing guanosine and DNA through photoinduced electron transfer mechanism, preferentially localize in the cytoplasm and induce cytotoxicity only upon photoactivation and hence can have potential use as phototherapeutic agents.

3.5. Conclusions

The photobiological studies of the viologen linked pyrene derivatives **1-3** clearly demonstrate that these systems undergo predominantly intercalative interactions with DNA and exhibit 2:1 preference for poly(dG).poly(dC) over poly(dA).poly(dT) duplexes. Photoexcitation of these bifunctional derivatives in the presence of PM2 DNA and subsequent analysis confirms that the charge-seperated base radical cation, once formed, results predominantly in the oxidative DNA damage. It was furthermore confirmed that most of the DNA damage

induced by these systems was recognized by Fpg protein, which is known to recognize oxidized DNA products such as 8-hydroxyguanosine and formamidopyrimidines. Further, the viologen linked pyrene derivatives, under investigation, were found to be non-toxic in the dark and as expected exhibited significant cytotoxicity only upon photoexcitation. These novel bifunctional systems are found to undergo efficient intercalative interactions DNA, localize in the cytoplasm and cleave DNA only through co-sensitization mechanism and can have potential use as phototherapeutic agents.

3.6. Experimental Section

3.6.1. General Techniques

An Elico pH meter was used for pH measurements. The electronic absorption spectra were recorded on a Shimadzu UV-VIS-NIR spectrophotometer. Fluorescence spectra were recorded on a SPEX-Fluorolog F112X spectrofluorimeter. The fluorescence quantum yields were determined by using optically matched solutions. Doubly distilled water was used in all the studies. A solution of calf thymus DNA was sonicated for 1 h to minimize complexities arising from DNA flexibility[24] and filtered through a 0.45 μm Millipore filter (M_w = 3 x 10^5 g mol^{-1}). The concentrations of DNA solutions were determined by using the average value of 6600 M^{-1} cm^{-1} for the extinction coefficient of a single nucleotide at 260 nm.[24] Polynucleotides were dissolved in phosphate buffer, and the concentrations were determined by using the average extinction coefficient

value of 7400 M^{-1} cm^{-1} at 253 nm for poly(dG).poly(dC) and 6000 M^{-1} cm^{-1} at 260 nm for poly(dA).poly(dT).[25] Viscosity measurements of DNA were carried out using calf thymus DNA (0.88 mM) in phosphate buffer (10 mM) containing 2 mM NaCl (pH 7.4) at 25 °C and also in the presence of various viologen linked pyrene derivatives and model derivative under similar conditions.

The DNA binding studies were carried out in 10 mM phosphate buffer (pH 7.4) containing 2, 100 and 500 mM NaCl. The intrinsic binding constant of the viologen linked pyrene derivatives with CT DNA was determined using absorbance at 344 nm recorded after each addition of CT DNA. The intrinsic binding constant K_{DNA} was determined from the half reciprocal plot of $D/\Delta\varepsilon_{ap}$ *vs* D, where D is the concentration of DNA in base pairs, $\Delta\varepsilon_{ap} = [\varepsilon_a - \varepsilon_F]$ and $\Delta\varepsilon = [\varepsilon_b - \varepsilon_F]$.[17] The apparent extinction coefficient, ε_a, is obtained by calculating $A_{[obsd]}$ / [pyrene derivatives]. ε_b and ε_F correspond to the extinction coefficient of the bound form of the pyrene derivatives and the extinction coefficient of the free pyrene derivatives, respectively. The data were fitted to Equation 3.1, with a slope equal to 1/ $\Delta\varepsilon$ and a y-intercept equal to 1/ ($\Delta\varepsilon K_{DNA}$). ε_b was determined from $\Delta\varepsilon$ and K_{DNA} was obtained from the ratio of the slope to the y-intercept. The binding site

$$D/\Delta\varepsilon_{ap} = D/\Delta\varepsilon + 1/(\Delta\varepsilon K_{DNA}) \quad (3.1)$$

size, n, of the viologen linked pyrenes was evaluated by carrying out DNA binding studies at an ionic strength of 10 mM phosphate buffer. The intersection of the two

straight lines drawn through the linear portions of the absorption titration curve gave the binding site size *n*, for the corresponding viologen linked pyrenes.

The counter ion release that accompanies binding of a ligand to DNA can be obtained from the slope of the $\log K_{DNA}$ vs. $-\log[Na^+]$[21] according to Equation 3.2,

$$-\delta \log K_{DNA} / \delta \log [Na^+] = -Z\Psi \qquad (3.2)$$

where Z is charge of the ligand and Ψ represents the average number of condensed and screened sodium ions associated with the DNA phosphate group. The non-electrostatic contributions to the association of ligand with DNA can be obtained from the Equation 3.3,

$$\ln K_{DNA} = \ln K_T^{\,0} + Z\xi^{-1}\ln(\gamma_{\pm}\delta) - Z\Psi \ln[Na^+] \qquad (3.3)$$

where $K_T^{\,0}$ is the equilibrium constant that does not include the free energy of ion release. For the B-form of DNA, the dimensionless polymer charge density ξ is 4.2. The variable δ is $0.33b$, where b is the average axial charge spacing, 1.7 A° for B-form of DNA. The mean activity coefficient at an appropriate salt concentration is $\gamma\pm$ 0.78 at 100 mM NaCl.

3.6.2. Materials

The synthesis of the viologen linked pyrene conjugates **1-3** was achieved in moderate yields through the S_N2 reaction of the corresponding bromoalkylpyrene derivative with 1-butyl-4,4'-bipyridinium bromide as described in Chapter 2 (Section 2.6.3) of this thesis. Calf thymus DNA (Pharmacia Biotech, USA), polynucleotides (Amersham Pharmacia Biotech Inc.) were obtained and used as

received. 1-Butyl-4,4'-bipyridinium bromide was obtained in 95% yield by the reaction of 4,4'-bipyridine with 1-bromobutane in the molar ratio of 3:1 in dry acetonitrile.[11] DNA from bacteriophage PM2 (PM2 DNA) was prepared according to the method of Salditt et al.[32] More than 95% was in the supercoiled form, as determined by the reported method. Formamidopyrimidine-DNA glycosylase[33] and Endonuclease were obtained from Dr. B. Epe.[34] T4 endonuclease V was partially purified by the method of Nakabeppu et al.[35] Exonuclease III was purchased from Boehringer. All repair endonucleases were tested for their incision at reference modifications under the applied assay conditions to ensure that the correct substrate modifications are fully recognized and no incision at non-substrate modifications take place.

3.6.3. Cell culture

L1210 cells were cultured in suspension in Rosewell Park Memorial Institute-1640 supplemented with antibiotics, 0.25 mg/mL L-glutamine, 107 μg/mL sodium pyruvate and 10% heat inactivated horse serum. Cell cultures were grown in a humidified atmosphere with 5% CO_2 in air at 37 ^{0}C.

3.6.4. Thermal Denaturation of DNA

The thermal denaturation temperature (T_m) of oligonucleotide duplexes in the presence and absence of viologen linked pyrenes were obtained in 10 mM phosphate buffer (pH 7.0) by using a thermoelectrically controlled Perkin Elmer spectrophotometer, interfaced to a PC-XT computer for the acquisition and

analysis of experimental data. The instrument was set at 260 nm and the temperature was scanned at a heating rate of 1 °C min^{-1}. The absorption data were plotted as a function of temperature. Under these conditions, the T_m value of 19 mer, [DNA(1).DNA(2)], without additive is 53 °C. The melting curves shown are the normalized melting curves. The percentage of hypochromicity in these measurements was calculated using equation 3.4,

$$H\% = \frac{\Delta A_0 - \Delta A_s}{\Delta A_0} \times 100 \qquad (3.4)$$

where, ΔA_0 and ΔA_s are the change in absorbance observed during complete denaturation of DNA in the absence and presence of a particular concentration of viologen linked pyrene derivatives, respectively.

3.6.5. DNA Relaxation Assay and Quantification of DNA Modifications in PM2 DNA

The exposure of PM2 DNA (10 μg/mL) to near-UV (360 nm, 9 and 18 kJ/m^2) radiation in the presence and absence of viologen linked pyrenes was carried out on ice in phosphate buffer (5 mM KH_2PO_4, 50 mM NaCl, pH 7.4) by means of a black light lamp (Osram HQV). The DNA was precipitated by ethanol/sodium acetate and re-dissolved in BE_1 buffer (20 mM Tris-HCl, pH 7.5, 100 mM NaCl, 1 mM EDTA) for damage analysis. A DNA relaxation assay was used to quantify endonuclease-sensitive modifications and strand breaks. It makes

use of the fact that supercoiled PM2 DNA is converted by either a single strand break (*SSB*) or the incision of a repair endonuclease into a relaxed (nicked) form which migrates separately from the supercoiled form in agarose gel electrophoresis. Quantification of both forms of DNA by staining with ethidium bromide followed by fluorescence scanning allows the determination of the number of single strand breaks per PM2 molecule (10^4 bp). If an incubation with repair endonucleases precedes the gel electrophoresis the number of single strand breaks plus endonuclease-sensitive sites (*ESS*) are obtained[42,43] through the equation 3.5,

$$SSB + ESS = -\ln[1.4 \times II/(1.4 \times I + II)] \qquad (3.5)$$

where, *I* and *II* are the fluorescence of the supercoiled and relaxed forms, respectively.

An aliquot of 0.3 μg of the modified PM2 DNA in 20 μL BE_1 buffer was incubated for 30 min at 37 °C with 10 μL of BE_1 buffer (for the determination of directly produced strand breaks) or with one of the following repair endonuclease preparations: (i) exonuclease III, 300 U/mL in 20 mM Tris-HCl, pH 8.0, 100 mM NaCl, 15 mM $CaCl_2$; (ii) FPG protein, 3 μg/mL in BE_1 buffer; (iii) endonuclease III, 40 ng/mL in BE_1 buffer; (iv) T4 endonuclease V, 90 μg/mL in BE_{15} buffer (BE_1 buffer containing 15 mM EDTA). The reactions were stopped by addition of 3 μL of 10% sodium dodecyl sulfate and the DNA applied to an agarose slab electrophoresis gel. After electrophoresis and staining with ethidium bromide, the

relative amounts of the supercoiled and nicked forms of the DNA were determined using a fluorescence scanner (FTR20, Sigma Instruments, Berlin). From these values the average number of single strand breaks per DNA molecule produced either directly by the damaging agent or by the subsequent enzymatic incision at the endonuclease-sensitive modifications were calculated according to the equation 6.

3.6.6. Cytotoxicity Studies

Cytotoxic studies were carried out using L1210 Cells. These cells were pre-incubated for 3-5 min with the viologen linked pyrene conjugates **1-2** in Ca^{2+} and Mg^{2+} free phosphate buffered saline (PBS) (140 mM NaCl, 3 mM KCL, 8 mM Na_2HPO_4, 1 mM KH_2PO_4, 0.1% glucose, pH 7.4) and then irradiated on ice (10^6 cells/mL) with visible light from a 1000 W halogen lamp (PF811) at a distance of 33 cm for 15 min, corresponding to 337.5 kJ/m^2 between 400 and 800 nm. The viologen linked pyrene conjugates **1-2** were removed by two centrifugation steps and resuspended in full medium at 1 or 2 x 10^5 cells/mL. Exponentially growing L1210 cells in suspension were counted after 48 using Coulter counter.

3.7. References

1. Lambert, B.; LePecque, J. –B. In *DNA-Ligand Interactions. From Drugs to Proteins*; Guschlbauer, W.; Saenger, W. Eds.; Plenum: New York, 1986, p 141.

2. Waring, M. J. In *Drug Action at the Molecular Level*; Roberts, G. K. Ed.; Macmillian: London, 1977, pp 167-189.

3. Pullman, B.; Jortner, J. *Molecular Basis of Specificity in Nucleic Acid–Drug Interactions*; Kluwer Academic Publishers: Netherlands, 1990.

4. Nielsen, P. E. *J. Mol. Recognit.* **1990**, *3*, 1-25.

5. Canter, C.; Schimmel, P. R. *Biophysical Chemistry*; W. H. Freeman and Co.: San Francisco, 1980, Vol. 2, p 398.

6. Kumar, C. V. In *Photochemistry in Organized Media*; Ramamurthy, V. Ed.; VCH: New York, 1991, pp 783-816.

7. Wemmer, D. E.; Dervan, P. B. *Curr. Opin. Struct. Biol.* **1997**, *7*, 355-361.

8. (a) Waring, M. J. *Annu. Rev. Biochem.* **1981**, *50*, 159-192. (b) Tomasz, M. In *Molecular Aspects of Anticancer-Drug Interactions*; Neidle, S., Waring, M. J., Eds.; Macmillan Press: Boca Raton, FL, 1994, Vol. 2, pp 312-349. (c) Bischofberger, N.; Shea, R. G. In *Nucleic Acid Targeted Drug Design*; Propst, C. L., Perun, T. J., Eds.; Dekker: New York, 1992, pp 579-612.

9. (a) Dougherty, T. J. *Photochem. Photobiol.* **1987**, *45*, 879-885. (b) Bonnett, R. *Chem. Soc. Rev.* **1995**, *24*, 19-33. (c) MacRobert, A. J.; Philips, D. *Chem. Ind.* **1992**, 17-19. (d) Kessel, D. *Photodynamic Therapy of Neoplastic Disease*; CRC Press: Boca Raton, FL, 1990, Vol. 2. (e) Henderson, B. W.; Dougherty, T. J. *Photochem. Photobiol.* **1992**, *55*, 145-153. (f) Bonnett, R. *Chemical Aspects of Photodynamic Therapy*; Gordon and Breach Science Publishers: The Netherlands, 2000.

10. (a) Foote, C. S. *Science* **1968**, *162*, 963-979. (b) Weishapaut, K. R.; Gomer, C. J.; Dougherty, T. J. *Cancer Res.* **1976**, *36*, 2326-2329. (c) Kochevar, I. E. *Photochem. Photobiol.* **1987**, *45*, 891-895. (d) Ben-Hur, E.; Carmichael, A.; Riesz, P.; Rosenthal, I. *Int. J. Radiat. Biol.* **1985**, *48*, 837-846.

11. (a) Laustriat, G. *Biochimie* **1986,** *68*, 771-778. (b) Piette, J.; Merville-Louis, M.-P.; Decuyoer, J. *Photochem. Photobiol.* **1986**, *44*, 793-802. (c) Cadet, J.; Berger, M.; Deccaroz, C.; Wagner, J. R.; van Lier, J. E.; Ginot, Y. M.; Vigny, P. *Biochimie* **1986**, *68*, 813-834. (d) Kochevar, I. E.; Dunn, D. A. in *Photosensitized Reactions of DNA*: *Cleavage and Addition*; Morrison, H. Ed., Bioorganic Photochemistry, Wiley: New York, 1990, pp. 273-316, Vol. 1.

12. (a) Epe, B. *Chem. Biol Interact.* **1991**, *80*, 239. (b) Halliwell, B.; Arumo, O. I. *FEBS lett.* **1991**, *281*, 9-19.

13. (a) Ciulla, T. A.; Van Camp, J. R.; Rosenfield, E.; Kochevar, I. E. *Photochem. Photobiol.* **1989**, *49*, 293-298. (b) Epe, B.; Mutzel, P.; Adam, W, *Chem. Biol. Interact.* **1988**, *67*, 149-165. (c) Piette, J.; Calberg-Bacq, C. -M.; van de Vorst, *Photochem. Photobiol.* **1981**, *49*, 293-298. (d) OhUigin, C.; McConnell, D. J.; Kelly, J. M.; van der Putten, W. J. M. *Nucleic Acids Res.* **1987**, *15*, 7411. (e) Schneider, J. E; Price, F. S.; Maidt, M. L.; Gutteridge J. M. C.; Floyd, R. A. *Nucl. Acid Res.* **1990**, *18*, 631-635. (f) Floyd, R. A.; West, M. S.; Schneider, J. E.; Watson, J. J.; Maidt, M. L. *Free Radic. Biol. Med*, **1990**, *9*, 76-81.

14. (a) Blazek, E. R.; Hariharan, P. V. *Photochem. Photobiol.* **1984**, *40*, 5-13. (b) Ben-Hur, E.; Fujihara, T.; Suzuki, F.; Elkind, M. M. *Photochem. Photobiol.* **1987**, *6*. 859-865. (c) Ramakrishnan, N. M.; Clay, E.; Xue, L. - Y.; Evans, H. H.; Rodriguez, A.; Oleinick, N. L. *Photochem. Photobiol.* **1988**, *48*, 297-303. (d) Uggla, A. H.; Sundell-Bergman, S. *Mutat. Res.* **1990**, *236*, 119-127.

15. (a) Averbeck, D. *Photochem. Photobiol.* **1989**, *6*, 859-882. (b) Lamola, A. A.; Yamane, T. *Proc. Natl. Acad. Sci. USA* **1967**, *58*, 443-446.

16. Leng, F.; Savkur, R.; Fork, I.; Prezewloke, T.; Priebe, W.; Chaires, J. B. *J. Am. Chem. Soc.* **1996**, *118*, 4731-4738.

17. Wilson, W. D.; Ratmeyer, L.; Zhao, M.; Strekovski, L.; Boykin, D. *Biochemistry* **1993**, *32*, 4098-4104.

18. Sammes, P. G.; Yahioglu, G. *Chem. Rev.* **1994**, 327-334.

19. (a) E. C. Long, J. K. Barton, *Acc. Chem. Res.* **1990**, *23*, 271-273. (b) H. M. Berman, P. R. Young, *Annu. Rev. Biophys. Bioeng.* **1981**, *10*, 87-114. (c) G. Dougherty, W. J. Prigram, *Crit. Rev. Biochem.* **1982**, *12*, 103-132. (d) C. Cantor, P. R. Schimmel, *Biophysical Chemistry*; W. H. Freeman: San Fransisco, 1980; Vol 2, pp 398-413.

20. Asato, A. E.; Zhang, B. W.; Denny, M.; Mirzadegan, T.; Liu, R. S. H. *J. Bioorg. Chem.* **1998**, *17*, 410-415.

21. (a) Kumar, C. V.; Asuncion, E. H. *J. Am. Chem. Soc.* **1998**, *115*, 8547-8553. (b) Modukuru, N. K.; Snow, K. J.; Perrin, B. S. Jr.; Thota, J.; Kumar, C. V. *J. Phys. Chem. B* **2005**, *109,* 11810-11818.

22. Petty, J. R.; Bordelon, J. A.; Robertson, M. E. *J. Phys. Chem. B* **2000**, *104*, 7221-7227.

23. (a) Dalgleish, D. G.; Peacocke, A. R. *Biopolymers* **1971**, *10*, 1853-1863. (b) Fiel, R. J.; Munson, B. R. *Nucleic Acids Res.* **1980**, *8*, 2835-2842. (c) Nordén, B.; Tjerneld, F. *Biopolymers* **1982**, *21*, 1713-1734. (d) Kubista, M.; Aakerman, B.; Nordén, B. *J. Phys. Chem.* **1988**, *92*, 2352-2356.

24. (a) Baguley, B. C.; Falkenhaug, E.-M. *Nucleic Acids Res.* **1978**, *5*, 161-171. (b) Deng, H.; Cai, J.; Xu, H.; Zhang, H.; Ji, L. *J. Chem. Soc. Dalton Trans.,* **2003**, 325-330.

25. Takenaka, S.; Ihara, T.; Takagi, M. *J. Chem. Soc., Chem. Commun.*, **1990**, 1485-1487.

26. (a) Gasparro, F. P. *Psoralen DNA Photobiology*; CRC Press Inc.: Boca Raton, Florida, 1988. (b) Patel, D. J.; Cannel, L. *Proc. Natl. Acad. Sci. USA* **1976**, *73*, 674-678.

27. Adam, W.; Berger, M.; Cadet, J.; Dall'Acqua, F.; Epe, B.; Frank, S.; Ramaiah, D.; Raoul, S.; Saha-Moller, C. R.; Vedaldi, D. *Photochem. Photobiol.* **1996**, *63*, 768-778.

28. (a) Epe, B.; Pflaum, M.; Haring, M.; Hegler, J.; Rudiger, H. *Toxicol. Lett.* **1993**, *67*, 57-72. (b) Epe, B.; Haring, M.; Ramaiah, D.; Stopper, H.; Abou-

Elzahab, M.; Adam, W.; Saha-Moller, C. R. *Carcinogenesis* **1993**, *14*, 2271-2276.

29. These experiments were carried out in collaboration with Professor Dr. B. Epe at the University of Mainz, Germany.

30. (a) Li, G.; Graham, A.; Chen, Y.; Dobhal, M. P.; Morgan, J.; Zheng, G.; Kozyrev, A.; Oseroff, A.; Dougherty, T. J.; Pandey, R. K. *J. Med. Chem.* **2003**, *46*, 5349-5359. (b) Hubbell, J. A. *Science*, **2003**, *300*, 595-596. (c) Savic, R.; Luo, L.; Eisenberg, A.; Maysinger, D.*Science* **2003**, *300*, 615-618.

31. (a) Dalton, W. S.; Sheper, R. J. *J. Natl. Cancer Inst.* **1999**, *91*, 1647–53. (b) Carreon, J. R.; Roberts, M. A.; Wittenhagen, L. M.; Kelley, S. O. *Org. Lett.* **2005**, *7*, 99-102.

32. Saldit, M.; Braunstein, S. N.; Camerini-Otero, R. D.; Franklin, R. M. *Virology* **1972**, *48*, 259-262.

33. Boiteux, S.; O' Conner, T. R.; Lederer, F.; Gouyette, A.; Laval, J. *J. Biol. Chem.* **1990**, *265*, 3916-3922.

34. Asahara, H.; Wistort, P. M.; Bank, J. F.; Bakerian, R. H.; Cunningham, R. P. *Biochemistry* **1989**, *28*, 4444-4449.

35. Riazzudin, S. In *Methods in Enzymology,* Grossman, L., Moldave, K. Eds.; Academic Press: New York, 1980, Vol. 65, pp 185-191.

Chapter 4

STUDY OF INTERACTIONS OF A FEW VIOLOGEN LINKED ACRIDINES WITH β-CYCLODEXTRIN

4.1. Abstract

Interactions of β–cyclodextrin (β–CD) with a few novel viologen linked acridine conjugates having rigid aromatic **1a–c** and flexible methylene **2a–c** spacer groups have been investigated through photophysical, chiroptical, electrochemical and atomic force microscopic (AFM) techniques. The dyads with *para*-tolyl **1a** and biphenyl **1c** spacer groups exhibited significantly decreased fluorescence quantum yields and lifetimes when complexed with β–CD, while negligible changes were observed for the *ortho*-isomer **1b**. In contrast, the conjugates **2a-c** with flexible spacer units, in the presence of β–CD, showed spacer length dependent significantly increased fluorescence quantum yields and lifetimes. Association constants for the complexes formed between β–CD and various dyads have been calculated and the complexation was confirmed using AM1 calculations, competitive ligand displacement, circular dichroism (CD), cyclic voltammetry (CV), ^{1}H NMR and AFM techniques. The intramolecular electron transfer rates (k_{ET}) have been estimated and are found to increase nearly 2-fold for

the dyads with *para*-tolyl and biphenyl spacer groups when complexed with β–CD, whereas significantly decreased k_{ET} values (ca. 15-fold) were observed for the dyads with flexible spacer group. These results demonstrate that the complexation of donor-acceptor conjugates having aromatic spacer group, with β–CD unusually leads to planarization of the conjugate resulting in enhanced electron transfer processes between the donor and acceptor moieties, while conformational unfolding of sandwich type of structure occurs in the dyads having flexible spacer groups.

4.2. Introduction

The study of interactions of cyclodextrins (CDs) with drugs and photoactive molecules has been an active area of research in recent years as they mimic the biological environment.[1] Cyclodextrins are cyclic oligosaccharides consisting of six to nine glucose units and are called α–, β–, γ–, and δ–cyclodextrins, respectively.[2] CDs are water soluble and have not only rigid,[3a] well–defined torus shape with relatively apolar interior, but also rotational symmetry with an asymmetric environment.[1-3] These cyclic systems are known to form inclusion complexes with a variety of compounds, ranging from low molecular weight non–polar aliphatic molecules, polar amino acids to high molecular weight polymeric materials, depending on the size of CD cavity and the cross sectional area of the guest molecules.[4] Because of these unique properties, CDs have found wide applications in pharmaceutical industry, catalysis,

separation technology, and recently in the design of biomimetic systems, supramolecular architectures and molecular machines.[5] Moreover, the hydrophobic and spatial control of CD inclusion processes have been extensively exploited for not only using them as drug carriers,[6] in catalysis[7] and separation technology,[8] but also in controlling the reactivity and in understanding the photochemical properties of a variety of functional molecules.[9] Of these systems, the electron donor–acceptor conjugates[10,11] have attracted great attention, since inclusion of such systems in CDs not only alter the interactions between the donor and acceptor moieties but also results in supramolecular architectures that are useful as molecular machines.[12,13]

The rate of intramolecular electron transfer (k_{ET}) in a donor–acceptor conjugate is dependent on several parameters. These include, free energy change, the distance between the donor and acceptor units, nature and their orientation, and the intervening medium.[14] Of these factors, the distance between the donor and acceptor, which also involves the nature of the spacer group is the most important factor, because of the approximately exponential decrease of the rates with increasing distance.[14,15] Although the interactions of CDs with donor–acceptor molecules having flexible spacers have been reported,[10,11,16] to the best of our knowledge, the systems with sterically bulky and rigid aromatic spacers have received less attention. This Chapter presents our results obtained through investigation of interactions of β–cyclodextrin (β–CD) with a few selected novel donor–acceptor dyads **1a–c** and **2a–c** (Figure 4.1), which are biologically

important and are efficient in cleaving DNA through the co–sensitization mechanism.[17] Upon inclusion in β–CD, we observed reduced k_{ET} for **2a–c** with

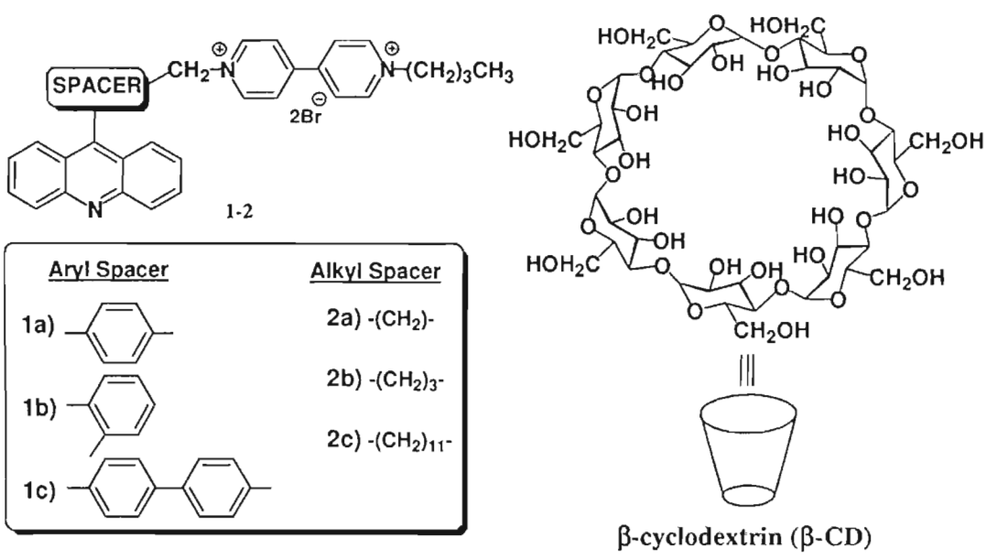

Figure 4.1. Structures of the viologen linked acridine derivatives **1a-c** and **2a-c** and β-cyclodextrin (β-CD) used in the present study.

flexible spacer, negligible changes for **1b** with sterically bulky spacer group but surprisingly enhanced k_{ET} for **1a** and **1c** with rigid aromatic spacer. Results of these investigations demonstrate for the first time that inclusion of the donor–acceptor dyads with the rigid aromatic spacer in β–CD leads to planarization of the dyad and thereby facilitates an effective interaction between the donor and acceptor moieties present in it.

4.3. Results

4.3.1. Synthesis of a Few Viologen Linked Acridines

Synthesis of the viologen linked tolylacridines **1a** and **1b** was achieved as shown in Scheme 4.1. The *ortho*- and *para*-tolylacridines **3a** and **3b**, respectively were synthesized by the reaction of diphenylamine with the corresponding toluic acids

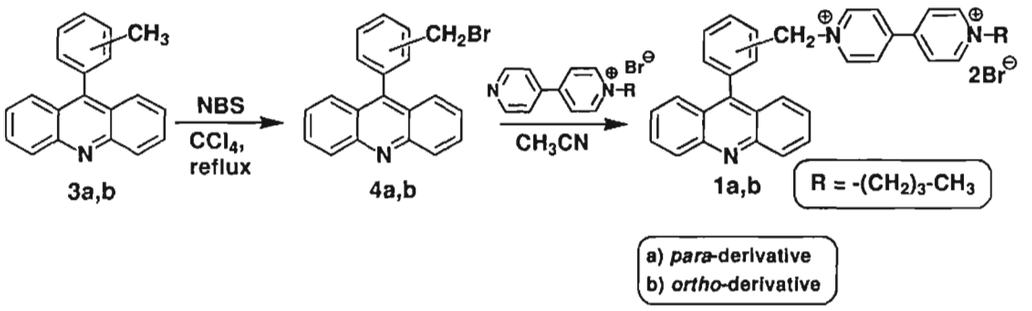

Scheme 4.1

in presence of anhydrous zinc chloride using a modified Bernthsen procedure.[18] These derivatives were then converted to the corresponding bromo derivatives **4a** (60%) and **4b** (56%) by the reaction with N-bromosuccinimide. Finally, the synthesis of the viologen linked tolylacridine derivatives was achieved by the reaction of the corresponding bromotolylacridine derivative with 1-butyl-4,4'-bipyridinium bromide. Thus, for example, the reaction of the bromo derivative **4a** with 1-butyl-4,4'-bipyridinium bromide yielded the viologen linked *para*-tolylacridine **1a** in 77% yield.[17a] Similarly, the reaction of **4b** with 1-butyl-4,4'-bipyridinium bromide, gave the viologen linked *ortho*-tolylacridine derivatives **1b** in quantitative yields.

Synthesis of the bromoalkylacridine **7** was achieved by a modified Bernthsen procedure (Scheme 4.2). The condensation reaction of diphenylamine with 4-methyl biphenylcarboxylic acid in presence of anhydrous zinc chloride gave 10% of the acridine derivative **7**, which in turn was converted to **8** (54%) by the reaction with N-bromosuccinimide as shown in Scheme 4.2. Reaction of **8** with 1-butyl-4,4'-bipyridinium bromide gave the product, **1c**, in 35% yield.

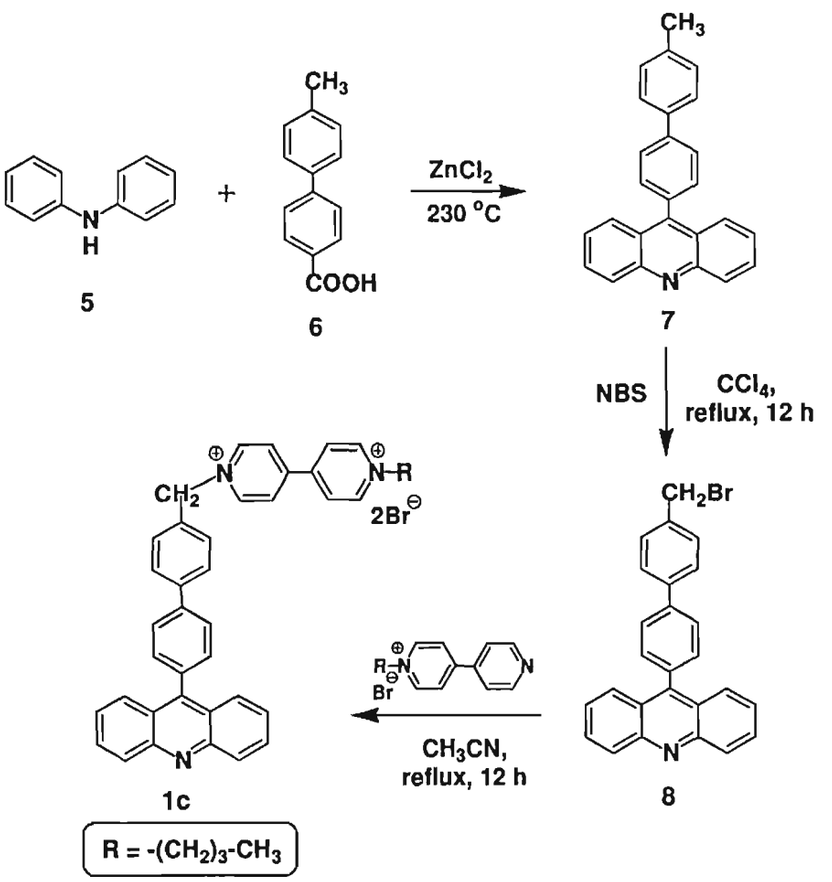

Scheme 4.2

Synthesis of the viologen linked acridine conjugates **2a-c** has been achieved as per the Scheme 4.3. S_N2 reaction of 1-butyl-4,4'-bipyridinium bromide with corresponding bromoalkylacridines **9-11** gave the viologen linked acridine conjugates **2a-c**, in 65-77% yield.[17b] All these compounds were purified through recrystallization and characterized on the basis of spectral data and analytical evidence. ^{1}H NMR spectrum of the viologen linked tolylacridine **1a** in DMSO-d_6, for example, showed a peak corresponding to the methylene group between the phenyl and viologen moieties at δ 6.3 as a singlet, while the aromatic protons

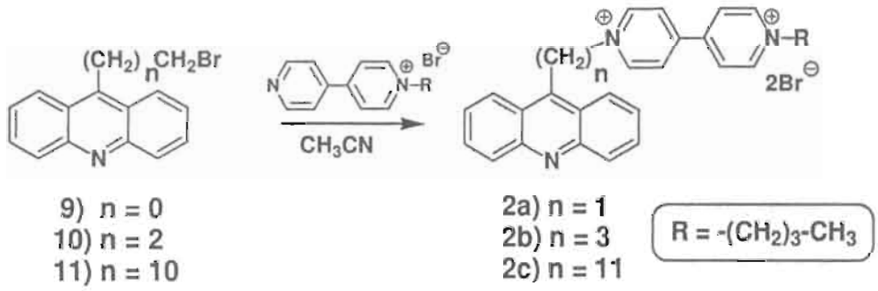

Scheme 4.3

corresponding to the acridine and viologen moieties appeared as multiplets in the region between δ 7.5 and δ 9.85. In the case of the viologen linked *ortho*-tolyl derivative **1b**, the methylene group between the phenyl and viologen moieties appeared at δ 5.6. On the other hand, viologen linked acridine **1c** showed peak corresponding to the methylene group between biphenyl and acridine moieties at δ 6.30, whereas aromatic protons corresponding to the acridine, biphenyl and viologen moieties appeared as multiplets in the region between δ 6.3 and δ 9.85. In the case of viologen linked acridine **2a**, the methylene group appeared at δ 7.16 as

a singlet, while the aromatic protons corresponding to the viologen and acridine moieties appeared as a multiplet at δ 7.79-9.37 (16H). ^{1}HNMR spectra of **2b** and **2c**, in addition to the other peaks, showed peaks corresponding to the methylene groups at δ 4.60-4.90. The ^{13}C spectrum of **1a** showed five sp^3 carbons appearing at δ 13.33, 18.77, 32.70, 60.64, and 63.87 corresponding to the four carbons of *n*-butyl group and one methylene carbon. The other aromatic carbons appeared in the region between δ 124.2 and δ 149.2. The mass spectra of the derivatives **1a-c** and **2a-c** gave a molecular ion peak in each case corresponding to M^+Br^-, indicating that one of the bromide ions is closely associated with the organic ligand (M^+).

4.3.2. Photophysical Properties in Presence of β-Cyclodextrin

The viologen linked acridine conjugates exhibited high solubility in aqueous medium and obeyed Beer's law under experimental conditions.[17] We observed no evidence for ground–state charge–transfer interaction between the acridine and viologen moieties present in these compounds under these conditions. Figure 4.2 shows the change in fluorescence spectra of **1a** with the increase in addition of β–CD. Upon increasing β–CD concentration, the fluorescence emission spectra corresponding to the acridine chromophore showed a significant quenching (ca. 2–fold). Similar observations were made with the dyad **1c** containing biphenyl spacer (Figure 4.3). In contrast, with the addition of β–CD,

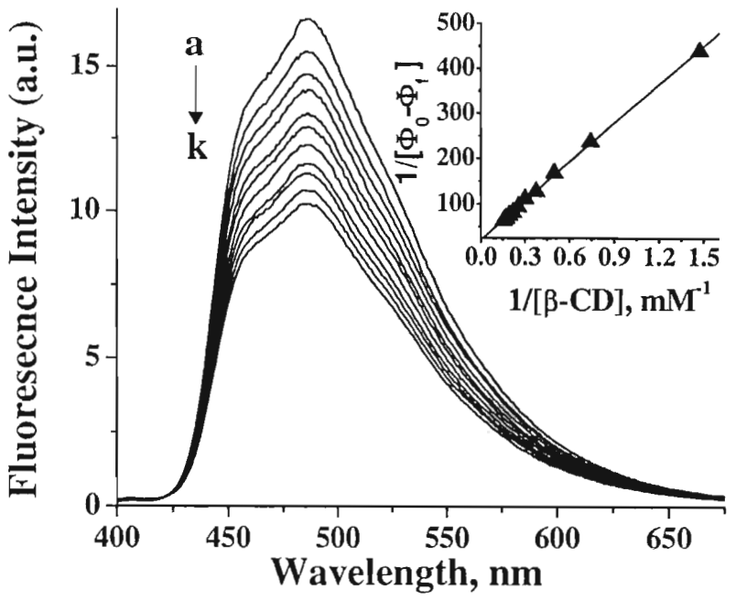

Figure 4.2. Effect of β–CD concentration on the fluorescence spectra of **1a** (4.1×10^{-5} M) and [β–CD] a) 0, (b) 0.68, (c) 1.35, (c) 2.01, (d) 2.67, (e) 3.31, (f) 3.94, (g) 4.57, (h) 5.19, (i) 5.80 and (k) 6.40 mM in water. Inset show the corresponding Benesi–Hildebrand plot.

negligible changes were observed in the absorption spectra of dyads **1a** (Figure 4.4) and also in the absorption (inset of Figure 4.4) and fluorescence spectra of the dyad with *ortho*-tolyl spacer **1b** (Figure 4.5). On the other hand, the donor–acceptor dyads **2a–c,** with the flexible spacer groups (methylene units of n = 1, 3 and 11; Figures 4.6-4.8), exhibited spacer–length dependent increase in fluorescence intensity with increase in addition of β–CD. For example, in the case of the viologen linked acridine conjugate **2c**, we observed ca. 15-fold enhancement in the fluorescence intensity with increase in concentration of β–CD.

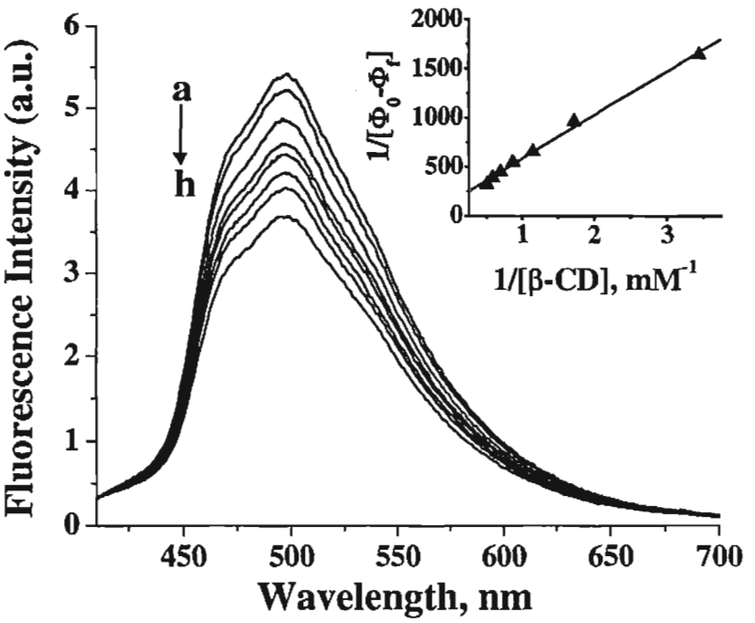

Figure 4.3. Effect of β-CD concentration on the fluorescence spectra of **1c** (9.1 x 10^{-5} M) and [β-CD] (a) 0, (b) 0.29, (c) 0.58, (d) 0.87, (e) 1.16, (f) 1.44, (g) 1.73, and (h) 2.01 mM in water. Excitation wavelength 360 nm. Insets show their corresponding Benesi-Hildebrand plots.

Benesi–Hildebrand analysis of the fluorescence changes (inset of Figures 4.2–4.3 and Figures 4.6-4.8), gave a 1:1 stoichiometry for the complexes formed between β–CD and the dyads **1a, 1c** and **2a–c**. The **1a**–β–CD complex showed an association constant (K_{ass}) of 239 M^{-1} and the corresponding change in free energy value of -13.7 kJM^{-1} (Table 4.1). In the case of the dyad with biphenyl spacer, **1c**– β–CD complex, we observed significantly higher association constant of 325 M^{-1} and change in free energy of -14.3 kJM^{-1}. On the other hand, **2c** with a flexible spacer length of n = 11, exhibited nearly ca. 124–fold higher association constant (K_{ass} = 29600 M^{-1} and ΔG = -25.7 kJM^{-1}), when compared to **1a** (Table 4.1).

However, the dyads **2a** and **2b** showed significantly reduced association constants of 36 and 219 M^{-1}, with the corresponding change in free energy of -8.9 and -13.4 kJM^{-1} respectively, when compared to **2c**.

Table 4.1. Association constants (K_{ass}), free energy change (ΔG) and fluorescence lifetimes (τ) for the complexes formed between β–CD and the donor–acceptor conjugates **1a–c** and **2a–c**.[a]

Compound	K_{ass}[b], M^{-1}	$-\Delta G$[c], kJM^{-1}	τ, ns	$\tau_{\beta-CD}$, ns
1a	239 ± 5[d]	13.7 ± 0.1	5.4 (100 %)	5.4 (69 %)
				0.9 (31%)
1b	Nil	Nil	10.6 (87 %)	e
			0.40 (13 %)	
1c	325 ± 6	14.3 ± 0.1	5.7 (100 %)	5.7 (40%)
				1.4 (60%)
2a	36 ± 2	8.9 ± 0.1	14.6 (100 %)	15.0 (100 %)
2b	219 ± 6[d]	13.4 ± 0.1	13.6 (81 %)	15.5 (82 %)
			2.80 (19 %)	5.80 (18 %)
2c	29600 ± 100	25.7 ± 0.4	14.7 (82 %)	15.0 (82 %)
			1.70 (18 %)	8.30 (18 %)

[a] Average of more than two experiments. [b] K_{ass} was calculated using Benesi–Hildebrand equation. [c] ΔG for the complexes was calculated using equation $-\Delta G = RT\ln K_{ass}$. [d] ^{1}H NMR titrations gave K_{ass} = 337 ± 9 and 224 ± 12 M^{-1} for **1a** and **2b**, respectively. [e] Negligible changes were observed.

To have a better understanding of fluorescence changes observed in presence of β–CD, we have analyzed the interaction of β–CD with the dyads **1a–c** and **2a–c** by picosecond time–resolved fluorescence technique. As shown in

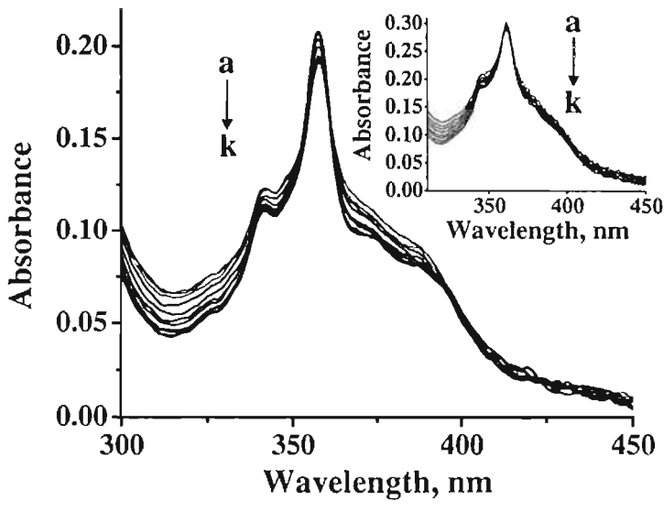

Figure 4.4. Effect of β-CD concentration on the absorption spectra of **1a** (4.1×10^{-5} M) in water. [β-CD] (a) 0, (b) 0.68, (c) 1.35, (d) 2.01, (e) 2.67, (f) 3.31, (g) 3.94, (h) 4.57, (i) 5.19, (j) 5.80 and (k) 6.40 mM. Inset shows the shows the effect of β-CD concentration on the absorption spectra of **1b** under same conditions.

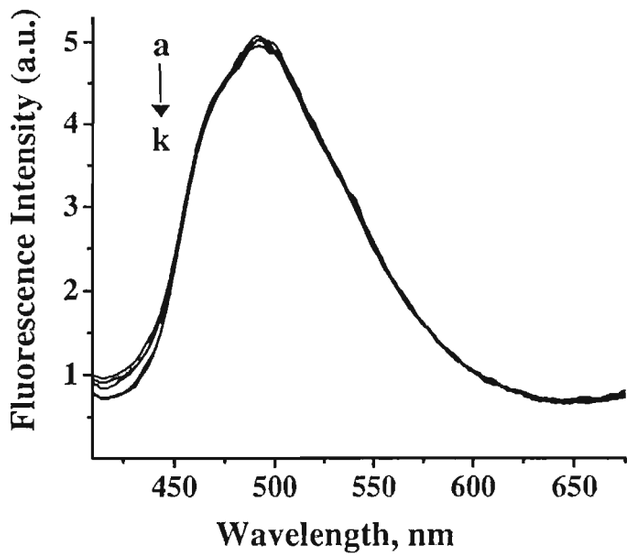

Figure 4.5. Effect of β-CD concentration on the fluorescence emission spectra of **1b** (4.1×10^{-5} M) in water. [β-CD] (a) 0, (b) 0.68, (c) 1.35, (d) 2.01, (e) 2.67, (f) 3.31, (g) 3.94, (h) 4.57, (i) 5.19, (j) 5.80 and (k) 6.40 mM. Excitation wavelength 360 nm.

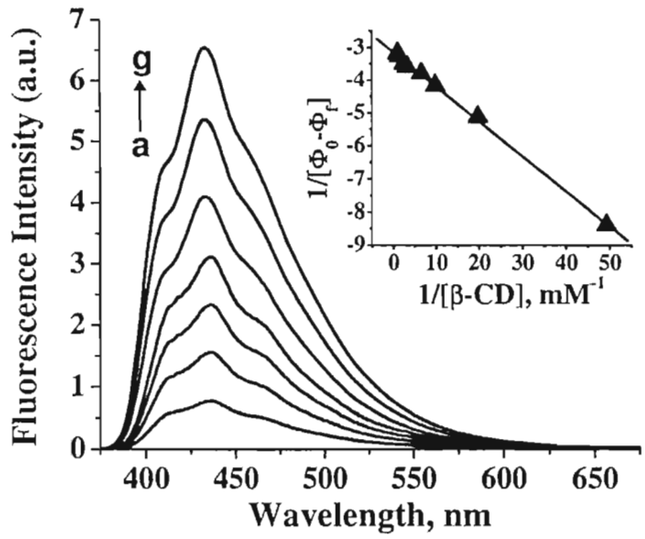

Figure 4.6. Effect of β–CD concentration on the fluorescence spectra of **2c** (4.1×10^{-5} M) and [β–CD] (a) 0, (b) 0.02, (e) 0.07, (g) 0.09 mM. Insets show their corresponding Benesi–Hildebrand plots.

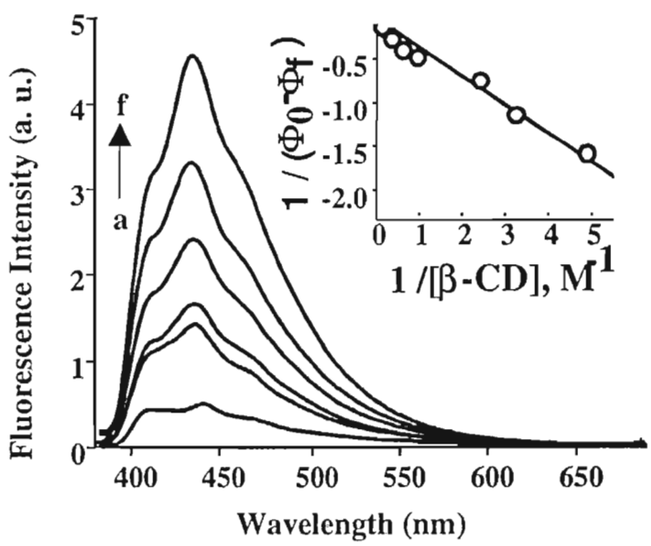

Figure 4.7. Effect of β-CD concentration on the fluorescence emission spectra of **2b** (1.23×10^{-6} M) in water. [β-CD] (a) 0, (b) 0.12, (c) 0.38, (d) 0.63, (e) 0.89 and (f) 6.3 mM. Excitation wavelength, 360 nm. Inset shows Benesi-Hildebrand plot for the change in absorption for **2b** with increasing concentration of β-CD.

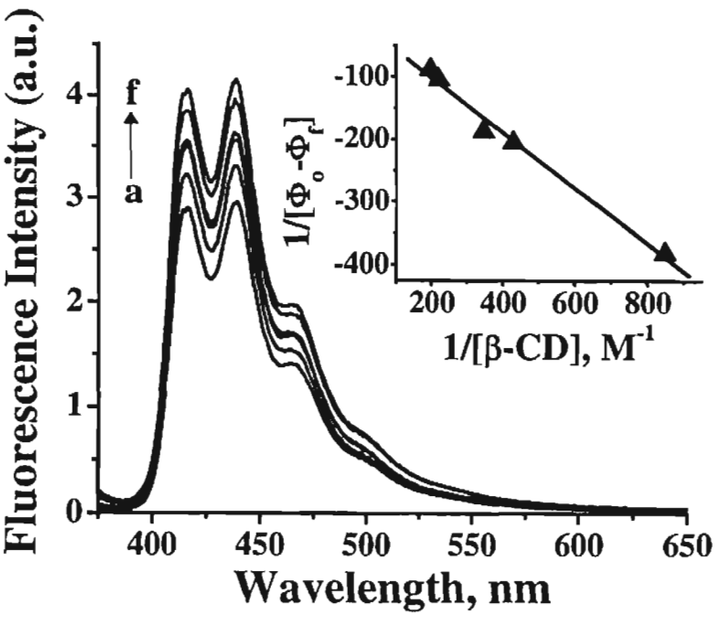

Figure 4.8. Effect of β-CD concentration on the fluorescence emission spectra of **2a** (1.73 x 10^{-6} M) in water. [β-CD] (a) 0, (b) 0.12, (c) 0.38, (d) 0.63, (e) 0.89 and (f) 6.3 mM. Excitation wavelength, 360 nm. Inset shows Benesi-Hildebrand plot for the change in absorption for **2a** with increasing concentration of β-CD.

Figure 4.9, the *para*-isomer **1a** exhibited monoexponential decay with lifetime of 5.4 ns. In the presence of β–CD, this dyad showed biexponential decay with lifetimes of 0.9 ns (31%) and 5.4 ns (69%) (Table 4.1). Similar observations were made with the dyad **1c** containing the biphenyl spacer group. The dyad **1c**, which showed monoexponential decay with lifetime of 5.7 ns, exhibited biexponential decay with lifetimes of 1.4 ns (60%) and 5.7 ns (40%) in the presence of β–CD. On the other hand, negligible changes were observed in the presence of β–CD in the case of the *ortho*–isomer **1b**, which showed biexponential decay with the

lifetimes of 10.6 ns and 0.4 ns (inset of Figure 4.9). In contrast, the dyads **2a–c** with the flexible spacer groups showed enhancement in lifetimes in the presence of β–CD. For example, the dyad **2a** showed monoexponential decay with a lifetime of 14.6 ns, but when complexed with β–CD, it exhibited a marginal enhancement in the lifetime (15 ns). The dyad **2b**, on the other hand, exhibited enhanced lifetimes of 15.5 and 5.8 ns in the presence of β–CD, as compared to its

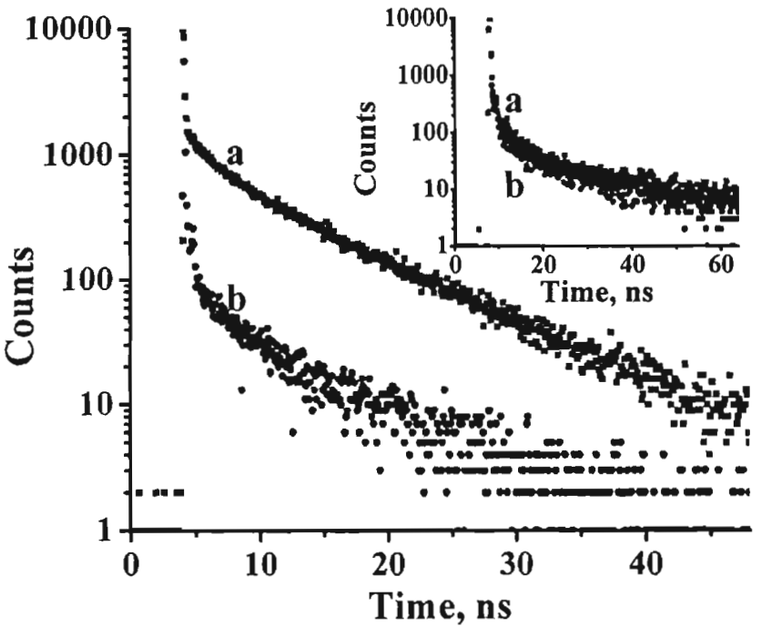

Figure 4.9. Fluorescence decay profiles of **1a** (1.23×10^{-6} M) in water (a) in the absence and (b) in the presence of β–CD. [β–CD] 6.40 mM. Inset shows the effect of β–CD concentration on the fluorescence decay profiles of **1b** (1.23×10^{-6} M) in water (a) in the absence and (b) in the presence of β–CD. [β–CD] 6.40 mM. Excitation and emission wavelengths are 360 and 485 nm, respectively.

lifetimes of 13.6 and 2.8 ns in the absence of β–CD. Similarly, the dyad **2c** with a long flexible spacer length of n = 11, showed biexponential decay with lifetimes of

14.7 and 1.7 ns. In the presence of β–CD, it exhibited significantly enhanced lifetimes of 15.0 and 8.3 ns. As indicated above, of the two lifetimes of the dyads **2b** and **2c**, only the short lived component exhibited significantly increased lifetimes (Table 4.1) in the presence of β–CD as compared to the long lived major component.

The values of k_{ET} for the electron transfer[17] for the dyads have been calculated using the fluorescence quantum yields and lifetimes. Unusually, k_{ET} increased from 1.17 x 10^{10} s^{-1} to 2.03 x 10^{10} s^{-1} for the dyad with *para*–tolyl spacer **1a** in the presence of β–CD. Similarly, ca. 2-fold enhancement was observed with the dyad containing biphenyl spacer group. In contrast to the dyads **1a** and **1c**, the dyad with flexible spacer group such as **2c** (n = 11) (k_{ET} = 0.6 x 10^{9} s^{-1}) exhibited significantly reduced rate of electron transfer by one order, when bound to β–CD (k_{ET} = 0.4 x 10^{8} s^{-1}). To understand the contrasting behavior of the dyads with flexible and rigid spacer groups in the presence of β–CD, we have investigated the interaction of these dyads with an alternative microenvironment medium such as micelles. Interestingly, irrespective of the nature of spacer group, the viologen linked acridine derivatives showed enhancement in the fluorescence quantum yields in the presence of micelles. For example, **1a** with rigid spacer and **2c** with fleixible spacer unit, exhibited enhancement in the fluorescence quantum yields ca. 16 and 2 fold, respectively (Figure 4.10) in the presence of sodium dodecyl sulphate micelles (SDS) as compared to the aqueous medium.

4.3.3. Characterization of β-Cyclodextrin Inclusion Complexes

Evidence for the interaction of the donor–acceptor dyads **1a**, **1c** and **2a–c** with β–CD and formation of the stable inclusion complexes is obtained through time-resolved fluorescence anisotropy, competitive ligand displacement,[19] ^{1}H NMR, circular dichroism (CD) and cyclic voltammetry (CV) techniques.

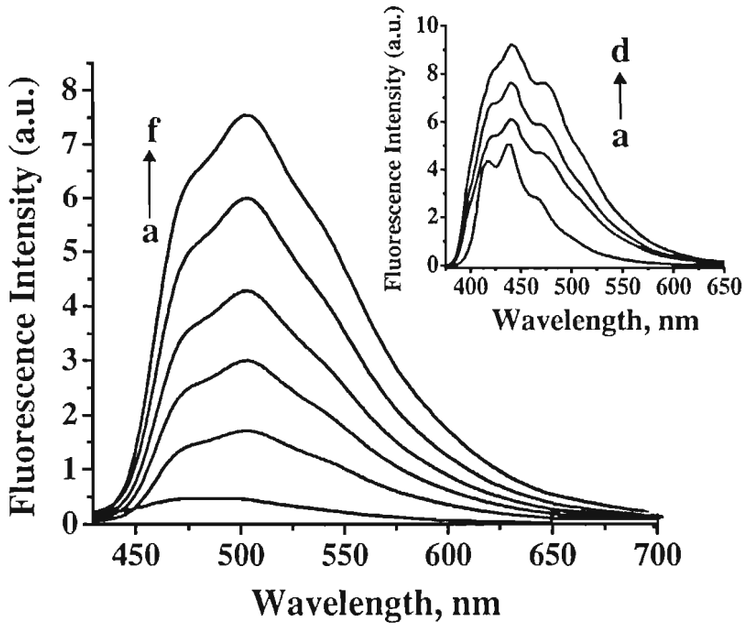

Figure 4.10. Effect of SDS concentration on the fluorescence emission spectra of **1a** (1.21×10^{-4} M) in water. [SDS] (a) 0, (b) 1.09, (c) 2.13, (d) 3.31, (e) 4.55 and (f) 6.57 mM; excitation wavelength 360 nm. Inset shows the effect of SDS concentration on the absorption spectra of **2c**. [SDS] (a) 0, (b) 2.13, (c) 4.55 and (d) 6.57 mM; excitation wavelength 360 nm.

Fluorescence anisotropy gives a physical insight into the extent of restriction imposed by the microenvironment on the dynamics of the molecule and thus can

be exploited for confirming the formation of stable inclusion complexes with β–CD.[20] Figure 4.11 shows the time–resolved anisotropy studies of the *para*-isomer **1a**–β–CD complex. We observed a monoexponential decay with rotational correlation time of 0.37 ns and r_0 value of 0.03–0.05. As expected, the *ortho*-isomer showed no anisotropic behavior under the same conditions, indicating its negligible interactions with β–CD. The calculated value for hydrodynamic radius of the 1:1 complex formed between **1a** and β–CD using the rotational correlation time was found to be 7.2 ± 0.5 Å, which corresponds to a diameter of 14.4 ± 0.5 Å, indicating the formation of a tight complex between β–CD and the dyad **1a**

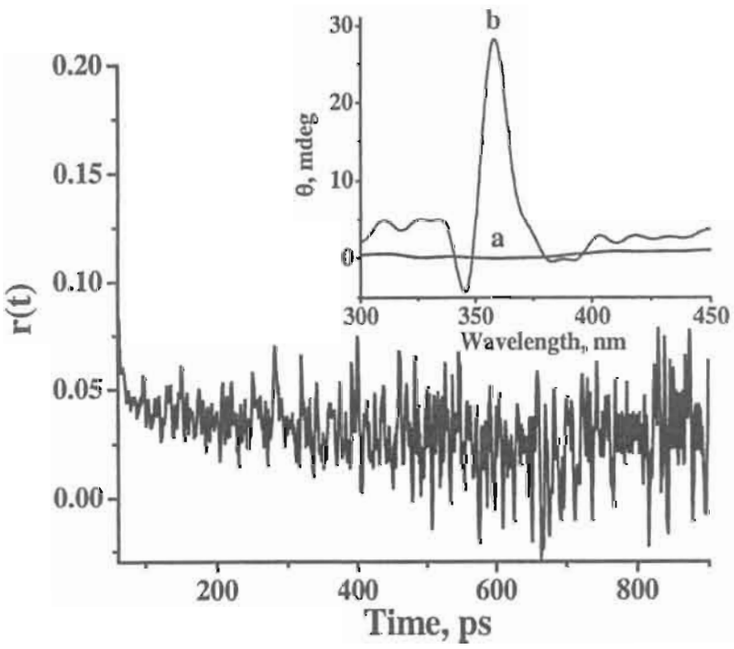

Figure 4.11. Time–resolved fluorescence anisotropy of **1a** (1.23 μM) in the presence of β–CD (6.40 mM). Inset shows the circular dichroic (CD) spectra of derivative **1a** (3.1 x 10^{-4} M) in the a) absence and b) presence of β–CD (6.40 mM).

having a diameter of 14.9 Å. These observations furthermore rules out the possibility of peripheral binding of β–CD with the dyad **1a**, since the diameter obtained from the anisotropy measurements is in good agreement with the theoretically determined diameter for the dyad **1a**.

Figure 4.12 shows the revival of the fluorescence intensity of the dyad **1a** through ligand displacement technique. The addition of β–CD results in the decrease in fluorescence intensity of **1a** followed by saturation at ca. 6.4 mM of β–CD. When AD–COOH, a known β–CD binding agent (K_{ass} = 1.14 x 10^3 M^{-1}),[19] was gradually added to this **1a**–β–CD complex, we observed the quantitative revival of the fluorescence intensity of **1a**, confirming thereby the effective displacement of **1a** by AD–COOH from the β–CD cavity. Figure 4.13 shows ^{1}H

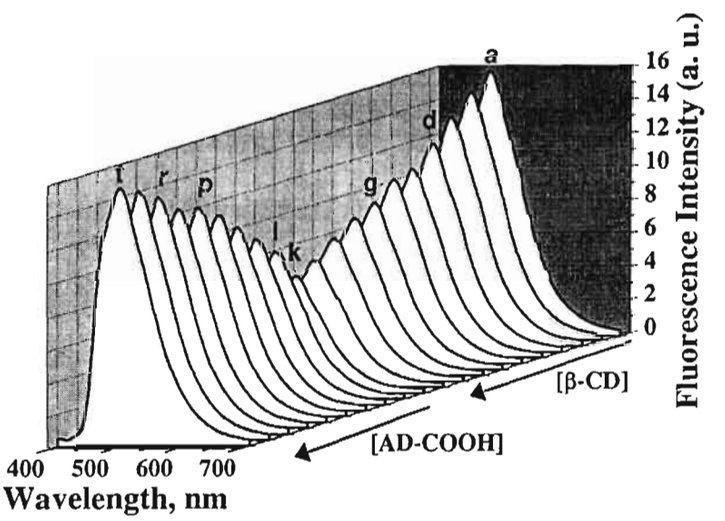

Figure 4.12. Effect of β–CD concentration on emission spectra of **1a** (4.1 × 10^{-5} M) in water. [β–CD] (a) 0, (d) 2.01, (g) 3.94, (k) 6.40 mM, followed by gradual addition of AD–COOH. [AD–COOH] (l) 0.12, (p) 0.61, (r) 0.85, (t) 1.21 mM.

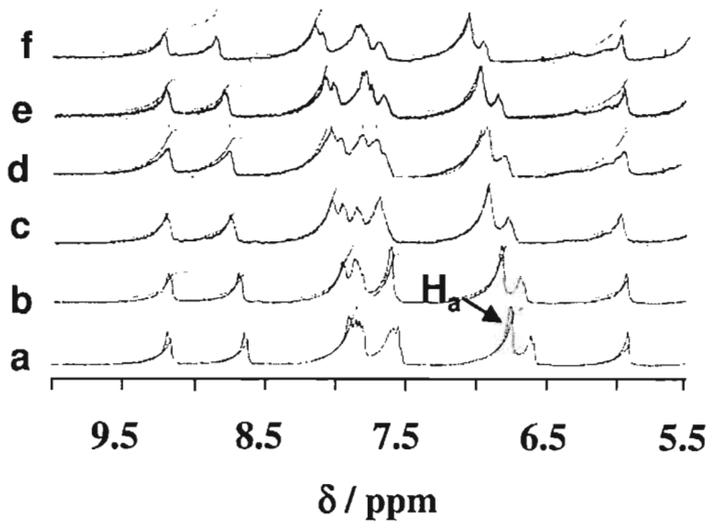

Figure 4.13. Effect of β–CD concentration on proton chemical shift of compound **1a** (37.2 mM) in water. [β–CD] (a) 0, (b) 0.55, (c) 1.03, (d) 1.45, (e) 1.84, (f) 2.49 mM.

NMR spectra of **1a** with the gradual addition of β–CD. In presence of β–CD, the dyad **1a** showed significant changes in chemical shift ($\Delta\delta$ = 0.3), for the proton corresponding to the spacer phenyl group. Analysis of the chemical shift changes through Benesi– Hildebrand plot (Figure 4.14) gave an association constant of 337 ± 12 M^{-1} for **1a**, which is relatively higher than the value obtained by fluorescence titrations (K_{ass} = 239 ± 5 M^{-1}). However, the NMR spectrum of the *ortho*-isomer **1b,** as expected showed negligible changes in the presence of β–CD (Figure 4.15).

Electrochemical studies of redox active ligands are highly useful in probing the ligand-β-CD interactions.[21] The complexation of a ligand within host molecule such as β-CD can reduce the mobility of the ligand thereby resulting in the decrease in the intensity of current. Moreover, ligands as such are also expected to

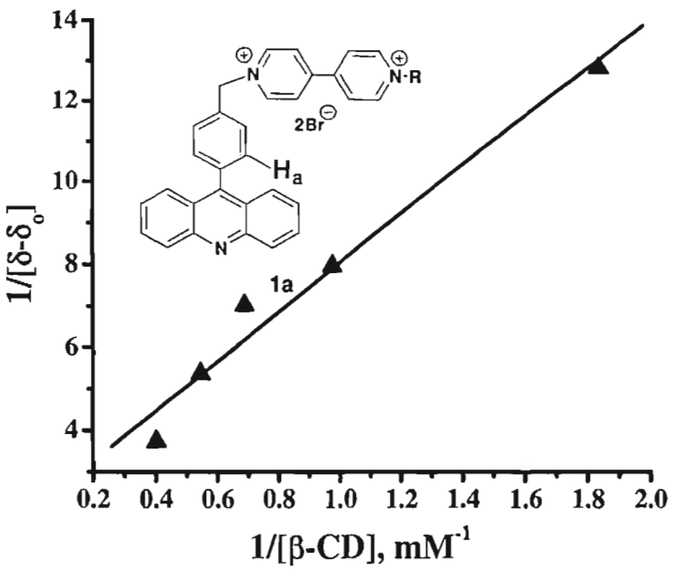

Figure 4.14. Benesi–Hildebrand plot of change in chemical shift of proton H_a of the dyad **1a** (37.2 mM) with increasing in concentration of β–CD in D_2O.

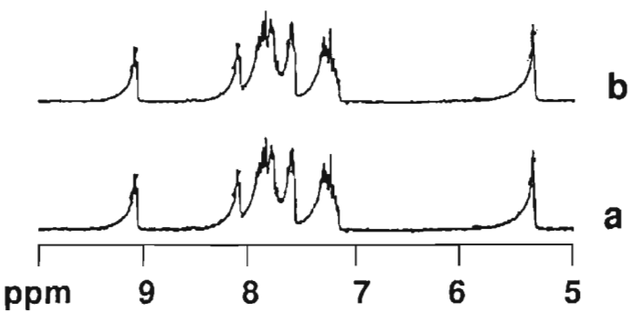

Figure 4.15. Effect of β-CD concentration on proton chemical shift of compound **1c** (35.6 mM) in water. [β-CD] (a) 0, (b) 2.49 mM.

exhibit significant changes in their redox properties when complexed with β-CD, depending on the nature of interactions involved. In this context, we examined the redox properties of the viologen linked acridines in presence of β-CD to

understand the nature of their complexation. Figure 4.16 shows the cyclic voltammograms of **1a**, which exhibited two reversible one–electron reduction processes centered at –0.44 and –0.73 V, characteristic of the viologen moiety.[21] With increase in addition of β-CD, we observed an increase in the reduction potentials by 66 and 10 mV, along with a decrease in current intensity of 35.7 μA (71%) and 15.7 μA (61%), respectively. The viologen linked acridine derivative **2b**, on the other hand, is found to have one reversible one–electron reduction

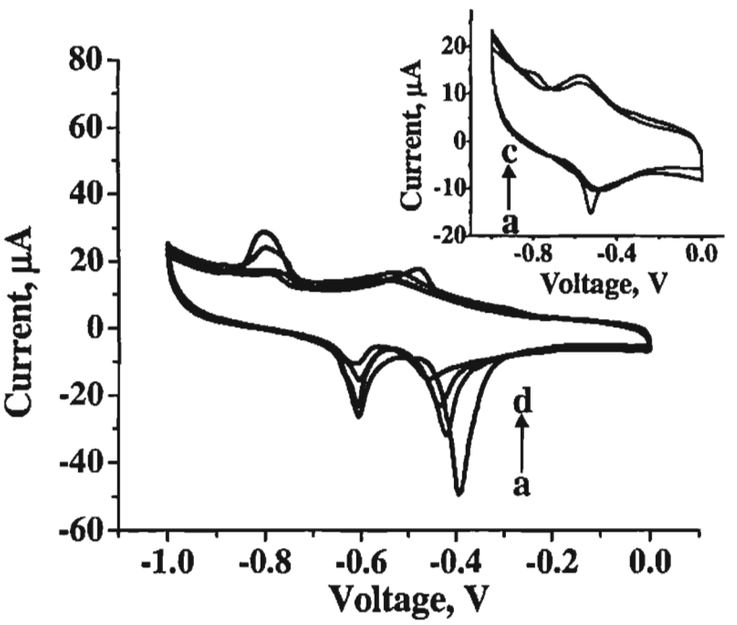

Figure 4.16. Cyclic voltammograms of **1a** (0.24 mM) in 24 mM NaCl with increasing concentrations of β–CD a) 0, b) 0.045, c) 0.09 and d) 0.18 mM. Scan rate, 100 mV/s. Inset shows cyclic voltammograms of **2b** (0.17 mM) in 17 mM NaCl with increasing concentrations of β–CD a) 0, b) 0.09 and c) 0.18 mM. Scan rate, 100 mV/s.

process centered at –0.54 V.[22] When β-CD was added, we observed a decrease in the reduction potentials by 38 mV (inset of Figure 4.16), along with a significant

decrease in current intensity of 6 μA (39%). These results indicate the formation of stable complexes between the dyads and β-CD and the importance of the spacer group on the current intensity of such complexes.

Circular dichroism studies are useful in understanding the complex formation of organic ligands with β-CD.[23] Binding of an achiral molecule within a chiral environment, such as β-CD, can lead to the induced optical activity of the bound species. Inset of Figure 4.11 shows the CD spectral changes of **1a** in the presence of β-CD. As shown in the inset of Figure 4.11, we observed induced CD signal corresponding to the acridine moiety of the dyad **1a** at higher concentrations of β–CD. In contrast, the CD studies of the *ortho*-isomer **1b** in the presence of β-CD, showed no induced CD signal,[24] confirming its negligible interactions with β-CD.

Understanding the interaction of molecules at the atomic level is gaining much attention in the recent years.[25] In contrast to the precision electron microscopes, atomic force microscopy is advantageous due to the non-invasive imaging of the materials. Particularly, tapping mode atomic force microscopy has been instrumental in imaging the soft materials such as organic molecules and biological samples. To understand how the viologen linked acridine conjugates interacts with β-CD, we have carried out tapping mode atomic force microscopic studies (TM AFM) of β-CD in the presence and absence of various representative ligands. β–Cyclodextrin alone showed a flaky, crystalline like structure with a height of 5 ± 1 nm, whereas in the presence of derivative **1a,** we observed drastic

changes in the in the morphology of β–CD resulting in the loss of crystalline structure (Figure 4.17). As expected, we observed negligible changes in the morphology of the β-CD in the presence of the *ortho*-isomer **1b**, which exhibits insignificant interactions with β-CD.

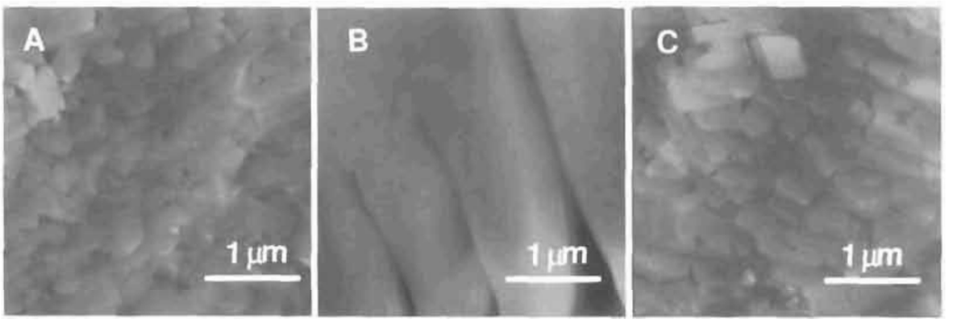

Figure 4.17. AFM images; A: β–CD (0.11 mM) alone, B: β–CD (0.11 mM) in the presence of **1a** (0.11 mM) and C: β–CD (0.11 mM) in the presence of **1b** (0.11 mM).

4.3.4. Molecular Modeling Studies

With a view to understand various photophysical properties of the viologen linked acridine derivatives in the presence and absence of β-CD, we have carried out semi–empirical AM1 calculations to find out the possible stable conformers for the dyads **1a–c** and **2a–c**. All the calculations have been carried out at AM1 level using a suite of Gaussian 03W programs. We obtained minimum energy conformers for the dyads **1a–c** and **2a–c** by geometry optimization of several conformers. Figure 4.18 shows structures of the energy–minimized conformations of the viologen linked acridine conjugates **1a–c** and **2a–c**. AM1 calculations show

that the viologen linked acridine derivatives **1a**, **1c** and **2a** exist in one extended form as the minimum energy conformer, while, the dyads **1b**, **2b** and **2c** have two minimum energy conformers. In agreement with the observation of various conformers through AM1 calculations, we obtained monoexponential fluorescence

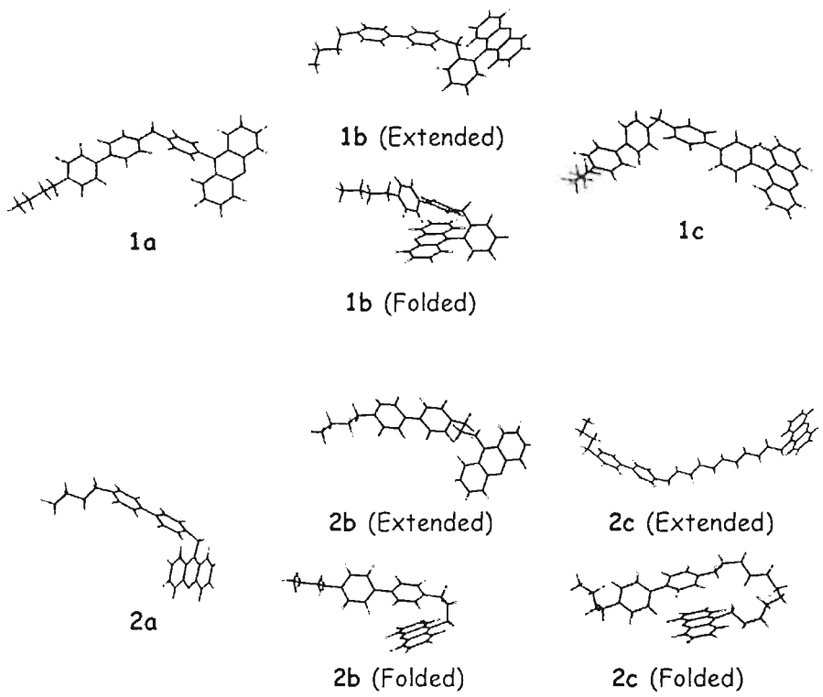

Figure 4.18. Minimum energy conformers of the viologen linked acridine derivatives **1a–c** and **2a–c**, obtained through AM1 calculations.

decay in the case of the dyads **1a**, **1c** and **2a** whereas the biexponential decay was observed for the dyads **1b**, **2b** and **2c**. From the orientation of the donor acridine chromophore with respect to the acceptor viologen moiety, we assign the major component (80–90%) with long lifetime to the lowest energy minimum conformer i.e. the extended form, while the minor (10–20%) and short lived species as that of

the folded conformer. However, in all these cases, the difference in the enthalpy of formation of these two conformations is marginal. Thus, the extended form is found to be slightly more stable than the folded one by 0.18–0.2 kcal mol^{-1}.

To understand the nature of the encapsulation of the viologen linked acridine containing *para*–tolyl spacer **1a** with β–CD, AM1 calculations have been carried out. Figure 4.19 shows the energy–minimized space–filling representation of the dyad **1a**-β–CD inclusion complex. It is apparent from this figure that the β–CD cavity fits neatly over the phenyl spacer group and should greatly restrict the

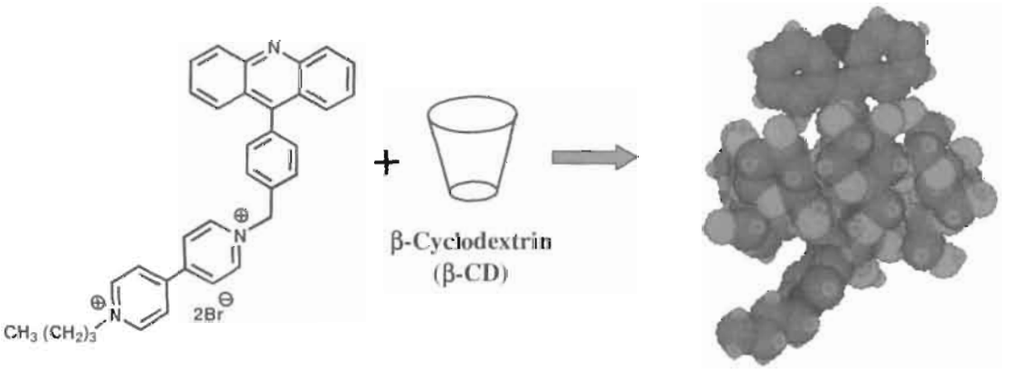

Figure 4.19. Minimum energy conformation for the complex **1a**–β–CD, obtained by the AM1 calculations.

rotational motions of the tolyl moiety. Evidence for such a complexation is obtained from the fluorescence anisotropy and ^{1}H NMR experiments, where we observed significant changes in chemical shifts of the spacer phenyl group when complexed with β–CD.

4.4. Discussion

For compounds in which a donor and an acceptor are separated by flexible or rigid spacer groups, the distance dependence of electron transfer reactions are well documented in the literature.[26-29] In such systems, both through–bond and through–space interactions play a key role in determining their photophysical properties. In the case of the dyads **1a** and **1c**, the observed decrease in fluorescence quantum yields (Fluorescence 'OFF', Figure 4.20) and the lifetimes in the presence of β–CD could be attributed to the increase in the rate of electron transfer from the excited state of the acridine chromophore to viologen moiety. This is evident, from the negligible changes in fluorescence quantum yields and the lifetimes observed for the dyad **1b**, which showed negligible interactions with

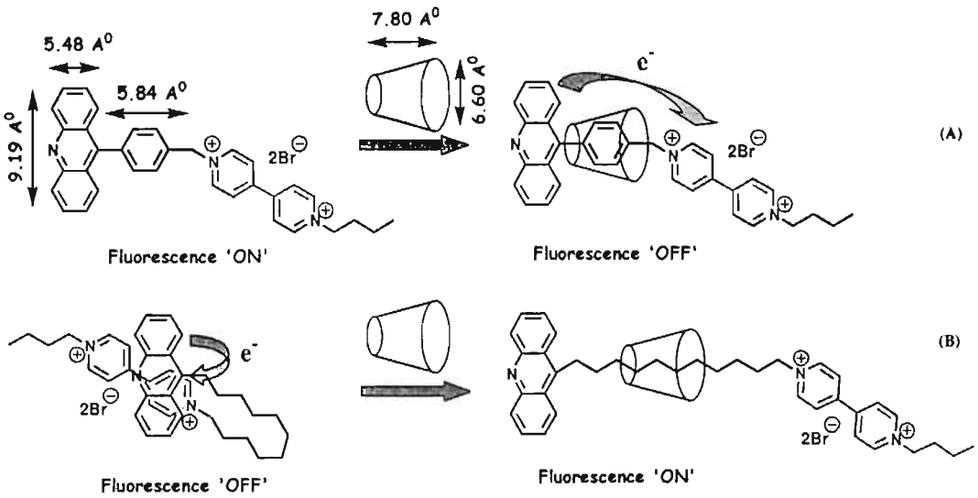

Figure 4.20. Schematic illustration of interactions between β–CD and (**A**) the dyad **1a** having rigid aromatic spacer and (**B**) the dyad **2c** consisting of flexible methylene spacer group (n = 11).

β–CD. On the other hand, the spacer length dependent enhancement in the fluorescence quantum yields and the lifetimes of the dyads **2a–c** was observed when complexed with β–CD (Fluorescence 'ON', Figure 4.20). This could be attributed to the decrease in the rate of electron transfer from the excited state of the acridine chromophore to viologen moiety in these cases. However, all these dyads **1a-c** and **2a-c** exhibited similar fluorescence enhancement in the presence of micelles. These results demonstrate that microencapsulation of all these derivatives occurs in micelles, whereas unusual planarization of the rigid spacer takes place in the β–CD cavity, particularly in the case of the dyads **1a** and **1c**. Further support for such planarization was obtained through electrochemical studies. We observed increase in the reduction potentials of the dyad **1a** corresponding to the viologen moiety in the presence of β–CD, whereas decreased values were observed for the dyad **2b** under similar conditions. This indicates the enhanced interactions between the donor and the acceptor moieties in the former case through planarization of the rigid spacer when complexed with β–CD.

As evident from the photophysical, electrochemical and chiroptical studies, all the dyads **1a** and **1c** (rigid), and **2a-c** (flexible), spacer groups undergo stable 1:1 complex formation with β-CD. Our results clearly demonstrate that the dyads **1a** and **1c** form tight complexes with β–CD through the inclusion of aryl spacer groups in the hydrophobic β–CD cavity, while the dyads **2a-c** through involvement of polymethylene spacer groups. This is based on the following facts:

i) observation of induced CD signal, ii) hydrodynamic radius of 14.4 ± 0.4 Å from the anisotropy measurements as compared to the theoretically calculated molecular length of 14.9 Å, iii) competitive displacement of the dyad **1a** from the **1a**–β–CD complex by AD–COOH, iv) change in chemical shift of the phenyl spacer group when complexed with β–CD, and v) observation of distinct AFM morphological changes of β–CD, when complexed with the dyad **1a**.

Inclusion of the *para*–tolyl moiety of the dyad **1a** in β–CD cavity obtained through AM1 calculations can be further understood as follows. Though the acridine unit can undergo interactions with β–CD[30] along the long molecular axis (radius = 9.19 Å), the substitution at the 9th position in the dyads **1a, 1c** and **2a–c**, prevents it from such interactions due to steric reasons (Figure 4.20). Therefore, β–CD binds to the dyads through the viologen unit leading to a less stable transition state[31] and then finally the complexed state, where β–CD is located on the spacer group. The *para*–tolyl moiety in **1a** with a length of 5.84 Å and width of 4.30 Å undergoes an effective encapsulation while **1b** with the *ortho*–tolyl spacer fails to interact with β–CD (Figure 4.20) due to steric constraints. This hypothesis is confirmed by the fact that the derivative **1c** with biphenyl moiety as a spacer unit has a length of 9.49 Å and width of 4.30 Å. As expected, the dyad **1c** is found to undergo an effective interaction with β–CD compared to **1a**, resulting in the formation of relatively a stable complex. Free energy changes observed during the β–CD complexation are found to be favorable for **1a** and **1c**, while in

the case of **2a–c**, it increases with the increase in methylene spacer length (Table 4.1). This could be attributed to the increase in entropy due to the displacement of water molecules from the β–CD cavity by the guest molecules. The observed spacer length dependent increase in the association constants of the dyads **2a-c** with flexible spacer groups with β-CD confirm the involvement of the flexible methylene groups in the formation of stable inclusion complexes from these cases.

4.5. Conclusions

In conclusion, the viologen linked acridine derivatives under investigation form stable complexes depending on the nature and length of the spacer group. Our results demonstrate the contrasting effects of the flexible and rigid spacer groups in the electron donor–acceptor dyads, when bound to β–CD. Upon β–CD complexation, the electron transfer process between the donor and acceptor moieties is inhibited in the dyads with flexible spacer groups, but significantly enhanced rate of electron transfer processes were observed with systems having the rigid aromatic spacer group. In the presence of β–CD, the viologen linked acridines containing flexible spacer group undergoes unfolding of the sandwich like folded structure, which results in the decrease in the interaction between the donor and acceptor moiety. In contrast, the enhanced electron transfer rates observed with systems having rigid spacer is attributed to the unusual planarization of the molecule, when encapsulated in the β–CD cavity. The results

of these investigations are important in understanding the interaction between donor-acceptor dyads, unusual effects of the organized media such as β–CD and also in the design of supramolecular drug delivery systems and molecular machines.

4.6. Experimental Section

4.6.1. General Techniques

All the molecular geometries were optimized at the semi–empirical level by using AM1 method as implemented in the Gaussian 03W suite of programs. All melting points are uncorrected and were determined on a Mel-Temp II melting point apparatus.[32,33] An Elico pH meter was used for pH measurements. The electronic absorption spectra were recorded on a Shimadzu UV–VIS–NIR spectrophotometer. Fluorescence spectra were recorded on a SPEX–Fluorolog F112X spectrofluorimeter. The fluorescence quantum yields were determined by using optically matching solutions. 9–Aminoacridine in methanol ($\Phi_f = 0.99$) was used as the standard.[34] The quantum yields of fluorescence were calculated using the equation 4.1, where, A_s and A_u are the absorbance of standard and unknown,

$$\Phi_u = \frac{A_s F_u n_u^2}{A_u F_s n_s^2} \Phi_s \qquad (4.1)$$

respectively. F_s and F_u are the areas of fluorescence peaks of the standard and unknown and n_s and n_u are the refractive indices of the standard and unknown

solvents, respectively. Φ_s and Φ_u are the fluorescence quantum yields of the standard and unknown compound. Fluorescence lifetimes and anisotropy were measured using an IBH Picosecond single photon counting system. Fluorescence lifetimes and anisotropy were determined by deconvoluting the instrumental function with mono or biexponential decay and minimizing the χ^2 values of the fit to 1 ± 0.1. The quenching rate constant k_q was calculated by employing Equations (4.2) and (4.3), where I_0 and I are the fluorescence intensities in the absence and presence of quencher (Q), K_{sv} the Stern–Volmer constant, and τ_0 the singlet lifetime of *para*–tolylacridine in the absence of quencher.

$$I_0/I = 1 + K_{SV}[Q] \qquad (4.2)$$

$$K_{SV} = K_q \times \tau_0 \qquad (4.3)$$

From the relative fluorescence quantum yields of the viologen–linked acridine derivatives and fluorescence lifetime of the model derivative *para*–tolylacridine, an estimate of the rate constant of electron transfer process k_{ET} can be made by using Equation 4.4, where Φ_{ref} and Φ are the relative fluorescence quantum yields of the model derivative *para*–tolylacridine and the viologen linked acridine derivative, respectively,

$$k_{ET} = [(\Phi_{ref} / \Phi) - 1] \tau_{ref} \qquad (4.4)$$

and τ_{ref} is the fluorescence lifetime of the model compound *para*–tolylacridine. Cyclic voltammetry was performed on a BAS CV50W Cyclic Voltammeter with potassium nitrate as supporting electrolyte in water. A standard three–electrode

configuration was used with a glassy carbon working electrode, a platinum auxiliary electrode, and a Ag/AgCl (3 M NaCl) reference electrode. The potentials were calibrated against the standard calomel electrode (SCE). ^{1}H and ^{13}C NMR were measured on a 300 MHz Bruker advanced DPX spectrometer. Circular dichroism spectra were recorded on Jasco Corporation, J–810 spectropolarimeter. NMR studies were performed with a Bruker 300 MHz system in D_2O at 298 ± 1 K. Association constants were determined using Benesi–Hildebrand equation for a 1:1 stoichiometric complex using equation 4.5, where K_{ass} is the association constant, Φ_f is the quantum yield of emission of a free viologen linked acridine,

$$1/(\Phi_f - \Phi_{ob}) = 1/(\Phi_f - \Phi_{ob}) + 1/K_{ass}(\Phi_f - \Phi_{ob})[\beta\text{-CD}] \qquad (4.5)$$

Φ_{ob} is the observed quantum yield in the presence of β–CD and Φ_{fc} is the quantum yield of emission of β–CD complex. The linear dependence of $1/(\Phi_f - \Phi_{ob})$ on the reciprocal of β–CD concentration indicates the formation of 1:1 molecular complex between β–CD and viologen linked acridine. Change in free energy (ΔG) associated with the complexation between viologen linked acridine derivatives and β–CD, was determined using the equation 4.6,[27a] where K_{ass} is the

$$\Delta G = -RT \ln K_{ass} \qquad (4.6)$$

binding constant. Doubly distilled water was used in all the studies. All experiments were carried out at room temperature (25 ± 1 °C), unless otherwise mentioned. Hydrodynamic radius (r_h) of the complex is related to rotational correlation time

(τ_R) as in the equation 4.7, where η is the viscosity of water, K is Bolktzmann's constant and T is the temperature.

$$r_h = \sqrt[3]{\frac{3KT\tau_R}{4\pi\eta}} \qquad (4.7)$$

Atomic force microscopy (AFM). Samples for the imaging were prepared by drop casting the β–CD solution in the absence and presence of viologen linked acridine derivatives on freshly cleaved mica at the required concentrations. AFM images were recorded under ambient conditions using a Digital Instrument Multimode Nanoscope IV operating in the tapping mode regime. Micro–fabricated silicon cantilever tips (MPP–11100–10) with a resonance frequency of 299 kHz and a spring constant of 20–80 Nm^{-1} were used. The scan rate varied from 0.5 to 1.5 Hz. AFM section analysis was done offline.

4.6.2. Spectrophotometric and Spectrofluorimetric Titrations

The linearity of absorbance *vs.* concentrations was determined in the concentration range of (10^{-4}–10^{-6} M) for all the derivatives. The sample concentrations were taken between 0.1–10 x 10^{-5} M, where it obeyed Beer's law and formed no aggregation of the solute in the aqueous solutions. The linearity of the fluorescence emission *vs.* concentrations was also checked in the same concentration range used. The absorbance of the excitation wavelength was maintained lower than 0.15. Titrations of β–cyclodextrin with donor–acceptor dyads were carried out in aqueous medium. 3 mL of these dyads were taken in a quartz

cuvette with a concentration ranging 0.1–10 x 10^{-5} M. Subsequently, a 0.090 M stock solution of β–cyclodextrin were added in 20 μl – 200 μl volume to 3 mL solution of these dyads. A series of ^{1}H NMR spectra were recorded upon addition of 50 μl of 8.7 mM stock solution of β–cyclodextrin to 0.75 mL of dyads.

4.6.3. Materials

Diphenylamine, β–cyclodextrin (β–CD) and 1–adamantanecarboxylic acid (AD-COOH) were purchased from Aldrich and were used without further purification. The synthesis of 9-(4-methylphenyl)acridine (**3a**), mp 188-189 °C (lit. mp 189 °C) and 9-(2-methylphenyl)acridine (**3b**), mp 212-213 °C (lit. mp 214 °C)[17a] was achieved as per reported procedures. 4–Methyl-4'–biphenylcarboxylic acid (**6**) mp 168-189 °C (lit. mp 169 °C)[35] was prepared by modification of the reported procedures. The starting materials, 9-bromomethylacridine (**9**), mp 162-163 °C (lit. mp 160-161 °C), 3-(acridin-9-yl)-1-bromopropane (**10**), mp 104-105 °C (lit. mp 103-104 °C), 11-(acridin-9-yl)-1-bromoundecane (**11**), 58-59 °C (lit. mp 58-59 °C),[17b] were prepared by modification of the reported procedures. 1-Butyl-4,4'-bipyridinium bromide was obtained in a 95% yield by the reaction of 4,4'-bipyridine with 1-bromobutane in the molar ratio of 3:1 in dry acetonitrile.[17b]

4.6.4. Synthesis of the viologen linked tolylacridines (1a and 1b)

A solution of 9-(4-methylphenyl)acridine (**3a**, 1 mmol), N-bromosuccinimide (NBS, 1 mmol) and benzoyl peroxide (20 mg) in dry CCl_4 (20 mL) was

refluxed for 8 h. The reaction mixture was cooled and filtered. The filtrate was concentrated to give a residue, which was chromatographed over silica gel column. Elution of the column with a mixture (1:4) of ethyl acetate and petroleum ether gave 9-(4-bromomethylphenyl)acridine **4a** in 60% yield, mp 203-204 °C; ^{1}H NMR ($CDCl_3$, 300 MHz) δ 4.7 (2H, s), 7.3-8.05 (8H, m), 8.25-8.50 (4H, m); ^{13}C NMR ($CDCl_3$, 75 MHz) δ 148.60, 146.28, 137.95, 136.04, 130.85, 129.96, 129.54, 129.06, 126.52, 125.69, 125.69, 124.92, 32.88; (HRMS-ESI) Calcd for $C_{20}H_{15}NBr$ 348.0388. Found 348.0384.

Similar reaction of 9-(2-methylphenyl)acridine (**3b**) with NBS in dry CCl_4 in presence of benzoyl peroxide yielded 9-(2-bromomethylphenyl)acridine **4b** in 56% yield, mp 136-137 °C; ^{1}H NMR ($CDCl_3$, 300 MHz) δ 4.05 (2H, s), 7.10-7.90 (10H, m), 8.15-8.45 (2H, m); ^{13}C NMR ($CDCl_3$, 75 MHz) δ 148.46, 144.04, 136.49, 135.30, 130.62, 129.75, 129.54, 129.07, 128.26, 126.23, 125.63, 124.96, 30.34; (HRMS-ESI) Calcd for $C_{20}H_{15}NBr$ 348.0388. Found 348.0394.

A solution of 9-(4-bromomethylphenyl)acridine (**4a**, 1 mmol) and 1-butyl-4,4'-bipyridinium bromide (2 mmol) in dry acetonitrile (30 mL) was stirred at 30 °C for 12 h. The precipitated solid was filtered, washed with dry acetonitrile and dichloromethane to remove the unreacted starting materials. The solid was further purified by Soxhlet extraction with dichloromethane and recrystallization from a mixture (4:1) of ethyl acetate and acetonitrile to give 77% of **1a**, mp 268-269 °C; ^{1}H NMR (DMSO-d_6, 300 MHz) δ 0.85-1.05 (3H, t, J = 2.89 Hz), 1.15-1.55 (2H,

m), 1.80-2.20 (2H, m), 4.70-4.90 (2H, t, J = 2.80 Hz), 6.3 (2H, s), 7.50- 8.40 (12H, m), 8.75-9.05 (4H, m), 9.42-9.60 (2H, m), 9.70-9.85 (2H, m); ^{13}C NMR (DMSO-d_6, 75 MHz) δ 149.23, 1483.61, 147.74, 146.19, 146.00, 145.76, 136.21, 134.42, 131.09, 130.64, 129.36, 128.94, 127.26, 126.79, 126.38, 126.21, 124.23, 63.87, 60.64, 32.70, 18.77, 13.33; MS m/z 561 (M^+Br^-, 5), 481 (M^+, 100), 424 (10); Anal. Calcd for $C_{34}H_{31}Br_2N_3$: C, 63.66; H, 4.87; N, 6.55. Found: C, 63.81; H, 5.09; N, 6.42.

Similar reaction of 9-(2-bromomethylphenyl)acridine (**4b**, 1 mmol) with 1-butyl-4,4'-bipyridinium bromide (2 mmol) in dry acetonitrile and purification as in the earlier case gave 75% of **1b**, mp 224-225 °C; ^{1}H NMR (DMSO-d_6, 300 MHz) δ 0.80-1.00 (3H, t, J = 2.89 Hz), 1.05-1.50 (2H, m), 1.70-2.10 (2H, m), 4.65-4.90 (2H, t, J = 2.85 Hz), 5.60 (2H, s), 7.15-8.70 (16H, m), 9.30-9.55 (4H, m); ^{13}C NMR (DMSO-d_6, 75 MHz) δ 148.50, 147.80, 145.82, 145.27, 142.77, 135.64, 132.08, 131.90, 131.36, 130.55, 130.44, 129.98, 129.47, 127.08, 126.68, 126.49, 125.95, 125.34, 124.24, 62.02, 60.64, 32.68, 18.78, 13.35; MS m/z 561 (M^+Br^-, 7), 481 (M^+, 100), 424 (7); Anal. Calcd for $C_{34}H_{31}Br_2N_3$: C, 63.66; H, 4.87; N, 6.55. Found: C, 63.69; H, 5.06; N, 6.46.

4.6.5. Synthesis of viologen linked 9–(biphenylyl–4–methyl)acridine (1c)

A mixture of 4–methyl-4'–biphenylcarboxylic acid (1.42 mmol), diphenylamine (1.42 mmol) and anhydrous $ZnCl_2$ (14 mmol) was heated at 230 °C

for 24 h. To the reaction mixture 20% H_2SO_4 (20 mL) was added and refluxed for 4 h. It was then cooled and neutralized with 25% aqueous NH_3 solution and the solid product thus obtained was chromatographed over silica gel. Elution of the column with a mixture of (1:1) of ethyl acetate and hexane gave 9–(biphenylyl 4–methyl)acridine (10%), mp 267–269 °C: ^{1}H NMR ($CDCl_3$, 300 MHz) δ 2.42 (3H, s), 7.31–8.17 (16H, m); ^{13}C NMR ($CDCl_3$, 75 MHz) δ 21.1, 126.4, 127.4, 128.9, 129.8, 130.5, 131.1, 134.9, 135.9, 136.7, 138.2, 140.4, 143.3, 143.8; HRMS (ESI) Calcd for $C_{26}H_{19}N$: 345.4358. Found: 345.4367.

A mixture of 9–(biphenylyl-4–methyl)acridine (0.1 mmol), N–bromosuccinimide (0.1 mmol) and AIBN in 10 mL dry CCl_4 was refluxed for 12 h. The reaction mixture was cooled and filtered. The filtrate was concentrated to give a residue, which was chromatographed over silica gel column. Elution of the column with a mixture (1:4) of ethyl acetate and petroleum ether gave the bromo derivative **8** (54%), mp 285–286 °C: ^{1}H NMR ($CDCl_3$, 300 MHz) δ 4.56 (2H, s), 7.52–8.05 (16H, m); ^{13}C NMR ($CDCl_3$, 75 MHz) δ 33.7, 126.7, 127.4, 128.5, 129.9, 130.5, 131.1, 134.9, 135.9, 138.2, 139.9, 142.1, 144.2, 145.8; HRMS (ESI) Calcd for $C_{26}H_{18}BrN$: 424.3319. Found: 424.3337.

To a solution of 9–(4–bromomethylbiphenyl)acridine (0.1 mmol) in dry acetonitrile (50 mL), 1–butyl–4,4'–bipyridinium bromide (0.1 mmol) was added and stirred at room temperature for 12 h. Precipitated product was filtered and dried to give **1c**, which was recrystallised from a mixture (7:3) of methanol and

ethylacetate. 35% yield, mp 291–293 °C: ^{1}H NMR (DMSO–d_6, 300 MHz) δ0.93–0.97 (3H, t, J = 7.4Hz), 1.35–1.38 (2H, m), 1.99–2.02 (2H, m), 4.79 (2H, t, J = 7.1Hz), 6.30 (2H, s), 7.37–8.27 (9H, m), 8.93–9.85 (8H, m); ^{13}C NMR (DMSO–d_6, 75 MHz) δ 13.4, 18.8, 32.7, 60.6, 62.8, 109.1, 124.2, 126.2, 126.4, 126.8, 127.3, 128.3, 129.1, 129.3, 130.5, 131.1, 134.5, 136.2, 145.8, 146.0, 147.9, 148.6, 149.2; HRMS (ESI) Calcd for $C_{40}H_{35}BrN_3$: 637.6301. Found: 637.6301. Anal. Calcd for $C_{40}H_{35}Br_2N_3$: C, 66.96; H, 4.92; N, 5.86. Found: C, 66.74; H, 5.01; N, 5.96.

4.6.5. Synthesis of the viologen linked acridines (2a-c)

A solution of ω-(acridin-9-yl)-α-bromoalkanes (1 mmol) and 1-alkyl-4,4'-bipyridinium bromide (1 mmol) in dry acetonitrile (30 mL) was stirred at 30 °C for 12 h. The precipitated solid thus obtained was filtered, washed with dry acetonitrile and dichloromethane to remove any unreacted starting materials. The solid was further purified by soxhlet extraction with dichloromethane to gave **2a-c** in quantitative to moderate yields.

2a (67%; obtained by the reaction of **9** with 1-alkyl-4,4'-bipyridinium bromide, was recrystallized from a mixture (1:4) of methanol-acetonitrile): mp 260-261 °C; ^{1}H NMR (DMSO-d_6) δ 0.94 (3H, t, J = 2.9 Hz), 1.30-1.37 (2H, m), 1.93-1.98 (2H, m), 4.70 (2H, t, J = 2.8 Hz), 7.16 (2H, s), 7.79-8.36 (4H, m), 8.51-8.72 (8H, m), 9.20-9.37 (4H, m); ^{13}C NMR (DMSO-d_6) δ 149.78, 148.91, 146.02,

145.69, 131.43, 130.97, 130.22, 128.70, 127.13, 126.92, 126.02, 124.36, 121.42, 61.02, 55.45, 33.01, 19.10, 13.67; (HRMS-ESI) Calcd for $C_{28}N_3H_{27}Br$: 484.1388. Found: 484.1372. Anal. Calcd for $C_{28}H_{27}Br_2N_3$: C, 59.49; H, 4.81; N, 7.43. Found: C, 59.28; H, 4.98; N, 7.31.

2b (71%; obtained by the reaction of **10** with 1-alkyl-4,4'-bipyridinium bromide, was purified by washing several times with a mixture (1:4) of methanol-acetonitrile): mp 253-254 °C; ^{1}H NMR (DMSO-d_6) δ 0.90 (3H, t, J = 2.7 Hz), 1.10-1.60 (2H, m), 1.70-2.20 (2H, m), 2.20-2.70 (2H, m), 4.75 (4H, t, J = 3.6 Hz), 7.60-8.30 (6H, m), 8.50-9.00 (6H, m), 9.30-9.75 (4H, m); ^{13}C NMR (DMSO-d_6) δ 149.45, 149.35, 146.18, 145.40, 133.29, 127.49, 127.19, 125.91, 124.96, 61.12, 60.73, 33.21, 33.05, 24.89, 19.28, 13.85; MS (FAB): m/z (%) 433 (M^+, 10), 408 (1), 376 (3), 347 (1). Anal. Calcd for $C_{30}H_{31}Br_2N_3$: C, 60.72; H, 5.27; N, 7.08. Found: C, 60.51; H, 5.21; N, 7.27.

2c (65%; obtained by the reaction of **11** with 1-alkyl-4,4'-bipyridinium bromide, was recrystallised from acetonitrile): mp 248 -249 °C; IR ν_{max} (KBr) 3032, 2933, 2859 (C-H), 1648 (C=N), 1559 (C=C) cm^{-1}; ^{1}H NMR (DMSO-d_6) δ 0.90-2.3 (27H, m), 4.7-4.9 (4H, t, J = 3.6 Hz), 7.50-8.00 (6H, m), 8.05-8.60 (6H, m), 8.70-9.30 (2H, m), 9.20- 9.30 (2H, m); ^{13}C NMR (DMSO-d_6) 148.98, 148.35, 147.65, 146.09, 130.49, 130.09, 127.02, 126.20, 125.15, 124.71, 61.25, 61.04, 33.07, 31.64, 31.15, 29.68, 29.26, 29.14, 28.76, 27.13, 25.80, 19.16, 13.72; MS

(FAB) m/z (%) 545 (M^+, 10), 488 (2), 429 (1), 323 (2), 270 (6). Anal. Calcd for $C_{38}H_{47}Br_2N_3$: C, 64.68; H, 6.71; N, 5.98. Found: C, 64.42; H, 6.44; N, 5.72.

4.7. References

1. (a) Monti, S.; Sortino, S. *Chem. Soc. Rev.* **2002**, *31*, 287–300. (b) Douhal, A. *Science* **1997**, *276*, 221. (c) Ball, P. *Nature*, **2003**, *423*, 25–26. (d) Nepogodiev, S. A.; Stoddart, J. F. *Chem. Rev.* **1998**, *98*, 1959–1976. (e) Connors, K. A. *Chem. Rev.* **1997**, *97*, 1325–1357.

2. (a) Kalyanasundaram, K. *Photochemistry in Microheterogenous Systems*; Academic Press: Orlando, Florida, 1987; pp 299–335. (b) Breslow, R.; Dong, S. D. *Chem. Rev.* **1998**, *98*, 1997-2011. (c) Li, S.; Purdy, W.C. *Chem. Rev.* **1992**, *92*, 1457–1490. (d) Komiyama, M. In *Cyclodextrins as Enzyme Models*: Atwood, J. L., Davies, J. E., MacNicol, D. D., Vogtle, F., Eds., Comprehensive Supramolecular Chemistry; Pergamon: Oxford, U. K., 1996; Vol. 3, pp 401–421.

3. (a) Breslow, R. Hydrophobic and Antihydrophobic Effects on Organic Reactions in Aqueous Solution. In *Structure and Reactivity in Aqueous Solution*; Cramer, C. J., Truhlar, D. G., Eds.; American Chemical Society: Washington, DC, 1994; pp 291-302. (b) Uekama, K.; Hirayama, F.; Irie, T. *Chem. Rev.* **1998**, *98*, 2045–2076.

4. (a) Rekharsky, M. V.; Inoue, Y. *Chem. Rev.* **1998**, *98*, 1875–1917. (b) D'Souza, V. T.; Lipkowitz, K. B. *Chem. Rev.* **1998**, *98*, 1741–1742.

5. Szejtli, J.; Osa, T. *Comprehensive Supramolecular Chemistry*; Elsevier: Oxford, U. K., 1996; vol. 3.

6. (a) Takahashi, K. *Chem. Rev.* **1998**, *98*, 2013. (b) Raymo, F. M.; Stoddart, J. F. *Chem. Rev.* **1999**, *99*, 1643–1663. (c) Wenz, G. *Angew. Chem. Int. Ed. Engl.* **1994**, *33*, 803–822. (d) Kawaguchi, Y.; Harada, A. *J. Am. Chem. Soc.* **2000**, *122*, 3797–3798.

7. Douhal A. *Chem. Rev.* **2004**, *104*, 1955–1976.

8. Schneider, H. J.; Hacket, F.; Rudiger, V.; Ikeda, H. *Chem. Rev.* **1998**, *98*, 1755–1785.

9. (a) Bakirci, H.; Zhang, X.; Nau, W. M. *J. Org. Chem.* **2005**, *70*, 39–46. (b) Szejtli, J. *Chem. Rev.* **1998**, *98*, 1743–1753. (c) Ikeda, H.; Nihei, T.; Ueno, A. *J. Org. Chem.* **2005**, *70*, 1237–1242.

10. (a) Park, J. W.; Song, H. E.; Lee, S. Y. *J. Phys. Chem. B* **2002**, *106*, 7186. (b) Park, J. W.; Lee, B. A.; Lee, S. Y. *J. Phys. Chem. B.* **1998**, *102*, 8209–8215. (c) Hwang, H. J.; Lee, S.; Park, J. W. *Bull. Korean Chem. Soc.* **2000**, *21*, 245–250. (d) Park, J. W.; Song, H. J. *Org. Lett.* **2004**, *6*, 24–26. (e) Park, J. W.; Lee, S. Y.; Song, H. J.; Park, K. K. *J. Org. Chem.* **2005**, *70*, 9505–9513.

11. (a) Yonemoto, E. H.; Kim, Y.; Schmehl, R. H.; Wallin, J. O.; Shoulders, B. A.; Richardson, B. R.; Haw, J. F.; Mallouk, T. E. *J. Am. Chem. Soc.* **1994**,

116, 10557–10563. (b) Yonemura, H.; Kasahara, M.; Saito, H.; Nakamura, H.; Matsuo, T. *J. Phys. Chem.* **1992**, *96*, 5765. (c) Yonemura, H.; Nojiri, T; Matsuo, T. *Chem. Lett.* **1994**, 2097–2100. (d) Saito, H.; Yonemura, H.; Nakamura, H.; Matsuo, T. *Chem. Lett.* **1990**, 535–538. (e) Watanabe, M.; Nakamura, H.; Matsuo, T. *Bull. Chem. Soc. Jpn.* **1992**, *65*, 164–169.

12. Harada, A. *Acc. Chem. Res.* **2001**, *34*, 456–464.

13. Badjic, J. D.; Balzani, V.; Credi, A..; Silvi, S.; Stoddart, J. F. *Science* **2004**, 303, *1845.*

14. Wasielewski, M. R. *Chem. Rev.* **1992**, *92*, 435–461.

15. (a) J. W. Verhoeven, *Pure Appl. Chem.* **1990**, *62*, 1585–1596. (b) Clark, C. D.; Debad, J. D.; Yonemoto, E. H.; Mallouk, T. E.; Bard, A. J. *J. Am. Chem. Soc.* **1997**, *119*, 10525–10531.

16. Yonemoto, E. H.: Saupe, G. B.; Schmehl, R. H.; Hubig, S. M.; Riley, R. L.; Iverson, B. L.; Mallouk, T. E. *J. Am. Chem. Soc.* **1994**, *116*, 4786–4795.

17. (a) Joseph, J.; Eldho, N. V.; Ramaiah, D. *J. Phys. Chem. B* **2003**, *107*, 4444–4450. (b) Joseph, J.; Eldho, N. V.; Ramaiah, D. *Chem. Eur. J.* **2003**, 9, 5926–5935. (c) Eldho, N. V.; Joseph, J.; Ramaiah, D. *Chem. Lett.* **2001**, 438–439.

18. (a) Bernthsen, A. *Justus Liebigs Ann. Chem.* **1884**, *224*, 1. (b) Jonker, S. A.; Ariese, F.; Verhoeven, J. W. *Recl. Trav. Chim. Pays-Bas* **1989**, *108*, 109-114.

19. Harries, D.; Rau, D. C.; Parsegian, V. A. *J. Am. Chem. Soc.* **2005,** *127*, 2184–2190.

20. (a) Mazzaglia, A.; Angelini, N.; Lombardo, D.; Micali, N.; Patane, S.; Villari, V.; Scolaro, L. M. *J. Phys. Chem.B* **2005**, *109*, 7258–7265. (b) Sen, P.; Roy, D.; Mondal, S. K.; Sahu, K.; Ghosh, S.; Bhattacharyya, K. *J. Phys. Chem. B* **2005**, *109*, 9716-9722.

21. Boulas, P. L.; Kaifer, M. G. ; Echegoyen, L. *Angew. Chem. Int. Ed.* **1998**, *37*, 216–247.

22. Mutz, M. W.; McLendon, G. L.; Wishart, J. F.; Gaillard, E. R.; Corin, A. F. *Proc. Natl. Acad. Sci. USA* **1996**, *93*, 9521–9526.

23. Harata, K.; Uedaira, H. *Bull. Chem. Soc. Jpn.* **1975**, *48*, 375-378.

24. Bakirci, H.; Zhang, X.; Nau, W. M. *J. Org. Chem.* **2005**, *70*, 39–46.

25. (a) Binnig, G.; Quate, C. F.; Gerber, Ch. *Phys. Rev. Lett.* **1986**, *56*930-937. (b) Rugar, D.; Hansma, P. K. *Phys. Today*, **1990**, *43*, 23-24.

26. Wasielewski, M. R. *Chem. Rev.* **1992**, *92*, 435-461.

27. Sessler, J. L.; Wang, B.; Harriman, A. *J. Am. Chem. Soc.* **1995**, *117*, 704-714.

28. Verhoewen, *Pure Appl. Chem.* **1990**, *62*, 1585–1596.

29. Le, T. P.; Rogers, J. E.; Kelly, L. A. *J. Phys. Chem. A* **2000**, *104*, 6778–6785.

30. (a) Schuette, J. M.; Ndou, T.; de la Pena, A. M.; Greene, K. L. ; Williamson, C. K.; Warner, I. M. *J. Phys. Chem.* **1991**, *95*, 4897–4902. (b)

Schuette, J. M.; Ndou, T.; Warner, I. M. *J. Phys. Chem.* **1992**, *96*, 5309–5314. (c) Schuette, J. M.; Ndou, T.; de la Pena, A. M.; Mukundan, S. Jr.; Warner, I. M. *J. Amer. Chem. Soc.* **1993**, *115*, 292–298.

31. Mirzoian, A.; Kaifer, A. E. *Chem. Eur. J.* **1997**, *3*, 1052–1058.

32. (a) Neelakandan, P. P.; Hariharan, M.; Ramaiah, D. *Org. Lett.* **2005**, *7*, 5765–5768. (b) Arun, K. T.; Ramaiah, D. *J. Phys. Chem. A* **2005**, *109*, 5571–5578. (c) Arun, K. T.; Epe, B.; Ramaiah, D. *J. Phys. Chem. B* **2002**, *106*, 11622–11627. (d) Jisha, V. S.; Arun, K. T.; Hariharan, M.; Ramaiah, D. *J. Am. Chem. Soc.* **2006**, *128*,

33. (a) Kuruvilla, E.; Joseph, J.; Ramaiah, D. *J. Phys. Chem. B* **2005**, *109*, 21997–22002. (b) Joseph, J.; Kuruvilla, E.; Achuthan, A. T.; Ramaiah, D.; Schuster, G. B. *Bioconjugate Chem.* **2004**, *15*, 1230–1235.

34. Weber, G.; Teale, F. W. J. *Trans. Faraday Soc.* **1957**, *53*, 646.

35. Abiraj, K.; Srinivasa, G. R.; Gowda, C. *Synlett,* **2004**, *5*, 877-879.

List of Publications of Mr. Mahesh Hariharan

1. Novel Bifunctional Viologen-Linked Pyrene Conjugates: Synthesis and Study of their Interactions with Nucleosides and DNA,
   M. Hariharan, J. Joseph and D. Ramaiah,
   J. Phys. Chem. B **2006**, *110*, 0000 (in press).

2. A Supramolecular ON-OFF-ON Fluorescence Assay for Selective Recognition of GTP,
   P. P. Neelakandan, **M. Hariharan** and D. Ramaiah,
   J. Am. Chem. Soc. **2006**, *128*, 11334-11335.

3. Site-Selective Binding and Dual Mode Recognition of Serum Albumin by a Squaraine Dye,
   V. S. Jisha, K. T. Arun, **M. Hariharan** and D. Ramaiah,
   J. Am. Chem. Soc. **2006**, *128*, 6024-6025.

4. Synthesis of a Novel Cyclic Donor-Acceptor Conjugate for Selective Recognition of ATP,
   P. P. Neelakandan, **M. Hariharan** and D. Ramaiah,
   Org. Lett. **2005**, 5765-5768.

5. Control over Chiral Switching: Kinetically and Thermodynamically Controlled Novel Self-Assembly of Squaraine Dyes in Solution and Thin Films,
   K. Jyothish, **M. Hariharan** and D. Ramaiah,
   Adv. Mater. (Communicated).

6. Unusual Planarization of Donor-Rigid Spacer-Acceptor Dyads through Encapsulation of β-Cyclodextrin,
   M. Hariharan and D. Ramaiah (To be communicated).

7. A Supramolecular Fluorescent Marker for the Detection and Quantification GTP and ATP in Buffer and Biological Fluids,
   D. Ramaiah, P. P. Neelakandan, **M. Hariharan**, a patent application No. # RRLT-179/2006 sent to CSIR on July 5, **2006** for filing in India and abroad.

PAPERS PRESENTED AT CONFERENCES

8. Synthesis and Study of Photophysical and DNA Binding Properties of Viologen Linked Pyrene Derivatives,
   M. Hariharan, J. Joseph and D. Ramaiah, Poster presented at *"IIIrd Trivandrum International Symposium on Recent Trends in Photochemical Sciences,"* Regional Research Laboratory, Trivandrum, India, **2004**, January 5-8.

9. DNA Oxidation Through Cosensitization Mechanism by Novel Viologen Linked Pyrene Derivatives,
   M. Hariharan, J. Joseph and D. Ramaiah, Poster presented at *"JNC Research Conference on Chemistry of Materials,"* Regional Research Laboratory, Trivandrum, India, **2005**, October 1-3.

10. Photoactivated DNA Cleavage Induced by Novel Viologen Linked Pyrene Conjugates,
    M. Hariharan, J. Joseph and D. Ramaiah, Poster presented at *"8th National Symposium in Chemistry,"* Indian Institute of Technology, Bombay, India, **2006**, February 3-5.